Politecnico di Torino

Master of Science Degree Programme in
Architecture, Construction and City

Master Thesis

Compounding Hazards in the San Francisco Bay Area:
Assessing Earthquake-Induced Gas Pipeline Damage and Fire Risk

Author | **Julia Demarchi Maciel**

Supervisors | **Gian Paolo Cimellaro & Kenichi Soga**

Co-supervisor | **Alessandro Cardoni**

A. Y. 2024/2025

“O que vale na vida não é o ponto de partida e sim a caminhada.
Caminhando e semeando, no fim, terás o que colher.”
- Cora Coralina

ACKNOWLEDGEMENTS

To Professor Gian Paolo Cimellaro, thank you for helping me broaden my academic horizon by introducing me to the challenging world of civil and environmental engineering. I am deeply grateful for the opportunity to blend my world of architecture with your world of engineering, an experience that has enriched me beyond measure. Thank you for opening so many doors and guiding me through them with patience and encouragement.

To Professor Kenichi Soga, my deepest gratitude for welcoming me into your team, for believing in me, and for trusting in what I could achieve. Thank you for the many hours spent together shaping this thesis and for your continuous support, both during my stay at UC Berkeley and after I returned home. Your counsel was essential for the conclusion of this work, your input invaluable, and your guidance truly vital.

I would also like to thank the UC Berkeley Visiting Scholar Program for granting me the opportunity to spend time at Berkeley and for providing the academic environment that made this work possible. I will never forget this incredible experience.

To Paola Lorusso, PhD student at UC Berkeley, I could not have done this without your help and advice. Having once stood where I stood, you understood how difficult this process could be. You took me under your wing, reminded me that I could do it, and supported me through countless meetings and coffee breaks. I am forever grateful to have met you.

To the Soga Research Group, thank you for welcoming me as one of your own, for sharing your expertise, and for all the moments of distraction and fun we had while I was in Berkeley. This experience would not have been the same without you.

To all my friends, old and new, thank you for your love and support since day one. You may be spread across the world, but you will always live in my heart, proof that friendships can endure long distances and multiple time zones.

Most important of all, I would like to thank my family. My deepest thanks to my mom, Alessandra, who taught me strength and resilience; to my dad, Ricardo, who taught me courage and drive; and to my brother, Enzo, who showed me what unconditional love truly is. Thank you for being the pillars that have held me up my entire life, and the lighthouse that guides me home when I am lost. Everything I am, I owe to you. Everything I do, I do for you. You have been, and always will be, the best part of me. This thesis would never have come this far without your support. Thank you for believing in me, even, and especially, when I didn't. *Eu amo vocês.*

ABSTRACT

California's natural gas infrastructure is essential to the state's energy system yet it still remains highly vulnerable to the combined effects of seismic events and fire activity. Traditional assessment approaches often overlook these interactions, limiting themselves to resilience planning. To bridge this gap, this thesis develops a quantitative, performance-based framework that integrates seismic hazard characterization, infrastructure vulnerability, and fire behavior into a unified multi-hazard analysis.

Applied to the San Francisco Bay Area through QGIS and the OpenSRA platform, the framework highlights where vulnerabilities concentrate and how cascading impacts may develop across interconnected systems. The findings show that compound risks are shaped by the convergence of physical conditions, infrastructure characteristics, and surrounding urban environments.

By establishing a more rigorous and transparent method for evaluating these dynamics, the research provides utilities and public agencies with a practical tool capable of informing targeted mitigation, investment prioritization, and integrated resilience strategies. The framework is broadly transferable and offers a path toward more robust multi-hazard assessment practices across California and the United States.

CONTENTS

LIST OF FIGURES

LIST OF TABLES

1. INTRODUCTION

California faces an increasingly complex and dynamic hazard environment shaped by the convergence of seismic activity, wildfire dynamics, climate change, population expansion, and aging infrastructure systems. As one of the most hazard-prone states in the United States, California has experienced significant evolution in its risk landscape over the last century. Historically, earthquakes have played the most defining role in shaping both public understanding and institutional approaches to disaster management. Landmark events such as the 1906 San Francisco earthquake and the 1989 Loma Prieta earthquake were pivotal in advancing seismic design, refining emergency response systems, and deepening scientific knowledge of crustal deformation and ground motion (Fielding Reid 1910; Lee et al. 2008). However, in recent decades, wildfires have eclipsed earthquakes as the state's most frequent and economically destructive hazard. Driven by persistent drought, vegetation stress, and intensifying development pressures in fire-prone regions, wildfire disasters have grown larger, more severe, and more costly (Li and Banerjee 2021; Westerling 2016; Keeley and Syphard 2019; Syphard et al. 2019).

Although earthquakes and wildfires are often analyzed as distinct hazard categories, their physical processes and societal impacts intersect in critical ways. These interactions exist within what disaster scholars increasingly describe as a multi-hazard or compounding hazard environment, one in which the occurrence of one hazard alters the probability, intensity, or consequence of another. In California, these interactions frequently involve infrastructure systems that bridge hazard domains, such as gas pipelines, electric power networks, and transportation corridors. When such systems fail during major earthquakes, compound, also known as cascading, effects can initiate secondary hazards that significantly magnify disaster impacts. Among the most consequential of these cascading processes is the phenomenon called fire following earthquake (FFE), also known as post-earthquake fire (PEF), which has historically been responsible for some of the most severe urban disasters in the state (Scawthorn 1986).

The San Francisco Bay Area provides a particularly compelling context for examining these interconnected risks. The region is situated atop one of the most active and geometrically complex sections of the boundary between the Pacific and North American tectonic plates, with the San Andreas, Hayward, Rodgers Creek, and Calaveras faults, each capable of producing high-magnitude events, cutting directly through densely populated urban corridors (Aagaard et al. 2016). Probabilistic assessments such as UCERF3 project a high likelihood of at least one major earthquake affecting the region in the coming decades (Field et al. 2014). Simultaneously, the Bay Area's Mediterranean climate, steep topography, diverse vegetation, and expanding wildland-urban interface (WUI) create conditions conducive to large, fast-moving wildfires. WUI growth places residential neighborhoods, infrastructure networks, and gas distribution systems in closer proximity to ignition-prone landscapes, increasing exposure and complicating emergency management.

Climate change further intensifies these risks by altering the environmental conditions that govern wildfire behavior. Rising temperatures, prolonged heat waves, declining snowpack, and increasing fuel aridity have extended the fire season well beyond its historical bounds (Keeley and Syphard 2016). These climatic shifts coincide with long-term vegetation stress, tree mortality, and hazardous fuel accumulation resulting from both ecological change and land-management practices. As a result, the Bay Area, and California more broadly, faces wildfire risks that are more extreme, more widespread,

and more difficult to manage than at any time in the past century (Westerling et al. 2011).

Despite this convergence of seismic and wildfire threats, hazard assessment practices continue to rely primarily on single-hazard frameworks. Seismic analysis typically focuses on ground-motion forecasting, structural response, liquefaction, lateral spread and landslide susceptibility, permanent ground deformation, and lifeline fragility. Wildfire research, in contrast, focuses on vegetation characteristics, ignition patterns, WUI expansion, meteorological drivers, and fuel dynamics to create fire-spread models (IUFRO and PROFOR 2020; Syphard et al. 2007). Neither take each other into careful consideration. While each field has developed advanced tools and methodologies to tackle their individual hazards, analytical separation obscures how earthquakes may create conditions favorable for fire ignition or how fire-prone environments may amplify the consequences of infrastructure failures triggered by seismic activity.

One of the most consequential yet understudied intersections between these hazard domains involves gas transmission and distribution pipelines. Many of California's gas pipelines were constructed decades ago, before modern seismic design standards were established (Bain 2023; Fournier et al. 2025). These systems, often composed of older or brittle materials and located in geologically complex terrain, are vulnerable to rupture, buckling, joint separation, or leakage when subjected to intense shaking or ground deformation such as liquefaction, lateral spreading, landslides, or surface fault rupture (O'Rourke and Liu 1999; Pitilakis et al. 2006). In the aftermath of a major earthquake, escaping natural gas can be easily ignited by downed electrical lines, damaged equipment, sparks, open flames, or static discharge. In dense urban areas where pipelines intersect buildings, transportation routes, and electrical infrastructure, multiple ignition events may occur simultaneously. If such ignition points arise within or near WUI zones, they may propagate into wildfires under severe fuel and weather conditions.

Historically, these cascading hazards have produced significant devastation. During the 1906 San Francisco earthquake, ruptured gas lines were a dominant source of ignition for the fires that ultimately destroyed more than 80% of the city's urban core (Fielding Reid 1910). Although firefighting capacity and infrastructure resilience have improved greatly since then, new vulnerabilities, including aging pipeline materials, population densification, and increasingly volatile fuel conditions, create renewed risk, especially following a major seismic event when water supply disruptions, roadway blockages, and emergency resource shortages may severely constrain fire response.
In the contemporary Bay Area, additional risk emerges from continued residential and infrastructural expansion into WUI landscapes. Housing expansion along ridge tops, in narrow valleys, and on densely vegetated slopes creates environments with high ignition potential and limited evacuation capacity. These constraints hinder fire suppression even under normal conditions; after an earthquake, when access routes may be compromised and water systems disrupted, containment becomes exponentially more difficult. Understanding where seismic vulnerability and wildfire potential overlap spatially is therefore essential for strengthening regional resilience and reducing compound hazard risk.

Despite mounting evidence of these interactions, significant analytical gaps remain unexplored in wildfire and earthquake research. While seismic studies have explored pipeline fragility under a range of hazard scenarios, and wildfire studies have advanced high-resolution spatial models of ignition and spread, few efforts integrate these approaches to identify where earthquake-pipeline-fire interactions are most likely to cascade. For regional planners, emergency managers, and utility operators, the absence of such integrated assessments limits the ability to identify and prioritize multi-hazard hotspots, namely, locations where earthquake-induced pipeline damage is likely to coincide with landscapes predisposed to rapid fire spread.

This thesis responds directly to these gaps by developing a spatially explicit, multi-hazard assessment of the San Francisco Bay Area that integrates seismic pipeline vulnerability modeling with wildfire risk analysis. Using a combination of GIS-based Multi-Criteria Decision Analysis (MCDA), the Analytic Hierarchy Process (AHP), and the OpenSRA seismic risk framework, the study produces a detailed spatial model of earthquake-pipeline-fire interactions. OpenSRA provides probabilistic estimates of pipeline damage under UCERF3 earthquake scenarios, incorporating parameters such as ground motion intensity, soil conditions, pipeline material, and installation characteristics. In parallel, a wildfire hazard surface is constructed using environmental, infrastructural, and historical ignition variables such as vegetation cover, proximity to roads, and past ignition locations (Syphard et al. 2007; Radeloff et al. 2018; CAL FIRE, n.d.). Integrating these layers reveals spatial patterns of compounding risk that remain obscured under single-hazard approaches.

The study has four primary objectives:

1. To develop a clear and understandable wildfire-risk surface for the Bay Area using environmental, infrastructural, and historical data.

2. To model pipeline-damage probability under UCERF3 earthquake scenarios using the OpenSRA framework.

3. To integrate the resulting hazard surfaces to identify combined hazard hotspots where earthquake-induced pipeline damage and wildfire potential intersect.

4. To evaluate the implications of these findings for hazard mitigation, emergency preparedness, and infrastructure planning across the region.

By situating this analysis in the Bay Area, a region defined by tectonic complexity, diverse ecosystems, and extensive infrastructure networks, this thesis offers insights relevant to other metropolitan regions facing similar multi-hazard dynamics. As climate extremes intensify and critical infrastructure continues to age, the urgency of developing integrated hazard assessments grows. Understanding where and how these risks intersect is essential not only for reducing disaster losses but also for supporting long-term planning, sustainable development, and community resilience. The chapters that follow therefore examine California's climate-driven wildfire context, its seismic hazard landscape, key theories of compounding hazards, the Bay Area's regional characteristics, and the methodological framework employed to evaluate earthquake–pipeline–fire interactions across the region.

2. CLIMATE CHANGE

One of the biggest and most pressing environmental concerns of the modern time is climate change. This phenomenon has, much quicker than expected, become a defining force that is constantly reshaping environmental, ecological, and societal conditions across the world, impacting countless lives. In response to that, a new trend in behavior has emerged among the youth, with constant protests and demonstrations demanding actions to counter the phenomenon, while governments and international bodies are beginning to rise up to the challenge by creating new policies, goals and increasing cross-border cooperation initiatives.

One of the countries highly affected by climate change, and the main focus of this research, is the United States, with California standing at the forefront of its accelerating impacts. Scientific evidence has been consistently demonstrating that anthropogenic greenhouse gas emissions have driven unprecedented global warming over the past century, resulting in climate shifts that are already altering hydrological systems, vegetation regimes, atmospheric dynamics, and the frequency and severity of natural hazards. Studies conducted in the beginning of 2025 have shown that global temperatures in 2024 exceeded over 1.5°C above pre-industrial levels, a considerable feat, making it the hottest year on record and the culmination of an uninterrupted series of extreme heat anomalies going back more than a decade (Schaeffer et al. 2025). NASA similarly confirms that humans are now observing climate-driven changes such as more intense heatwaves, shrinking ice sheets, sea-level rise, and increased drought faster than previously anticipated, with some of these changes being completely irreversible (NASA 2024). A University Corporation for Atmospheric Research (UCAR) scientific assessment further corroborates these findings, projecting additional warming of up to 4 or 5°C by the end of the century if emissions remain high. This considerable increase in temperature could fundamentally alter precipitation regimes, extreme weather patterns, ocean chemistry, and ecosystem structures (UCAR 2025). In sum, the evidence is strong in illustrating that climate change is not a distant risk but a present reality, one that is greatly affecting every region of the United States.

Across the country, the manifestations of a warming climate are most prominently evident in the intensification of climate-related disasters. Hurricanes striking the Atlantic and Gulf coasts have become stronger due to warmer ocean waters (Vernick 2025), extreme rainfall events have increased in both frequency and magnitude, and major flooding has devastated many communities from the Midwest to the Southeast (US EPA 2024). Heatwaves have grown longer, hotter, and more widespread, contributing to significant mortality rates and placing added stress on energy systems and public health infrastructures that are already in high-demand (Schaeffer et al. 2025). Water resources are under similar stress, being more limited each day. The severity of droughts in the Southwest has gotten much worse as warming has led to a decline in snowpack, which is melting earlier and earlier each year, threatening water supply reliability and even food production, increasing human vulnerability (NASA 2024). These national trends help form the backdrop against which California's unique climate vulnerabilities have become especially pronounced.

The state of California is widely recognized as one of the United States' most climate-sensitive regions. This is due to many factors, including its rapidly rising temperatures, atmospheric aridity, recurrent droughts, and complex topography. In recent decades, these factors have converged to dramatically intensify wildfire behavior across the state. Research by Abatzoglou and Williams (2016) further corroborates that anthropogenic warming is one of the main causes behind increased fuel aridity across

the western United States. It has accounted for more than half of observed increases in vapor pressure deficit, a key variable controlling forest flammability. Building on this work, Williams et al. (2019) show that climate change has also doubled the cumulative forest area burned in the western U.S. since the 1980s. More recently, Turco et al. (2023) measured how much climate change has affected California's wildfire trends. They found that almost all of the fivefold increase in summer burned area between 1971-1995 and 1996-2021 is linked to human-caused warming. Their results show a 172% increase in burned area directly connected to rising temperatures, which confirms that heat-driven vegetation drying, rather than natural climate variation, is the main force behind California's current wildfire behavior. State-level records also reinforce these conclusions. The California climate indicators report shows that annual burned area has increased sharply since the early 2000s, with 2020 alone burning an unprecedented 4.2 million acres followed by 2.6 million acres in 2021, making both years some of the worst in California's recorded history (Sapsis et al. 2022). The number of very large fires (taken to be over 10,000 acres in area) has risen dramatically, with nearly all of the state's largest fires occurring since 2000. These megafires have caused widespread destruction, with two of its most infamous fires being the 2018 Camp Fire, the deadliest and most destructive in California history, and the 2020 August Complex Fire, the state's first "gigafire" exceeding one million acres (Sapsis et al. 2022). However, the fires alone are not the only problem to be considered. Postfire impacts are equally worthy of discussion and investigation, as they cascade across communities, ecosystems, and critical infrastructure systems, resulting in horrible and at times dangerous air-quality periods of time, extensive economic damages to both the population and the government, habitat loss, tree mortality, and, most important for this research, severe disruption of public services systems and networks.

Climate-driven wildfire escalation in California is also tightly connected to weakened forest resilience and elevated vegetation stress (NASA 2024). Vegetation modeling by Ackerly et al. (2015) shows that climate change is causing major changes in the types and locations of plant communities in the San Francisco Bay Area, even in places that were once thought to be protected from climate impacts. These transitions significantly influence fuel loads, setting the stage for more extreme fire seasons. Atmospheric research further demonstrates that warming-induced increases in vapor pressure deficit intensify the speed at which fuels dry, producing more days of extreme fire weather and lengthening the fire season into months that previously had little fire activity (Schaeffer et al. 2025).

Apart from the growing threat of wildfires, climate change in California is increasingly reshaping people's lives, with extreme heat emerging as one of the most concerning hazards. Recent scientific reviews indicate that a rising share of the global population is being pushed outside the historical "human climate niche," which is described as the range of climatic conditions in which human societies have traditionally settled in (Schaeffer et al. 2025). As heat extremes surpass levels that are physiologically tolerable in some regions, more communities are being forced to reconsider where and how they live. This shift is already contributing to patterns of displacement, as households relocate in search of safer temperatures, reliable livelihoods, and more stable living conditions. In addition to that, rising temperatures put an added strain on vulnerable populations such as outdoor workers, the elderly, and low-income communities, exacerbating health and socioeconomic disparities (Do et al. 2023).

These social effects are further intensified when climate-driven hazards interact

with critical service systems. Research on infrastructure interdependencies shows that wildfires, heatwaves, and extreme weather can trigger cascading disruptions across energy, transportation, communication, and water networks (Sfetsos et al. 2021). In California, wildfires have repeatedly damaged transmission lines, prompted preemptive grid shutdowns, and hindered emergency response, with national analyses indicating that extreme weather accounts for over 60% of prolonged power outages affecting medically vulnerable populations (Do et al. 2023), illustrating how climate hazards compound existing social inequalities. These patterns mirror global trends documenting that socially and economically marginalized communities bear disproportionate burdens from climate disasters (Ibarrarán Viniegra et al. 2009; Vernick 2025).

In addition to these more immediate hazards, climate change has also been linked to the change in long-term geophysical processes. Studies in Alaska by Sauber and Ruppert (2013) and Sauber et al. (2021) show that rapid ice mass loss can influence crustal stress fields and modulate seismicity. While these processes are most pronounced in regions undergoing significant deglaciation, they illustrate broader principles linking climate processes to geological hazards. Similar research in East Asia demonstrates that interglacial warming periods have historically aligned with elevated intraplate seismicity (Kim and Lee 2023), suggesting that climate-induced mass redistribution may influence seismic risk in certain contexts. Though this phenomenon is certainly less significant in California than its dominant tectonic forces, it is still an interesting point of research. As sea levels continue to rise and alter coastal mass distribution, future changes in ocean loading along California's coast could, at least in principle, have subtle effects on regional stress fields, making this a topic worth monitoring as climate change progresses.

In summary, the literature paints a coherent and urgent picture: climate change is intensifying environmental hazards and California is paying a high price as one of the most acutely affected regions. Wildfires have become larger, more destructive, and more frequent; heatwaves are growing more intense; droughts are deepening; and critical infrastructure systems are increasingly vulnerable. These impacts interact with socioeconomic inequalities, increasing risks for marginalized communities and amplifying the costs of inaction. Climate change in California represents not a singular threat but a system-wide transformation affecting ecosystems, human life and health, infrastructure, governance, and long-term environmental stability. The trajectory of these impacts will depend heavily on near-term mitigation and adaptation strategies, as emphasized by NASA (2024), UCAR (2025), and the Intergovernmental Panel on Climate Change (IPCC) (Schaeffer et al. 2025). Immediate reductions in greenhouse gas emissions, combined with coordinated adaptation planning, will determine the extent to which California and the nation can preserve a livable future in a rapidly changing climate prone more and more to more devastating natural disasters.

3. NATURAL DISASTERS

Natural disasters are severe natural events that exceed a community's capacity to respond, shaped by both physical processes and societal vulnerability (Quarantelli 2000). Their frequency and impact have grown due to urbanization, environmental degradation, and climate change (Saunders et al. 2025). In 2024 alone, 393 natural hazard-related disasters caused 16,753 fatalities, affected 167 million people, and generated US$242 billion in losses (CRED 2025). Despite advances in forecasting and management, disasters continue to reveal global inequalities, often harming low-income communities the most (Botzen et al. 2019; Kharb et al. 2022; Rentschler et al. 2022).

Floods, storms, droughts, heatwaves, and earthquakes remain the most common disasters globally. Floods caused the highest number of fatalities in Africa and Asia in 2024, while tropical cyclones such as Typhoon Yagi and Cyclone Remal affected millions across Southeast Asia. At the same time, severe droughts in southern Africa and the Amazon damaged ecosystems and agricultural systems (Delforge et al. 2025). Extreme heat events are also becoming a major threat, illustrated by the 2024 Saudi Arabia heatwave that killed over 1,300 Hajj pilgrims (CRED 2025). These trends underscore the links between climate change, population growth, and hazard exposure.

Disaster impacts are mediated by governance and infrastructure quality. Wealthier nations experience high economic losses but lower mortality due to stronger emergency systems, while lower-income regions face disproportionate fatalities and slower recovery (Botzen et al. 2019; Kharb et al. 2022). Weak data systems further exacerbate risk: EM-DAT, the most widely used disaster database, lacks consistent reporting in low-income regions and underrepresents smaller events (Delforge et al. 2025; Gall et al. 2009; Mazhin et al. 2021). This limits accurate assessments for policy and investment.

Improving resilience requires better data integration and communication. Research emphasizes that effective early-warning systems depend not only on accurate forecasts but also on public understanding, trust, and communication clarity (Saunders et al. 2025; Twigg 2003; Golding 2022). Emerging technologies, like satellite imagery, crowdsourced observations, and machine-learning models, enable more localized and timely warnings (Kaku 2019). These innovations align with global policy frameworks like the Hyogo and Sendai Frameworks, which promote data-driven, preventive approaches to disaster risk reduction (UNISDR 2015; Delforge et al. 2025). Yet implementation gaps persist, especially where institutional capacity is limited.

Overall, natural disasters are no longer isolated natural phenomena; they are systemic challenges shaped by social inequality, climate change, and infrastructure vulnerability. Data quality, communication, and governance remain central to improving resilience and reducing future losses (CRED 2025; Delforge et al. 2025; Saunders et al. 2025).

3.1 Earthquakes

Earthquakes occur when accumulated stress in the Earth's crust is released along faults, generating seismic waves and surface shaking (Kanamori and Brodsky 2004). The elastic rebound process explains how stress builds gradually and is suddenly released when rock strength is exceeded (Hardebeck and Okada 2018). Although tectonic motion is the primary driver, environmental factors such as glacial retreat, permafrost thaw, groundwater depletion, and human activities can influence fault

stress.

Climate-related surface changes are particularly significant in Alaska. Rapid glacier melt has reduced crustal loading, increasing stress on nearby faults. Sauber and Ruppert (2013) found that ice loss brought faults between the coast and the 1979 aftershock zone closer to failure by roughly 0.2-1.2 MPa. Subsequent research showed that seasonal snow loading, deglaciation, and permafrost thaw alter stress fields in ways that promote seismicity on upper-crustal faults (Sauber et al. 2021). These findings build on earlier work by Plafker (1969), whose mapping of uplift and subsidence patterns after the 1964 Alaska earthquake established the basis for linking glacial mass change and crustal deformation.

Similar processes occur in California through human-induced hydrological change. Groundwater pumping in the Central Valley has caused crustal uplift and reduced normal stress on the San Andreas Fault. Amos et al. (2014) demonstrated that this unburdening helps explain the seasonal pattern of microearthquakes near Parkfield. Such studies show that seismicity responds to changes at Earth's surface, not just deep tectonic forces.

Earthquakes create profound and lasting societal impacts. The 1994 Northridge earthquake damaged over 114,000 structures and caused US$41.8 billion in losses, making it one of the costliest disasters in U.S. history (Petak and Elahi 2001). Fires ignited by gas and electrical failures further increased destruction (Eguchi et al. 1998). Similarly, the 1964 Alaska earthquake caused major coastal uplift and subsidence, drastically altering shorelines, damaging ports, and affecting nearshore ecosystems (Plafker 1969).

Furthermore, earthquakes often trigger secondary hazards, including tsunamis, landslides, liquefaction, and urban fires. The 1906 San Francisco earthquake illustrates this interaction: roughly 80% of total destruction resulted from fires that ignited after gas and electrical systems failed. More recent research highlights that earthquake-related fire remains one of the most significant compounding urban hazards (Vitorino et al. 2024).

In sum, earthquakes are not isolated geological events but dynamic interactions between tectonic processes, climate-driven mass changes, human activities, and infrastructure vulnerability. It is, therefore, imperative to learn how to analyze these factors together for better planning in a changing environment.

3.2 Wildfires

Wildfires are uncontrolled fires that burn vegetation across forests, shrublands, and grasslands, with their spread governed by fuel conditions, weather, and topography (Keane et al. 2008; McLauchlan et al. 2020). They propagate through surface fuels, ladder fuels, and tree canopies, and their intensity increases under dry, hot, and windy conditions that promote rapid combustion. Although lightning and other natural processes can ignite fires, human activities now account for the majority of ignitions, including power-line malfunctions, equipment sparks, and accidental or negligent behavior (Balch et al. 2017; Farid et al. 2024). This mixture of natural and anthropogenic drivers establishes wildfires as both ecological processes and socio-environmental hazards.

The ecological impacts of fire are multifaceted. Many western U.S. ecosystems evolved with periodic low-intensity burning, which facilitates nutrient recycling, opens habitat, and stimulates regeneration (McLauchlan et al. 2020). Yet the benefits of fire are increasingly overshadowed by the prevalence of high-severity events. When fire frequency or intensity exceeds ecological thresholds, vegetation loss, soil hydrophobicity, and shifts in species composition become widespread (Keane et al. 2008). These degradative effects extend beyond the burn perimeter as post-fire erosion and sedimentation impair water quality in rivers and reservoirs (Farid et al. 2024). Thus, contemporary wildfires destabilize landscape processes in ways that differ markedly from pre-suppression fire regimes.

A major source of modern wildfire risk is long-term fuel accumulation, driven primarily by twentieth-century fire suppression. After catastrophes like the 1910 Great Fire, U.S. land agencies adopted suppression policies that minimized the role of natural burning (Marlon et al. 2012). Although intended to protect timber and settlements, these policies produced denser forests and heavier fuel loads, making current fires larger, faster, and more intense. Scientific recognition of fire ecology has since shifted management toward prescribed burning and managed fire (Huffman et al. 2020), but the scale of accumulated fuels far exceeds current treatment capacity. This historical backdrop helps explain why recent fires behave in ways uncharacteristic of many fire-adapted ecosystems.

Climate change is now amplifying these structural vulnerabilities. Warmer temperatures, earlier snowmelt, and prolonged drought reduce fuel moisture and lengthen fire seasons across the western United States (Keane et al. 2008; McLauchlan et al. 2020). Quantitative attribution studies estimate that between 33% and 82% of the burned area in several western ecoregions from 1992–2020 is attributable to anthropogenic climate change, along with roughly 49% of smoke exposure (Feng et al. 2024). Wildfires themselves contribute to further warming through the release of carbon dioxide, methane, and black carbon (Farid et al. 2024). This feedback loop, warming that fuels fires, and fires that in turn reinforce warming, illustrates the deep interconnection between climatic and ecological processes.

Another critical component shaping wildfire impacts is human settlement in the wildland-urban interface (WUI). WUI expansion has increased ignition likelihood and placed millions of homes and residents at direct risk (Balch et al. 2017). The juxtaposition of flammable vegetation with dispersed housing, limited road access, and inadequate defensible space complicates both suppression and evacuation efforts. Smoke exposure further magnifies the human cost, contributing to respiratory and cardiovascular health effects across wide regions (Feng et al. 2024; Edgeley et al. 2025). As such, the WUI transforms wildfire from a largely ecological phenomenon into a complex socio-technical hazard.

Collectively, these factors have produced a wildfire regime in California that is fundamentally different from previous decades. Although ignition frequency has not dramatically increased, the area burned and severity of fires have risen significantly, straining suppression resources and complicating post-fire recovery (Farid et al. 2024). Addressing these challenges requires integrated approaches that combine ecological fuel management, climate adaptation, land-use planning, and the hardening of communities and infrastructure. Only with such multi-dimensional strategies can

California move toward a more sustainable coexistence with wildfire in an era of accelerating environmental change.

4. COMPOUND HAZARDS

Compound hazards occur when multiple drivers or events interact, producing impacts greater than the sum of their individual effects (Zscheischler et al. 2018; Brett et al. 2025). These interactions are especially critical in urban environments where infrastructure systems, like water, power, gas, and transportation, are tightly interconnected. When one system fails, cascading disruptions can propagate quickly and non-linearly (Alexander and Pescaroli 2019). Earthquakes combined with fires represent one of the clearest and most destructive examples of such compound behavior: seismic shaking damages buildings and lifelines, ruptures utilities, and impairs emergency response, while fires ignite and spread under compromised conditions (Scawthorn et al. 2006).

Historical earthquakes around the world consistently illustrate that fire is a major contributor to total losses. The 1906 San Francisco and 1923 Great Kantō events demonstrate that when ignition rates are high and water systems are damaged, fires, not the shaking, dominate fatalities and property destruction (Scawthorn et al. 2006; Schencking 2013). More recent events such as Northridge (1994), Kobe (1995), and the 2011 Great East Japan earthquake also reaffirm the strong coupling between seismic impacts, gas infrastructure failure, and urban fire spread (Cruz and Suarez-Paba 2019). Compound-hazard research has traditionally focused on climate-related pairs (e.g., heat-drought, flood-storm-surge), leaving technologically mediated events, such as earthquake-triggered fires or NaTech disasters, comparatively underexamined (Zscheischler et al. 2018; Brett et al. 2025). Yet the urban and technological dimensions of these hazard cascades are increasingly relevant as cities densify, infrastructure ages, and climate change alters baseline stressors on energy systems.

Against this backdrop, understanding how earthquakes interact with fire dynamics and gas networks is essential for anticipating catastrophic outcomes and addressing remaining gaps in multi-hazard modeling.

4.1 Post-Earthquake Fires

Post-earthquake fires (PEFs) are among the most devastating secondary hazards in seismic regions. Historical earthquakes show that fires can surpass shaking-related losses when lifelines fail and ignition sources proliferate. In the 1906 San Francisco earthquake, more than 80% of total destruction resulted from fires that burned for days after gas and water systems were damaged (Vitorino et al. 2024; Baquedano Juliá et al. 2021). A similar pattern occurred in the 1923 Great Kantō earthquake, where over 110,000 fatalities, most fire-related, were caused by widespread ignitions and the collapse of response capabilities (Vitorino et al. 2024).

Despite these precedents, PEFs remain insufficiently integrated into seismic design standards. Building codes generally prioritize structural resistance but rarely account for fire following earthquake (FFE) conditions, leaving buildings vulnerable once fireproofing, connections, or partitions are compromised (Vitorino et al. 2024; Mousavi et al. 2008). This gap is particularly pronounced for steel moment frames and reinforced concrete structures, where seismic damage can sharply reduce fire resistance (Alasiri et al. 2021; Dashti et al. 2025).

Ignition patterns in PEF scenarios follow strong empirical trends. A global review of 49 events shows that fires correlate more closely with shaking intensity and time of day than with earthquake magnitude (Vitorino et al. 2024). Mealtime hours generate higher ignition rates due to appliance use. Common ignition sources include ruptured

gas lines, electrical faults, and open flames, often triggered or exposed by structural collapse (Hua et al. 2025). These fires then spread more readily when roads are blocked, water networks are damaged, or communications fail, as seen in Northridge (1994) and Kobe (1995) (Scawthorn 1986; Tian et al. 2025; Nishino 2023).

Modeling capabilities for PEFs have advanced substantially, with early geometric approaches having been replaced by probabilistic, GIS-based, and physics-informed methods (Baquedano Juliá et al. 2021). Ren and Xie (2004) incorporated Huygens' Principle to simulate urban fire spread under varying winds and densities. More recently, Nishino et al. (2023) developed Monte Carlo and hierarchical Bayesian frameworks that integrate ignition uncertainty, urban morphology, firefighter mobility, and infrastructure fragility, allowing realistic scenario generation even in data-limited contexts. These tools help planners test interventions, evaluate worst-case outcomes, and prioritize investments.

Mitigation strategies span building-level, urban, and regional scales. At the structure level, maintaining active fire systems (sprinklers, alarms), securing utilities, and upgrading passive fire protection are essential (Mousavi et al. 2008). At the city scale, flexible gas connections, water system redundancy, alternative water sources, firebreak corridors, and coordinated emergency communication networks are crucial (Kürüm Varolgüneş and Varolgüneş 2025; Vitorino et al. 2024). BIM-based simulations further support evacuation planning by showing how smoke can render corridors impassable within minutes (Lofti et al. 2021).

Even with improved science, significant gaps remain. Social behavior, delayed evacuations, and community-led response are rarely modeled; most analyses rely on U.S. and Japanese case studies, leaving large parts of the world without tailored assessments (Vitorino et al. 2024). European historical districts, for example, pose unique challenges, as highlighted by Baquedano Juliá et al. (2021), due to narrow streets, combustible materials, and limited fire separations.

PEFs therefore represent a decisive component of earthquake risk, requiring integrated, multi-scale planning and recognition of their central role in urban disaster outcomes.

4.2 Earthquake-Gas Pipeline-Fire Relationship

Earthquakes and urban fires are tightly linked through the vulnerability of natural gas infrastructure. Buried pipelines experience deformation from fault rupture, liquefaction, lateral spreading, and wave-propagation strain. Older systems, particularly cast-iron pipes and brittle joints, are highly susceptible to breakage, with failure probabilities increasing sharply once peak accelerations exceed ~0.7g (Ueno et al. 2004). When leaks ignite due to electrical faults, sparks, or open flames, cascading urban fires can develop and quickly overwhelm limited suppression capabilities (Lee et al. 2008).

Historical events repeatedly illustrate this pattern. In the 1906 San Francisco earthquake, gas mains ruptured across the city, contributing to dozens of simultaneous ignitions (Scawthorn et al. 2006). The 1994 Northridge earthquake produced around 110 post-quake fires, many linked to natural gas failures, including the Balboa Boulevard fire that destroyed multiple homes (Cruz and Suarez-Paba 2019). During the 1995 Kobe earthquake, damage to buried gas facilities and joint failures led to over 200 gas-leak fires and disrupted service to roughly 857,000 customers (Cruz and Suarez-Paba 2019). NaTech incidents, such as the refinery fires during the 2011 Great East Japan earthquake, further illustrate how technological systems amplify earthquake impacts. Modeling the earthquake-gas-fire chain remains challenging. Fragility functions for pipelines are limited and often derived from small datasets, urban fire models seldom integrate lifeline failure, and proximity effects, such as clustering of gas corridors and dense housing, are difficult to represent accurately (Piccinelli et al. 2013; Krausmann et al. 2019). Yet the mechanisms are well understood: ground deformation causes leaks, ignition likelihood rises with interaction between utilities, and compromised water systems reduce suppression capacity (Jones et al. 2008).

This nonlinearity matters because small changes in ignition probability or response delay can shift outcomes from isolated fires to block-level conflagrations. Co-location of faults, liquefaction zones, and densely built neighborhoods creates hazard "hot spots" where gas infrastructure and population exposure overlap. Fires can also feed back into infrastructure failure by damaging power lines, substations, and telecommunications equipment.

Targeted interventions offer substantial risk reduction. Automatic shutoff valves, excess-flow limiters, sectionalized mains, and prioritized replacement of brittle pipes all reduce leak likelihood. Water system redundancy, like firefighting cisterns, fireboats, and emergency hydrants, improves suppression under lifeline failure. San Francisco's Marina District during the 1989 Loma Prieta earthquake is a notable example: liquefaction destroyed hydrants, but the fireboat Phoenix provided critical water supply that prevented widespread conflagration.

In summary, the interaction between earthquakes, gas networks, and fire is a classic cascading hazard. Damage to pipelines increases ignitions, water network failures limit suppression, and urban density accelerates fire spread. Addressing this requires integrated, multi-hazard data, coupled simulations, and infrastructure-aware planning that reflects the realities of interconnected urban systems (Zscheischler et al. 2018; Piccinelli et al. 2013; Jones et al. 2008).

5. CALIFORNIA HAZARD LANDSCAPE

California's hazard landscape has grown increasingly complex due to climate change, aging infrastructure, and continued development in high-risk areas. While earthquakes have traditionally shaped statewide preparedness, wildfires now occur more frequently and impose greater socioeconomic impacts. From 1953 to 2024, the state experienced 386 federal disaster declarations, with nearly one-third since 2015 and 289 linked to wildfire (Ermagun et al. 2025). Burned area has increased nearly fivefold between 1971-1995 and 1996-2021 (Turco et al. 2023), driven largely by anthropogenic climate change (Dahl et al. 2023; Turco et al. 2023). In contrast, earthquakes accounted for only 7% of emergency declarations from 1950 to 2017 (Legislative Analyst's Office 2019), though their potential for cascading failures remains severe (Li et al. 2024; Comfort 2021).

The current problem of climate change only amplifies risk across hazard types. Warmer conditions increase vapor pressure deficits, drying vegetation and intensifying fire seasons (Turco et al. 2023). At the same time, critical infrastructure, designed for historical climate conditions, struggles to withstand modern extremes (Moftakhari and AghaKouchak 2019). Compound events such as wildfire-rainfall sequences also pose growing threats, exemplified by the 2018 Montecito debris flows following severe wildfire (Moftakhari and AghaKouchak 2019). As temperatures rise, these multi-hazard sequences are expected to increase (Nemeth et al. 2024).

Energy systems face elevated exposure to compound hazards. Wildfire, landslide, erosion, and runoff threaten both above- and below-ground pipeline infrastructure, particularly in Northern and Central California (Moftakhari and AghaKouchak 2019). Above-ground gas facilities melt or fail under wildfire conditions, while underground lines are damaged by flooding, sedimentation, and ground movement. Projections suggest that even currently low-risk regions, such as the Mojave and Sonoran Deserts, will experience increased compound hazard exposure in coming decades.

Social vulnerability further intensifies this bleak hazardscape. More than 2.9 million Californians live within one kilometer of oil and gas infrastructure in wildfire-prone areas, disproportionately affecting Black, Hispanic, and Native American communities (González et al. 2024), with many lacking access to mitigation resources, insurance, or resilient infrastructure (MacCarthy et al. 2024; Thomas 2024). Meanwhile, aging networks amplify risks: gas systems face safety and compliance challenges as midstream networks deteriorate (Saran et al. 2024), and electricity systems suffer escalating outage potential as assets exceed design lifespans (Lo et al. 2019; Do et al. 2023).

Risk communication systems also lag behind these evolving threats. Public frameworks often treat hazards in isolation, failing to convey the interconnected nature of wildfire, infrastructure vulnerability, and post-earthquake risks (Nemeth et al. 2024). This communication gap disproportionately harms socially vulnerable communities and complicates emergency response.

Mitigation requires integrating land management, infrastructure upgrades, and inclusive planning. Fuel treatments (prescribed burns, thinning, grazing) reduce wildfire severity when applied systematically (Oliveira et al. 2016; Murray et al. 2023). Transportation and utility networks need safe-to-fail design with redundancy to withstand cascading events (Fraser et al. 2022). Zoning reforms, updated building codes, and community-centered resilience planning are crucial for long-term adaptation (Shives et al. 2025; Bondi and Kaewwilai 2020; MacCarthy et al. 2024).

California's hazard environment is thus defined by the convergence of climate pressures, infrastructure fragility, and social inequity. Understanding this context is essential for assessing risk to critical systems such as gas networks and for advancing resilience across diverse communities.

5.1 WUI Zones

The wildland-urban interface (WUI), where homes meet or intermingle with flammable vegetation, is one of the fastest-growing and most hazardous landscapes in California (Radeloff et al. 2005; 2018). Over one-third of California households now reside in WUI areas, with nearly 1.5 million new homes built there from 1990 to 2020 (Greenberg et al. 2024). This expansion places millions at heightened wildfire risk due to direct exposure to flames, radiant heat, and wind-driven embers (Wilkin et al. 2025). California's fire-adapted ecosystems and steep topography further intensify this threat (Thapa et al. 2023).

Most WUI fires are human-caused, by accidents, infrastructure failures, or negligence, raising ignition likelihood as development expands (Radeloff et al. 2018; Calviño-Cancela et al. 2016). Firefighting is further complicated by dispersed housing, narrow roads, and limited water supply, making evacuations dangerous. The 2018 Camp Fire showed how bottlenecks and limited exit routes can turn evacuations into life-threatening events, especially for elderly or mobility-limited residents (Thapa et al. 2023).

Compliance with defensible space and fire-resistant construction codes remains inconsistent. Inspections show that a majority of WUI homes fail to meet vegetation clearance or ember-resistant standards (Wilkin et al. 2025). Meanwhile, WUI growth disrupts ecosystems, fragments habitats, and introduces invasive species (Radeloff et al. 2005; 2018). Fire suppression to protect homes further alters natural fire regimes, increasing fuel accumulation (Thapa et al. 2023). Smoke from burning structures also produces toxic pollution with regional health impacts (Qiu et al. 2025).

Socioeconomic dynamics intensify vulnerability. Wealthier residents often seek scenic WUI locations, benefiting from insurance and political resources, while California's housing shortage pushes lower-income households into more isolated, high-risk WUI areas (Debats Garrison and Huxman 2020; Greenberg et al. 2024). Recovery after fires often follows inequitable trajectories: affluent households rebuild more easily, while vulnerable groups experience permanent displacement (Amiri et al. 2025).

Advances in WUI mapping and modeling provide better tools for managing risk. Gong et al. (2024) incorporate housing density, vegetation cover, and fire occurrence to delineate high-risk zones. Masoudvaziri et al. (2021) integrate wildfire hazard, exposure, and demographic vulnerability to identify hotspot communities, particularly useful for regions like the Sierra Nevada foothills. These methods support planning for evacuation routes, fuel treatments, and zoning restrictions.

Recent events underscore the urgency of better governance. The 2025 Los Angeles fires caused US$250 billion in damages and destroyed over 16,000 structures, largely in WUI neighborhoods (Qiu et al. 2025). Such fires illustrate that WUI disasters are not simply ecological problems but socio-technical crises shaped by settlement patterns, building practices, and infrastructure limitations.

Policy solutions must combine fuel management, resilient building standards, equitable insurance models, and land-use planning. Without coordinated intervention, ongoing WUI expansion and climate change will deepen California's wildfire crisis and increase exposure to cascading hazards.

5.2 Gas Networks

California's natural gas networks, comprising high-pressure transmission pipelines, local distribution lines, and underground storage, form a critical energy lifeline. They support heating, electricity generation, and industrial operations while interacting with water, electricity, and transportation systems. Their complexity makes them particularly vulnerable to disruption during natural hazards, especially earthquakes.
Seismic damage to pipelines arises from fault rupture, liquefaction, lateral spreading, and differential settlement. The 1994 Northridge earthquake ruptured both transmission and distribution lines along Balboa Boulevard, igniting fires that destroyed five homes (O'Rourke and Palmer 1994; Bain et al. 2024). Older oxy-acetylene welds performed poorly compared to modern electric arc welds (Bain 2023). The 1989 Loma Prieta earthquake caused liquefaction-induced failures in San Francisco's Marina District, where ruptured gas mains ignited fires and hydrant failure forced reliance on the fireboat Phoenix (Schmidt et al. 2014; O'Rourke and Palmer 1994; Scawthorn et al. 1992).

Minor ground deformation can also cause significant pipeline damage, as documented by Schmidt et al. (2014). Similar vulnerabilities are observed in global incidents such as the 2004 Ghislenghien explosion in Belgium and the 2010 Dalian disaster in China. U.S. events, including the 2018 Merrimack Valley explosions and the 1965 Natchitoches pipeline tragedy, highlight failures related to over-pressurization, mismanagement, corrosion, and outdated materials (Ly 2019).

California's system has faced high-profile failures, such as the 2015 Aliso Canyon blowout, the largest methane release in U.S. history, caused by corrosion and inadequate maintenance. These cases underscore that pipeline risk arises not only from natural hazards but also from aging infrastructure, operational errors, and regulatory gaps.
Multi-hazard perspectives are essential for understanding pipeline vulnerability. Wildfire can melt above-ground equipment; floods, landslides, and erosion can expose or rupture buried lines; and earthquakes can generate widespread leaks that lead to urban fires. Integrated GIS-based models that combine seismicity, liquefaction susceptibility, WUI expansion, infrastructure age, and population exposure can guide targeted retrofits and risk mitigation.

In this context, strengthening California's gas networks requires replacing brittle materials, improving corrosion monitoring, enhancing shutoff and pressure-control technologies, and prioritizing upgrades in geohazard-prone zones. As climate pressures and urban expansion continue, the resilience of these systems is central to reducing the severity of future disasters.

6. CASE STUDY: SAN FRANCISCO BAY AREA

This section of the thesis brings together all the elements discussed in previous chapters in order to frame the San Francisco Bay Area as the case study investigated in this work. Commonly referred to as the Bay Area, the location is one of the most dynamic and complex regions in California, both socially and environmentally. It encompasses nine counties (San Francisco, Alameda, Contra Costa, Marin, Napa, San Mateo, Santa Clara, Solano, and Sonoma - see Figure 1) and includes a diverse mix of urban, suburban, and rural environments. The region is centered around the San Francisco Bay, an estuarine system that significantly influences the area's climate, ecology, and development patterns. The Bay Area's delimitation as a distinct geographic and socio-economic unit is rooted in its interconnected infrastructure, shared environmental systems, and integrated economy. Its boundaries are not merely administrative but reflect a cohesive region tied together by daily commuting flows, regional planning agencies such as the Metropolitan Transportation Commission (MTC) and the Association of Bay Area Governments (ABAG), and shared vulnerabilities to natural hazards.

Socially, the Bay Area is home to over 7.7 million residents and stands as one of the most densely populated and economically significant regions in the United States (Bay Area Census 2020). It is characterized by a strong concentration of technological industries, particularly in Silicon Valley, which contributes to both regional affluence and socio-spatial inequality. The region's infrastructure, comprising dense transportation networks, energy systems, and extensive urban settlements, makes it particularly sensitive to compounding hazards. The proximity between residential areas and critical lifelines, such as gas transmission networks operated by Pacific Gas and Electric (PG&E), increases the potential for multi-hazard interactions, especially in the aftermath of earthquakes.

Natural characteristics further heighten the Bay Area's complexity and vulnerability. The region is defined by its position along the Pacific coast and its proximity to major active fault systems, including the San Andreas and Hayward faults. These faults have historically generated significant seismic events, such as the 1906 San Francisco earthquake and the 1989 Loma Prieta earthquake, both of which caused widespread infrastructure damage and secondary fires (Scawthorn et al. 2006). The presence of these faults, combined with a dense gas pipeline network, creates conditions under which earthquakes can easily trigger compounding hazards like gas leaks and fires, making the area an ideal case study for research on earthquake impacts on gas infrastructure and subsequent fire activity.

Environmental diversity is another defining feature of the Bay Area. The region's Mediterranean climate supports a mix of vegetation types, ranging from coastal scrublands and grasslands to dense chaparral and oak woodlands. These ecosystems are highly flammable during the dry summer and fall months, when prolonged droughts, low humidity, and high winds amplify wildfire risks (Keeley and Syphard 2018). The region also contains extensive wildland-urban interface (WUI) zones. These areas, found prominently in the East Bay Hills, Marin County, and parts of Santa Clara and Sonoma counties, represent some of the highest fire risk zones in California, as the combination of fuel continuity, steep topography, and human presence facilitates ignition and rapid fire spread (Radeloff et al. 2018).

The proximity of the ocean further influences the Bay Area's microclimates and vegetation distribution. Coastal fog and marine breezes help moderate temperatures and occasionally provide moisture that can delay the onset of fire season in some

locations. However, these same meteorological conditions can also transport smoke and pollutants from inland fires toward coastal communities, amplifying air quality issues and regional health impacts. The ocean's moderating effect also contrasts with the dry inland valleys, creating sharp climatic gradients that influence vegetation flammability and hydrological patterns across short distances (Martin 2008; Weiss et al. 2013; Chow et al. 2022).

The Bay Area's significance extends beyond its own boundaries, as its infrastructure, economy, and environmental systems are deeply interconnected with those of surrounding regions. Energy transmission lines, transportation corridors, and supply chains link the Bay Area with Central and Northern California, meaning that any disruption, such as a large earthquake or widespread fire, could have cascading consequences at the state and national level. The region's ports, financial institutions, and technological industries are vital to California's and the U.S. economy, reinforcing the importance of safeguarding its critical infrastructure from multi-hazard events (Tam and Johnson 2020; Cal OES 2023).

For these reasons, the Bay Area is a highly significant study area for investigating the relationship between earthquake-induced damage to gas networks and subsequent fire activity. Its unique combination of dense population, active fault lines, aging energy infrastructure, and extensive WUI zones provides a natural laboratory for understanding compounding and cascading hazards. Research in this region not only contributes to local disaster resilience but also offers insights applicable to other seismically active urban regions worldwide. The Bay Area's social, infrastructural, and environmental vulnerabilities, when analyzed together, highlight the urgent need for integrated risk assessment approaches capable of addressing the intersection between seismic and fire hazards in an era of increasing urbanization and climate stress.

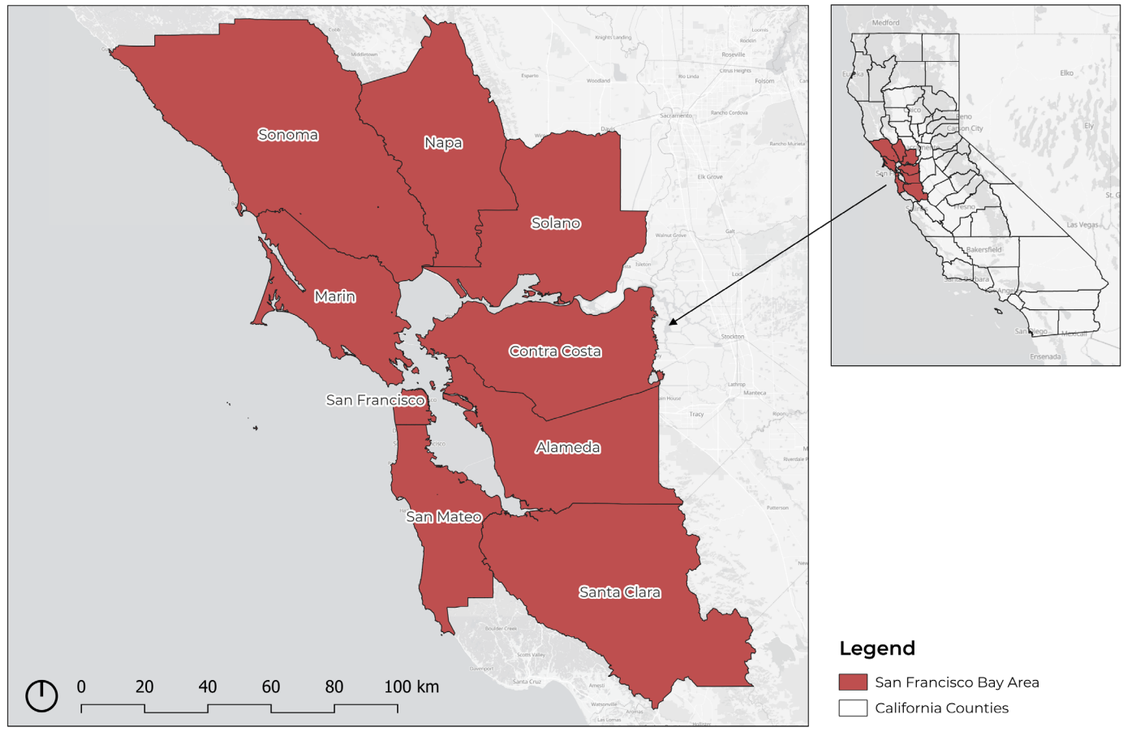

Figure 1 *State of California and Bay Area counties.*

7. METHODOLOGY

The methodology developed for this study combines geospatial analysis, multi-criteria decision-making, and seismic risk modeling in order to evaluate compound hazards in the San Francisco Bay Area. The first component of the analysis involved the use of Geographic Information System (GIS) data processed in QGIS to create a detailed fire risk index map. This map was developed through spatial analysis techniques and the application of Multi-Criteria Decision Analysis (MCDA) using the Analytic Hierarchy Process (AHP), which allowed the weighting and integration of several fire-related parameters selected by the author. The second component focused on seismic activity modeling performed in OpenSRA, applying the Uniform California Earthquake Rupture Forecast, Version 3 (UCERF3) model, to assess potential ground failure and its effects on gas transmission infrastructure. Finally, the results from both analyses were combined to examine how earthquake-induced pipeline damage may interact with fire susceptible zones, providing an integrated perspective on the interaction and progression of compound hazards across the region.

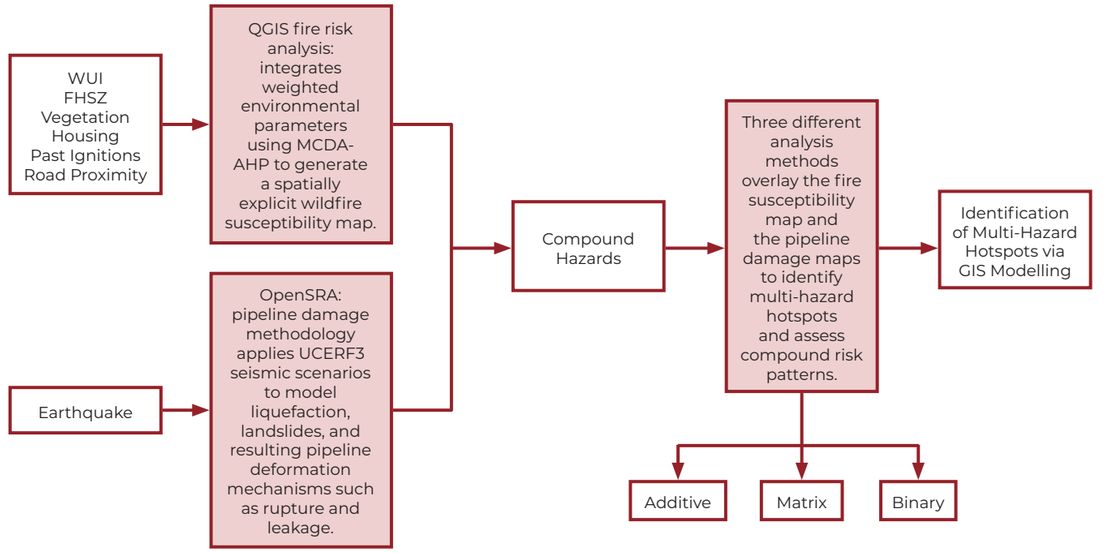

Figure 2 *Methodology framework.*

7.1 GIS-MCDA-AHP

Geographic Information Systems (GIS) have become an indispensable tool in natural hazard research, providing the capacity to integrate, analyze, and visualize complex datasets within a spatial framework. Their value lies in the ability to unify diverse information into coherent models that capture the dynamics of risk across both natural and built environments. Unlike purely statistical or engineering approaches, GIS situates hazards within their geographic and socio-ecological contexts, enabling a more complete understanding of where multiple threats converge. This integrative capability is particularly relevant in multi-hazard assessments, where compounding risks frequently emerge at the intersection of seismic activity, wildfire exposure, and infrastructure vulnerability (Burrough and McDonnell, 1998; Goodchild, 2006).

Within this framework, Multi-Criteria Decision Analysis (MCDA) represents a prominent application of GIS, allowing multiple spatial criteria to be combined according to their relative importance. The method enables the construction of composite indices that represent spatial variations in hazard susceptibility and has been widely adopted for wildfire risk mapping. Malczewski (1999) established the theoretical basis for integrating MCDA within GIS, emphasizing its ability to incorporate both expert judgment and empirical evidence. Among MCDA methods, the Analytic Hierarchy Process (AHP) has become one of the most widely used due to its structured pairwise comparison approach, which provides a transparent and consistent mechanism for assigning weights to different factors (Saaty 1987; 1990). Studies have shown that AHP effectively balances qualitative and quantitative criteria, reduces subjectivity through consistency checks, and allows replication across diverse spatial. For these reasons, the AHP method was selected for this study as the most appropriate approach to systematically weight and integrate the parameters influencing wildfire susceptibility in the Bay Area.

The effectiveness of GIS-based MCDA-AHP has been demonstrated in numerous wildfire assessments. In California, Chuvieco et al. (2014) and Keeley and Syphard (2018) applied weighted overlay techniques to map wildfire risk and prioritize management zones, while other studies used similar approaches to support post-fire restoration planning. Beyond California, studies in Greece, Turkey, and Iran have applied GIS-AHP to model wildfire hazard under future climate scenarios, integrating biophysical and social factors to identify areas of highest vulnerability. At a finer scale, Li et al.(2021) enhanced Wildland-Urban Interface (WUI) mapping in California by combining building footprint and vegetation data, illustrating the adaptability of AHP-based GIS frameworks to detailed landscape analysis. These studies collectively support the reliability and transferability of GIS-AHP methods for regional hazard assessment.

Although GIS-based wildfire assessments are widely developed, relatively few studies have explicitly addressed the interaction between fire risks and pipeline vulnerability. This represents a significant gap in hazard research, as gas transmission infrastructure can play a critical role in amplifying the impacts of natural disasters. Gas leaks and explosions are known to intensify fire behavior and complicate suppression efforts, particularly when they occur alongside seismic events. Post-earthquake fires are a well-documented secondary hazard, often resulting from ruptured pipelines or damaged gas distribution systems. Historical examples such as the 1994 Northridge earthquake, which triggered multiple fires following pipeline ruptures, illustrate the potential for infrastructure damage to escalate into large-scale fire incidents (Yegian et al. 1995; Seismic Safety Commission 1995). Despite the precedents, the spatial relationship between seismic-induced pipeline damage and wildfire exposure has rarely been examined through an integrated modeling framework. Addressing this gap offers an opportunity to advance vulnerability assessment by revealing new pathways of cascading risk in seismically active and fire-prone regions.

California provides an ideal setting for exploring this interconnection. The state combines some of the most severe wildfire recurrence patterns in the world with an extensive and aging gas transmission network that traverses active fault systems and densely populated Wildland-Urban Interface (WUI) zones (Radeloff et al. 2018). Its complex topography, Mediterranean climate, and history of both large wildfires and damaging earthquakes make it an unparalleled case study for evaluating the overlap of seismic and fire hazards. Furthermore, California's regulatory and data-rich environment provides the necessary foundation for implementing a comprehensive, GIS-based multi-hazard analysis.

Parameters	Description	Publication	Website
Wildland-Urban Interface (WUI)	*GIS data integrating U.S. Census information and USGS National Land Cover Data (NLCD) to spatially represent the Wildland-Urban Interface (WUI) as defined by the Federal Register (66:751, 2001).*	*Radeloff, Volker C., David P. Helmers, H. Anu Kramer, et al. 2018. "Rapid Growth of the US Wildland-Urban Interface Raises Wildfire Risk." Proceedings of the National Academy of Sciences 115 (13): 3314–19. https://doi.org/10.1073/pnas.1718850115.*	*https://silvis.forest.wisc.edu/data/wui-change/*
Vegetation Coverage			
Housing Density			
Historical Ignition Points	*GIS data containing a spatial database of wildfire ignition points in the United States from 1992–2020, compiled from federal, state, and local fire agency reports.*	*Short, K. C. 2014. "A Spatial Database of Wildfires in the United States, 1992-2011." Earth System Science Data 6 (1): 1–27. https://doi.org/10.5194/essd-6-1-2014.*	*https://www.fs.usda.gov/rds/archive/catalog/RDS-2013-0009.6*
Road Network	*GIS data depicting road networks in the San Francisco Bay Region, compiled from county-level shapefiles by the Metropolitan Transportation Commission.*	-	*https://opendata.mtc.ca.gov/datasets/MTC::san-francisco-bay-region-roadways/about*
Fire Hazard Severity Zones (FHSZ)	*GIS data from CAL FIRE delineating Fire Hazard Severity Zones (FHSZ), based on datasets from CAL FIRE FRAP, CANSAC, the U.S. Census Bureau, the U.S. Geological Survey, and other public GIS databases.*	-	*https://osfm.fire.ca.gov/what-we-do/community-wildfire-preparedness-and-mitigation/fire-hazard-severity-zones*

***Table 1** Selected parameters and their sources.*

Building on the strengths of earlier GIS-based wildfire assessments and addressing the clear research gap in multi-hazard modeling, this study develops a Fire Risk Index for the San Francisco Bay Area by integrating six spatial parameters identified as key drivers of wildfire susceptibility: Wildland-Urban Interface (WUI) zones, Fire Hazard Severity Zones, vegetation coverage, housing density, historical ignition point density, and road proximity to ignition sources. These layers were processed and standardized in QGIS to ensure comparability and were later combined into a single composite map that represents the spatial distribution of fire risk across the region. This index then serves as the foundation for linking wildfire susceptibility with seismic pipeline damage, enabling a detailed assessment of cascading hazard potential.

To establish how much each parameter contributes to overall fire risk, the study applied the Analytic Hierarchy Process (AHP) developed by Saaty (1987). AHP was chosen because it provides a structured way to transform literature-based evidence and expert judgment into numerical weights through pairwise comparisons. This approach is widely used in wildfire susceptibility studies due to its transparent and repeatable method for ranking multiple interacting factors (Adaktylou et al. 2020; Greene et al. 2011; Gigović et al. 2018).

7.1.1 Definition of the Parameters

The first step of the MCDA-AHP analysis was to define the goal of the model and identify the criteria that influence wildfire susceptibility in the Bay Area. The objective was to create a single wildfire risk map that represents the combined effect of several environmental and human-related factors. Six parameters were selected based on their relevance in wildfire research: Wildland-Urban Interface (WUI) zones, Fire Hazard Severity Zones (FHSZ), vegetation coverage, housing density, historical ignition density, and road proximity to ignition sources.

The datasets used for each parameter were collected from established and reliable sources, which are summarized in Table 1. After gathering the data, each parameter was processed in QGIS to ensure consistency across the entire study area. Because the datasets came in different formats and units, they were first converted into a raster format, allowing the landscape to be represented as a uniform grid of cells that can be compared directly across layers. Each raster was then normalized to a 1-5 scale, with the risks being classified as:

1 = Very Low
2 = Low
3 = Moderate
4 = High
5 = Very High

This normalization step ensures that all parameters contribute proportionally to the final model and prevents differences in measurement units from influencing the results. Once standardized, each parameter produced its own risk map, and these individual layers were later overlapped and combined using the AHP-derived weights to generate the final integrated wildfire risk map.

7.1.1.1 Wildland-Urban Interface (WUI)

The wildland-urban interface (WUI) constitutes a zone of particular concern for wildfire risk, because it combines human ignition sources, built infrastructure, and combustible fuels. Research demonstrates that both interface zones (where structures meet wildland) and intermix zones (where structures and fuels intermingle) carry elevated risk compared to developed areas isolated from fuel (Taccaliti et al. 2023; Mell et al. 2010).

For that reason, WUI was selected as a parameter. The WUI map developed by Radeloff et al. (2018) was selected for this study, imported into QGIS and reclassified into three categories: non-WUI (areas beyond or separated from wildland fuel), interface WUI and intermix WUI. Recognizing that intermix zones typically present the greatest vulnerability (fires can ignite in vegetation and transition into structures, while structural fuels can also contribute to spread), values of 1, 3 and 5 were assigned respectively (see Figure 3), within the established 1-5 scoring framework, to map relative risk contributions. The choice of 1-3-5 (rather than a linear 1-2-3) reflects the need to preserve meaningful separation between low, moderate and high risk, and to maintain compatibility with other criteria in the composite overlay risk calculation.

In doing so, the WUI parameter is ensured to contribute appropriately to the overall fire-risk map, directing attention and resources toward those zones (especially intermix WUI) which, according to empirical studies, are at greatest risk of ignition, fire spread and built-environment damage (Taccaliti et al. 2023).

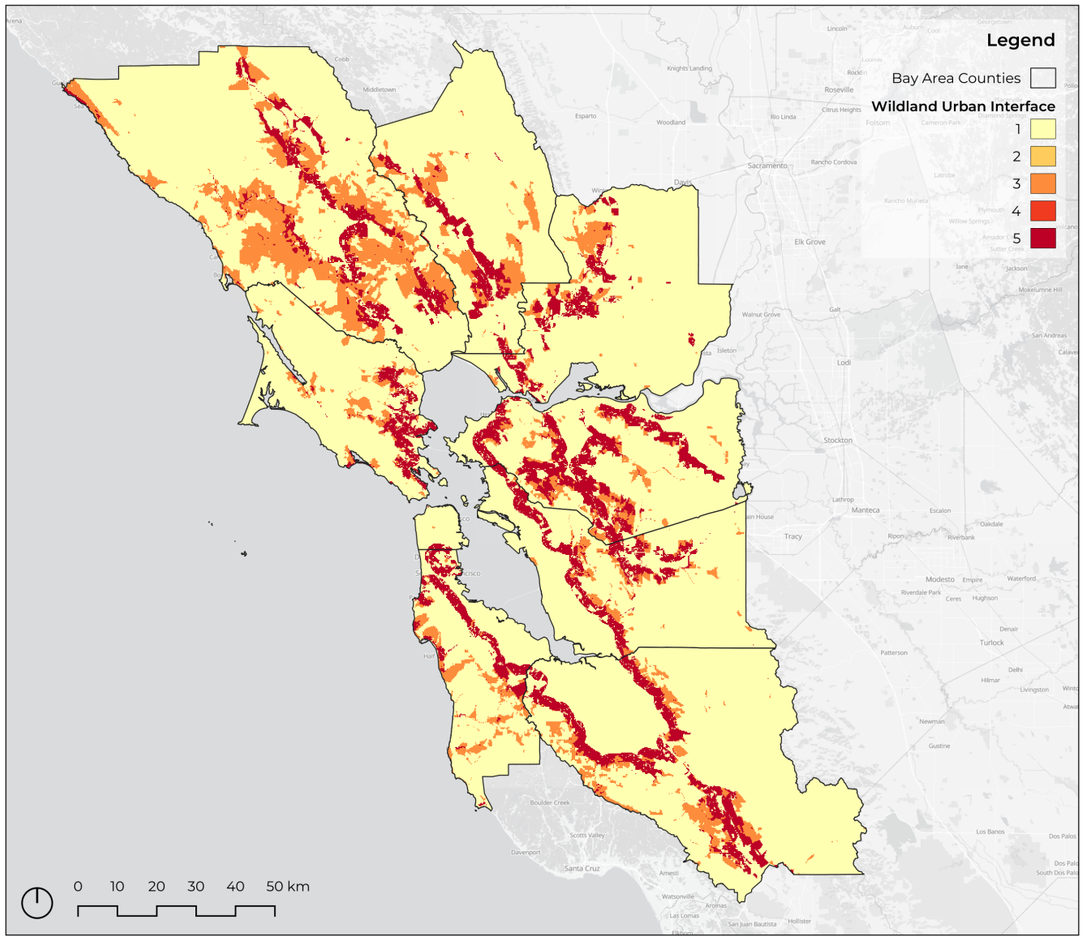

Figure 3 *Intermix and interface WUI zones in the Bay Area.*

7.1.1.2 Fire Hazard Severity Zones (FHSZ)

Fire hazard severity zones were integrated into the fire risk model using official data from the California Department of Forestry and Fire Protection (CAL FIRE), which classifies all areas of the state into three risk categories: moderate, high, and very high. Using this dataset ensures consistency with state-level fire management and hazard assessment frameworks while providing a scientifically validated basis for further spatial analysis. The map was clipped to fit the Bay Area, focusing the assessment on the study region's local geographic and environmental conditions.

To maintain consistency across all fire risk parameters, the CAL FIRE map was reclassified. The original three categories were aligned with values 3, 4, and 5. A buffer zone was created around the CAL FIRE severity zones to represent transitional areas with lower but still relevant exposure to wildfire hazard. This buffer was assigned a value of 2, acknowledging that fire risk does not decrease abruptly outside mapped hazard boundaries, as ignition and spread often extend beyond these zones (Chuvieco et al. 2014).

All remaining areas in the Bay Area not covered by either the official severity zones or the buffer were assigned the value 1. This ensures full spatial coverage while maintaining proportional differentiation of hazard across the study area. The resulting five-class map (see Figure 4) allows for finer granularity and comparability across parameters, which is consistent with established methodologies for multi-criteria fire risk mapping (Fiorucci et al. 2024).

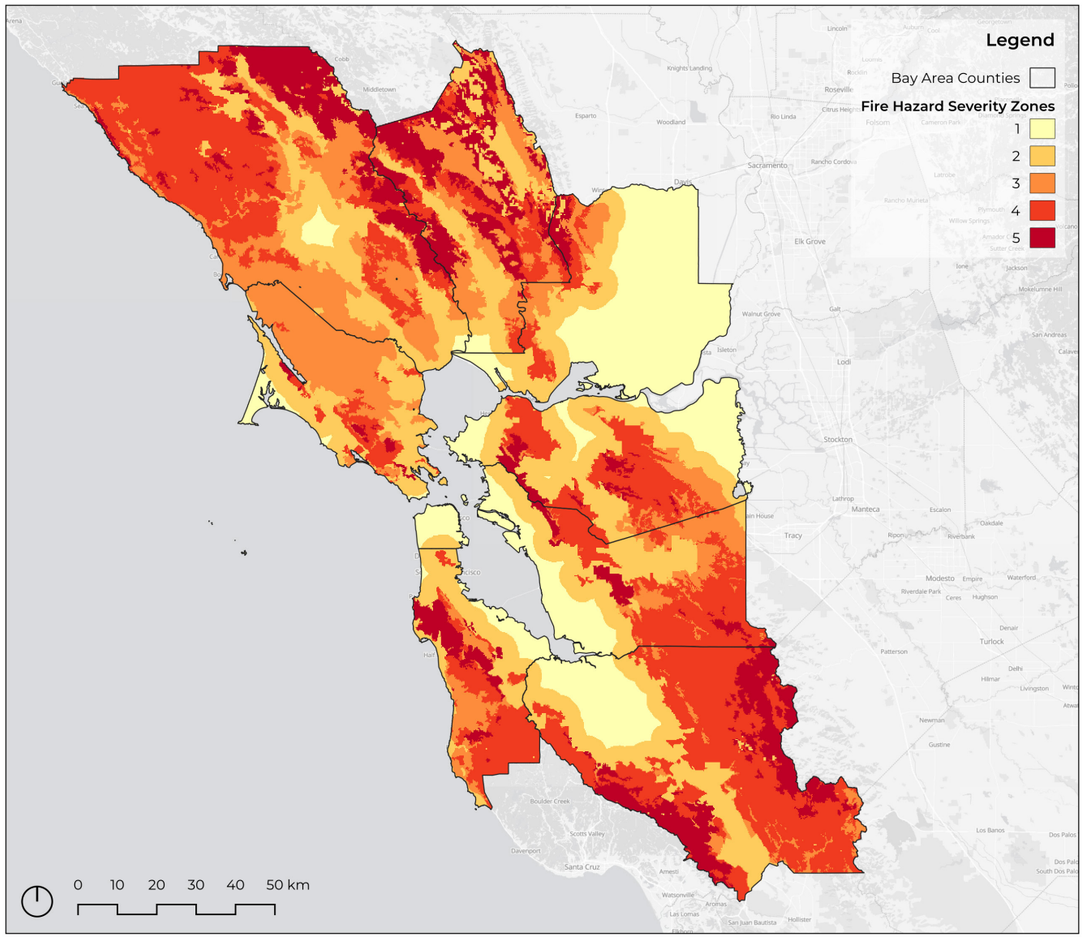

Figure 4 *Fire Hazard Severity Zones in the Bay Area.*

7.1.1.3 Vegetation Coverage

Vegetation was selected as a core parameter due to its fundamental role in both the ignition and propagation of fires. Vegetation represents the primary source of combustible material within a landscape, directly influencing the likelihood, intensity, and spread of wildfires. Areas with higher proportions of vegetation, particularly those containing dry or continuous fuel loads, are more prone to ignition and sustain faster rates of fire spread once ignited.

The role of vegetation as a determinant of fire behavior has been extensively documented in wildfire ecology and risk modelling literature. Loudermilk et al. (2022) describe vegetation as not only the fuel for fires but also a structural element that shapes how fires behave across the landscape, influencing factors such as flame height, heat release, and rate of spread. Similarly, Thonicke et al. (2010) demonstrate through global vegetation-fire modelling that vegetation characteristics, including composition, structure, and continuity, are among the primary controls of fire dynamics and burned area extent. The composition and dryness of vegetation therefore have direct implications for the probability of ignition and the potential severity of a fire event.

Fires originating in vegetated areas behave differently from those in urban or built environments. In vegetated regions, the continuity of fuel allows fires to spread rapidly, driven by abundant biomass and the presence of ladder fuels that facilitate vertical fire movement. The presence of shrubs, grasslands, and forested areas contributes to higher heat release rates and broader spatial propagation compared to ignition in built-up areas, where fire spread is generally constrained by breaks in fuel continuity. According to Chuvieco et al. (2014), the spatial configuration of vegetation cover is one of the key determinants of wildfire propagation, as continuous vegetation provides the necessary connectivity for fire expansion across the landscape.

In this study, vegetation was incorporated as a quantitative variable expressed as the percentage of vegetation cover. Data were extracted from available census and land cover datasets, comprising categories such as forests, grasslands, and wetlands. This approach allowed for the spatial representation of fuel availability, providing a basis for comparison among regions with varying vegetation densities. Areas with higher vegetation percentages were assigned higher risk values, on a scale of 1 to 5, as they represent environments with greater combustible potential and, consequently, a higher probability of fire ignition and spread. The raw data used for classification of the vegetation patterns can be seen in Table 2.

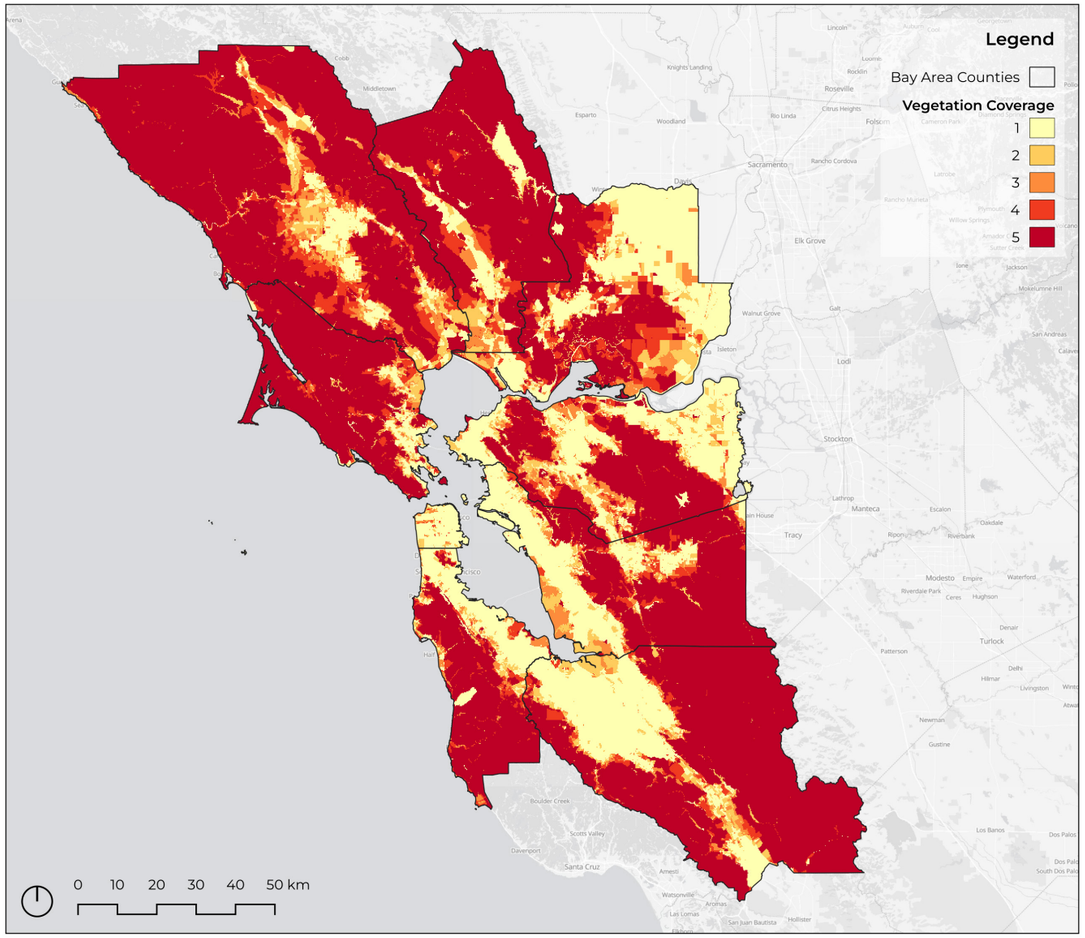

Figure 5 *Vegetation coverage in the Bay Area.*

Hazard Class	Wildland vegetation in %
1	0 - 9.5
2	9.5 - 31.2
3	31.2 - 56.7
4	56.7 - 82.6
5	82.6 - 100

Table 2 *Wildland vegetation cover and the hazard classes assigned to each range. Data refers to 2019 surveys.*

7.1.1.4 Housing Density

Housing density was included because it influences both the likelihood of ignition and the vulnerability of people and structures during wildfire events. Areas with many homes have more human activity and more potential ignition sources, and they also contain larger populations and a greater number of buildings that may be threatened. High housing density therefore reflects elevated exposure for residents as well as a higher potential for loss of homes.

The relevance of this parameter is well established in wildfire research, especially in the Wildland Urban Interface (WUI), where residential areas directly border flammable vegetation. Homes in these zones are highly exposed to embers, radiant heat, and advancing flames (Radeloff et al. 2018; Cohen 2000). In California, continued growth within the WUI has substantially increased structure loss and risks to human life during wildfire events (Syphard et al. 2019).

Typical construction practices also add to the importance of this factor. Approximately 90 to 94% of homes in the United States are built with light wood framing and drywall, which ignite easily and allow fire to spread once exposed to heat or embers. Wind-driven embers can ignite structures far ahead of the flame front, and burning homes can ignite others nearby, especially in dense developments (Alexandre et al. 2016).

This map, like the others, was assigned values of risk between 1 and 5 in order to maintain continuity between datasets (see Figure 6). It is possible to see a clear pattern of urbanization in the areas in closest proximity to the San Francisco Bay, with housing density decreasing in areas where vegetation is most prevalent. Table 3 shows the original dataset of housing density (units/km^2) in the Bay Area, 2020, before it was converted into hazard classes. The table also shows what hazard value each range was assigned to.

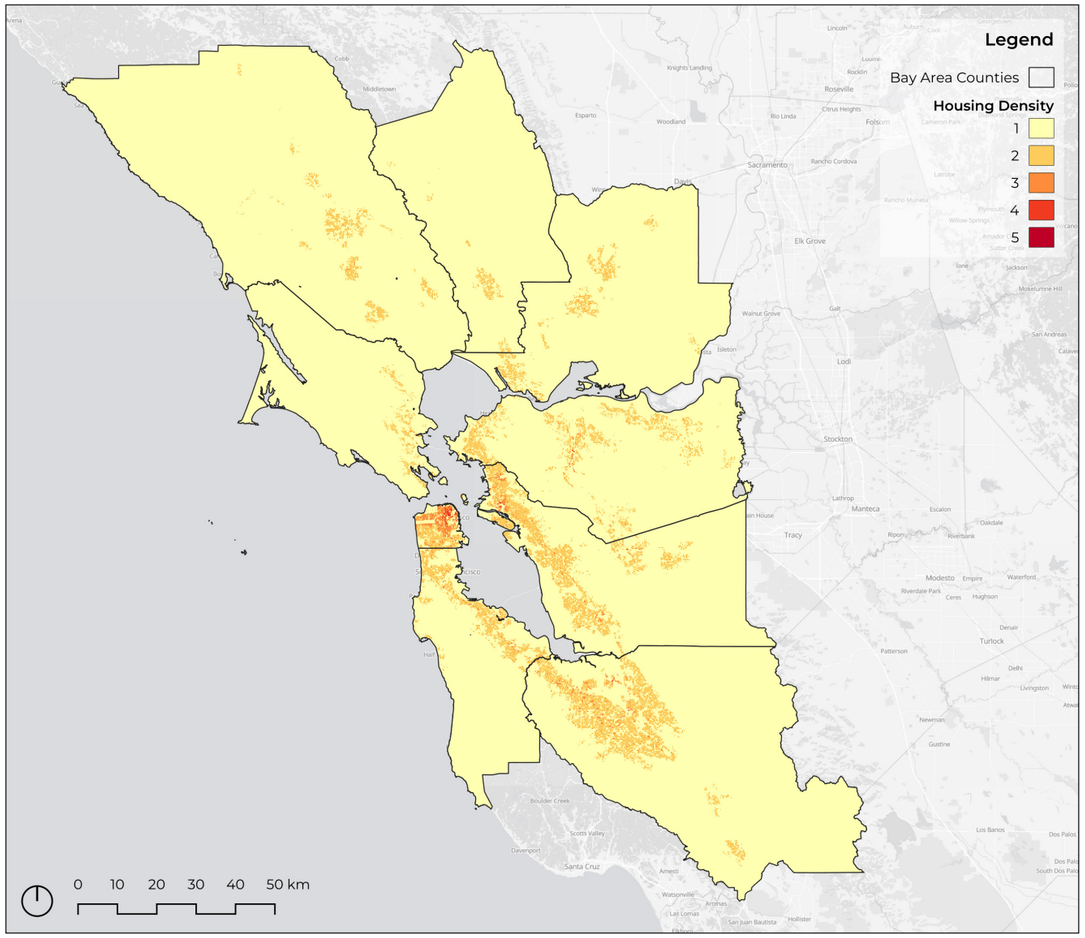

***Figure 6** Housing density in the Bay Area. The urban corridors are very obviously located around the Bay, be-*

Hazard Class	Housing density (units/km^2)
1	0 - 868
2	868 - 4014
3	4014 - 13217
4	13217 - 41291
5	41291 - 99649

***Table 3** Housing density in the Bay Area and the hazard classes assigned to each range. Data refers to 2020 surveys.*

7.1.1.5 Ignition Density

Another fundamental parameter was the spatial distribution of historical ignition points. These represent the geographical locations where fires have been recorded in the past and therefore constitute a direct indicator of areas with demonstrated susceptibility to fire ignition (Costafreda-Aumedes et al. 2016). The ignition point dataset was imported into QGIS for spatial analysis and visualization. The first analytical step consisted of generating a kernel density heatmap, which converts discrete ignition points into a continuous surface representing ignition density. This process allows the identification of hotspots of fire activity, where ignition events are spatially clustered and thus indicate areas of heightened ignition likelihood. The heatmap was subsequently rasterized to ensure compatibility with other layers. However, because some areas contained no ignition points, portions of the Bay Area fell outside the resulting raster coverage. To maintain consistency across layers, all of which must share the same spatial extent to allow accurate calculation of summed raster values, these gaps were filled with cells assigned a value of 0. This preserves the ability to overlay the heatmap with the other datasets while ensuring that the added cells do not influence the final analysis, as they represent a separate, non-impactful class.

Using historical ignition data as a primary fire-risk criterion is well established in the literature. Historical ignitions have been demonstrated to be strong predictors of future fire occurrence, since they capture the combined effect of environmental, climatic, and human factors influencing fire likelihood over time (Chuvieco et al. 2014). Furthermore, kernel density estimation (KDE) has been widely adopted in wildfire risk mapping as an effective means of transforming point occurrences into continuous probability surfaces that facilitate spatial modeling and comparison (Guo et al. 2024; Oliveira et al. 2016). By rasterizing this layer, the analysis ensured methodological consistency among all datasets and allowed for weighted overlay analysis in subsequent steps.

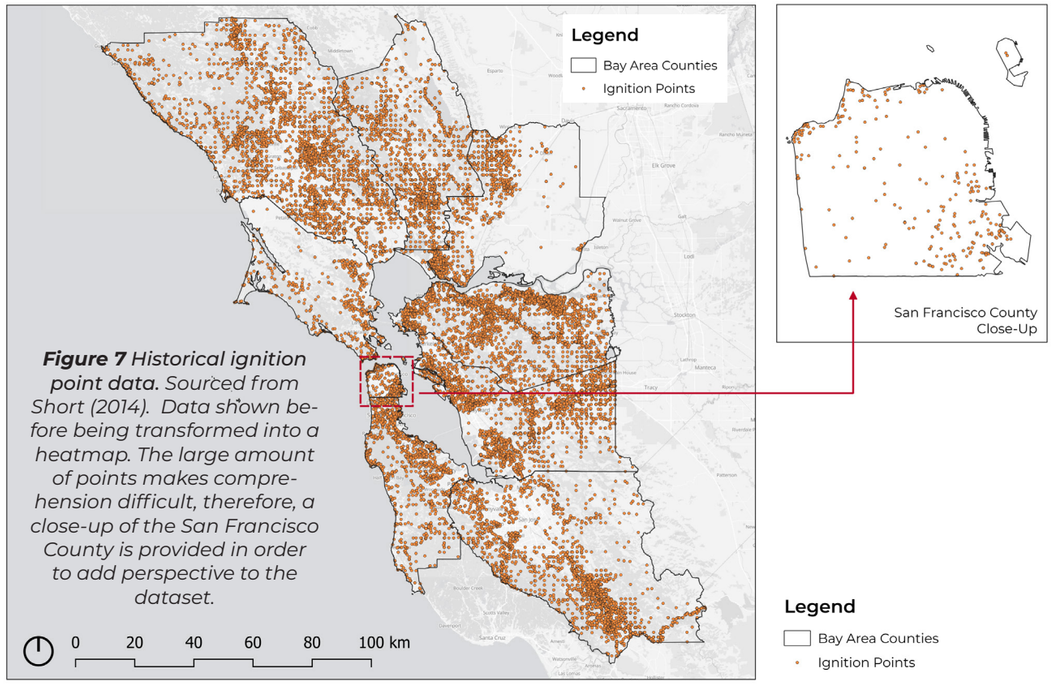

***Figure 7** Historical ignition point data. Sourced from Short (2014). Data shown before being transformed into a heatmap. The large amount of points makes comprehension difficult, therefore, a close-up of the San Francisco County is provided in order to add perspective to the dataset.*

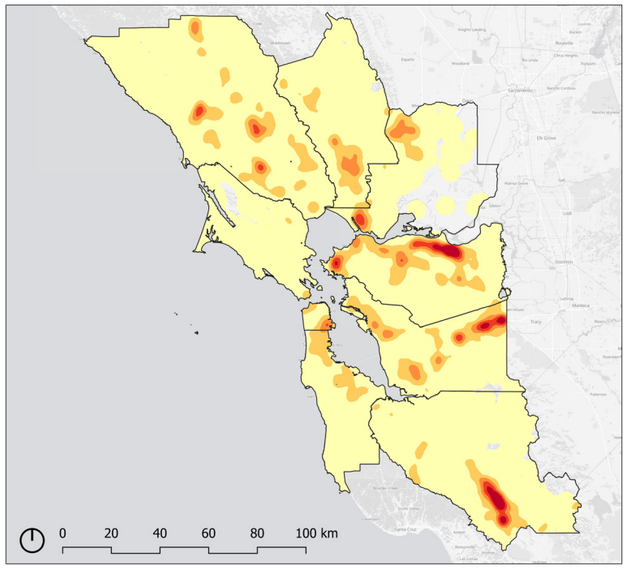

***Figure 8** Initial ignition density pattern. It is possible to see how the county of Solano has large sparse areas of no data. That region was assigned a value of 0 so the map could have the same resolution and spatial boundaries as the others, ensuring a proper overlay later on in the analysis.*

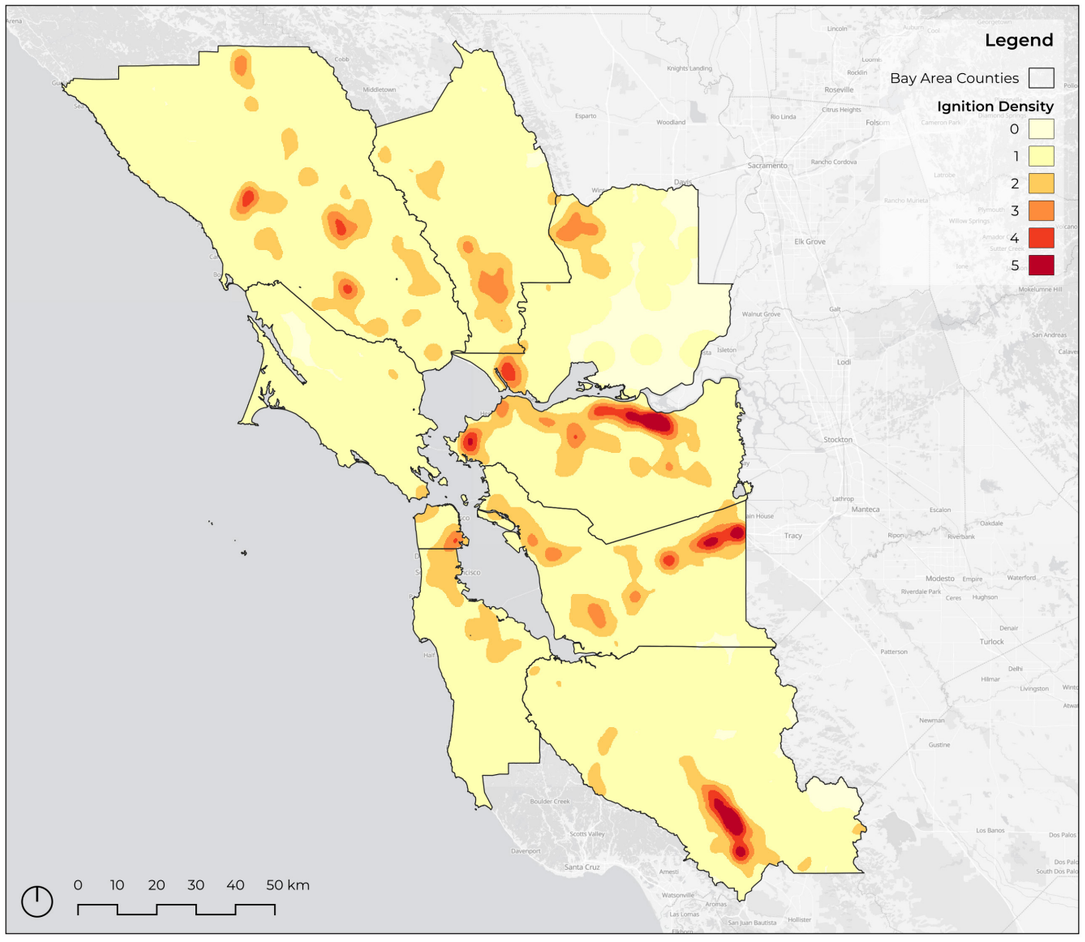

***Figure 9** Ignition density in the Bay Area.*

7.1.1.6 Road Proximity to Ignition Sources

The road network was also chosen as a key parameter due to its strong association with human-caused ignitions and its critical role in both the onset and management of wildfires. Roads represent one of the most influential forms of human infrastructure in relation to ignition probability, particularly where they intersect vegetated or non-urbanized areas. Numerous studies have demonstrated that wildfires are disproportionately ignited near roads, primarily as a result of human activities such as smoking, mechanical sparks, and vehicle malfunctions (Ricotta et al. 2018; Narayanaraj and Wimberly 2012). These anthropogenic causes are especially frequent along highways and rural routes that traverse or border natural landscapes, where fuel continuity allows small ignition sources to develop into larger fires.

Beyond direct human influence, roads modify their surrounding environment by increasing sunlight exposure and wind flow along roadside edges, which can reduce fuel moisture and promote ignition (Ricotta et al. 2018). Moreover, the close spatial relationship between major roads and other critical infrastructure, such as gas transmission lines, can amplify the consequences of potential ignitions through cascading failures or explosions.

In this study, a buffer of 200 meters was applied to each road segment to capture the adjacent vegetated zones likely affected by road-related ignition risks. These buffered zones were intersected with historical ignition point data from the Bay Area to quantify the relationship between roads and fire occurrences. Roads that overlapped with one or more ignition points were classified on a five-level risk scale, where a higher number of intersections indicated greater risk. This approach follows evidence from fire science literature showing that ignition likelihood decreases exponentially with distance from roads. The cells that fell outside the scope of the roads were assigned a value of 0 so as to not interfere with the final product of the overlapped layers.

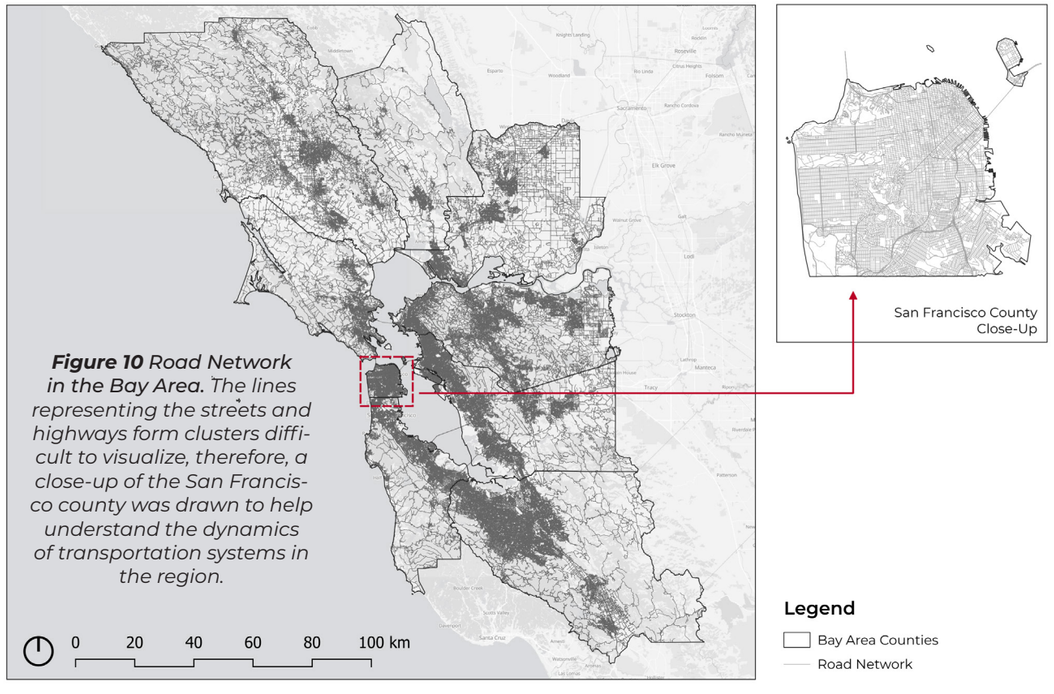

***Figure 10** Road Network in the Bay Area. The lines representing the streets and highways form clusters difficult to visualize, therefore, a close-up of the San Francisco county was drawn to help understand the dynamics of transportation systems in the region.*

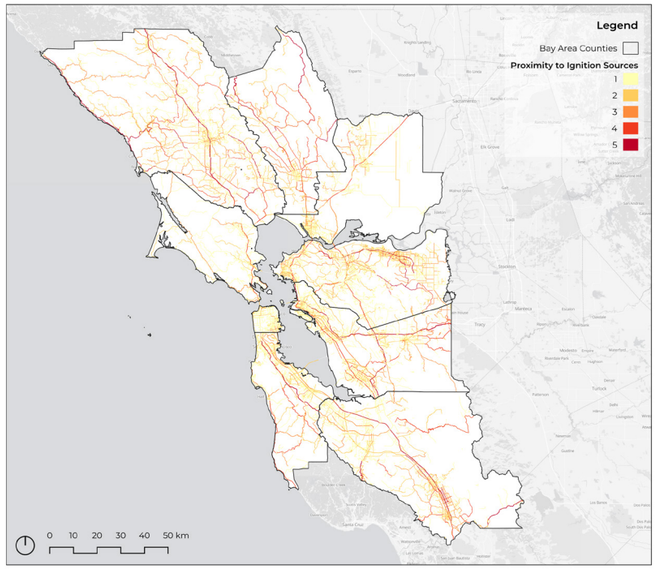

***Figure 11** Road network intersected with ignition sources. Streets were buffered and overlapped with historical ignition points. This created a map where the roads were classified by how many times each segment overlapped with different ignition points. Because this data left a big gap in area not covered by the network (seen as white in the map), it was necessary to manually add a value to all "no data" pixels within the boundary used for the analysis. The value assigned was 0, so as to not interfere with actual relevant spatial data during the multi-hazard analysis performed later in the study. Figure 12 shows all classes (1-5) alongside the 0 class.*

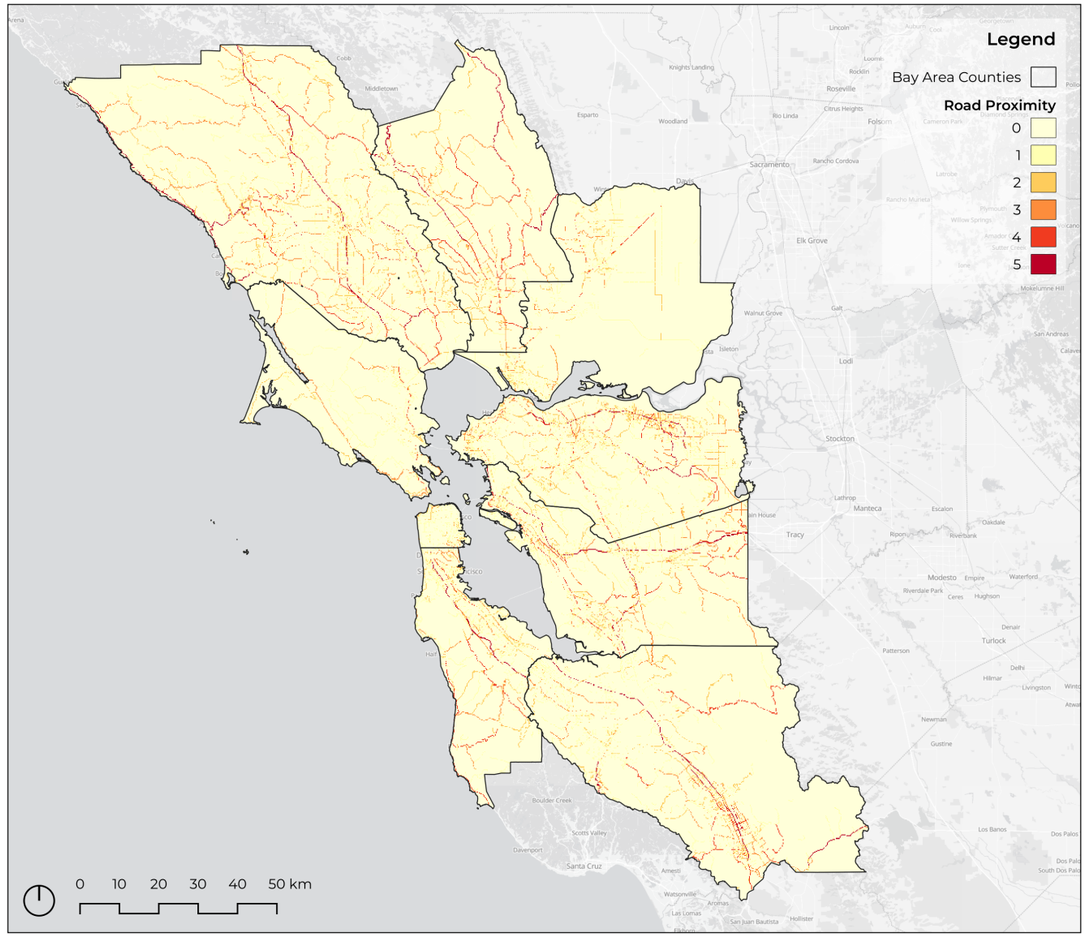

***Figure 12** Road Proximity to Ignition Sources in the Bay Area.*

7.1.2 Construction of the Pairwise Comparison Matrix

A pairwise comparison matrix $A = [a_{ij}]$ was constructed to assess the relative importance of each parameter with respect to the main goal (see Table 5). Each element a_{ij} represents the importance of factor *i* compared to factor *j*, with reciprocal relationships defined as $a_{ji} = 1/a_{ij}$. The scale proposed by Saaty (1990) was used to assign comparative values between 1 and 9, where 1 denotes equal importance and 9 denotes extreme importance of one parameter over another. Saaty's Fundamental Scale, where these values are explained, can be seen in Table 4.

Importance value	Definition	Explanation
1	Equal importance	Two activities contribute equally
3	Moderate importance	One activity is slightly favored over another
5	Strong importance	One activity is strongly favored over the other
7	Very strong importance	One activity is very strongly favored over the other
9	Extreme importance	The evidence favoring one activity over the other is of the highest possible order of affirmation
2, 4, 6, 8	Intermediate values	Numerical compromises between values as sometimes it is not possible to describe one activity over another in simple terms
1/x	Reciprocal value when the inverse relationship applies	A comparison where the smaller element is used as a reference unit to estimate how many times larger the other element is.

***Table 4** Saaty's Fundamental Scale. Adapted from Saaty (1990).*

In this study, the WUI zones and Fire Hazard Severity Zones were assigned the highest relative importance, as these represent areas of both high fuel availability and high human exposure. The next most important parameter was Vegetation Coverage, followed by Housing Density, Ignition Density, and Road Proximity to Ignition Sources, which exert secondary but still relevant influence on fire dynamics.

	WUI Zones	FHSZ	Vegetation Coverage	Housing Density	Ignition Density	Road Proximity
WUI Zones	1	1	2	4	7	9
FHSZ	1	1	2	4	7	9
Vegetation Coverage	0.5	0.5	1	3	6	7
Housing Density	0.25	0.25	0.333	1	5	6
Ignition Density	0.143	0.143	0.167	0.2	1	3
Road Proximity	0.111	0.111	0.143	0.167	0.333	1

***Table 5** The final 6×6 pairwise comparison matrix A. Constructed based on the author's judgments, forming the foundation for weight calculation. The reciprocal structure of the matrix ensured internal consistency and symmetry.*

7.1.3 Derivation of Weights

After constructing the pairwise comparison matrix, the next step involved the calculation of the relative weights of each criterion, which represent their proportional contribution to the overall wildfire risk. The process followed the normalization and averaging method proposed by Saaty (1987).

First, the sum of each column of the pairwise comparison matrix was calculated. Then,

every element in each column (a_{ij}) was divided by the total of its respective column. This operation normalizes the data and produces a new normalized matrix (*N*), shown in Table 6, ensuring that the sum of each column equals 1:

$$n_{ij} = \frac{a_{ij}}{\sum_{i=1}^{n} a_{ij}}$$

	WUI Zones	FHSZ	Vegetation Coverage	Housing Density	Ignition Density	Road Proximity
WUI Zones	0.333	0.333	0.354	0.323	0.266	0.257
FHSZ	0.333	0.333	0.354	0.323	0.266	0.257
Vegetation Coverage	0.166	0.166	0.178	0.243	0.228	0.2
Housing Density	0.083	0.083	0.059	0.081	0.189	0.171
Ignition Density	0.048	0.048	0.029	0.016	0.038	0.086
Road Proximity	0.037	0.037	0.026	0.014	0.013	0.029

***Table 6** Normalized matrix N.*

Once the matrix was normalized, each row of this new matrix was averaged to obtain the weight vector (*w*), which expresses the mean relative importance of each factor across all comparisons:

$$w_i = \frac{\sum_{j=1}^{n} n_{ij}}{n}$$

The resulting vector $w = [w_1, w_2, ..., w_n]$ contains the normalized weights of the criteria, where the sum of all weights equals 1.

Parameters	Weight
WUI Zones	0.311
FHSZ	0.311
Vegetation Coverage	0.197
Housing Density	0.111
Ignition Density	0.044
Road Proximity	0.026

***Table 7** Weight vector w. The two highest weights (WUI and FHSZ) reflect the predominance of these factors in determining fire susceptibility. Vegetation and housing density also play relevant roles, followed by historical ignition points and road proximity to past ignition sources.*

To verify the consistency of the matrix and to prepare for the subsequent step, the original comparison matrix (*A*) was then multiplied by the weight vector (*w*) to obtain the product vector *Aw*:

$$Aw = \begin{bmatrix} a_{11} & a_{12} & \cdots & a_{1n} \\ a_{21} & a_{22} & & a_{2n} \\ \vdots & & \ddots & \vdots \\ a_{n1} & a_{n2} & \cdots & a_{nn} \end{bmatrix} \cdot \begin{bmatrix} w_1 \\ w_2 \\ \vdots \\ w_n \end{bmatrix}$$

Each resulting element of *Aw* represents a weighted sum of the judgments for each parameter.

Subsequently, each element of the vector Aw was divided by the corresponding element of the weight vector (*w*) to obtain a set of λ_i values:

$$\lambda_i = \frac{(Aw)_i}{w_i}$$

This operation yields one eigenvalue (λ_i) per parameter. In this case, there are six resulting values corresponding to the six selected factors, as seen in Table 8.

λ1	6.437
λ2	6.437
λ3	6.532
λ4	6.378
λ5	6.045
λ6	6

***Table 8** All eigenvalues computed.*

The maximum eigenvalue (λ_{max}) was then estimated as the average of these six eigenvalues, calculated with the formula:

$$\lambda_{\max} = \frac{\sum_{i=1}^{n} \lambda_i}{n}$$

Given that *n* = 6, the computation produced a result of λ_{max} = 6.305.

7.1.4 Consistency Verification

To ensure that the pairwise comparisons were logically coherent, the Consistency Index (CI) and Consistency Ratio (CR) were calculated using the principal eigenvalue λ_{max}. The formulas proposed by Saaty (1987) are:

$$CI = \frac{\lambda_{\max} - n}{n - 1}$$

$$CR = \frac{CI}{RI}$$

where *n* is the number of parameters used and RI is the random index for a matrix of that order. In this case, *n* = 6. The RI values, as proposed by Saaty (1987), are as follows:

n	1	2	3	4	5	6	7	8	9	10
Random Index (RI)	0	0	0.58	0.9	1.12	1.24	1.32	1.41	1.45	1.49

***Table 9** Random Consistency Index adapted from Saaty (1987).*

The maximum eigenvalue obtained was λ_{max} = 6.305, leading to:

$$CI = \frac{6.305 - 6}{6 - 1} = 0.061$$

$$CR = \frac{0.061}{1.24} = 0.049$$

The resulting Consistency Ratio (CR = 0.049) is well below the accepted threshold of 0.10, indicating that the matrix judgments are highly consistent and no adjustments were necessary.

7.1.5 Weighted Linear Combination (WLC)

After the weights were validated, they were applied to the standardized raster layers of each criterion to compute the Fire Risk Index (FRI) through a weighted linear combination model. The general equation used was:

$$FRI = \sum_{i=1}^{n} w_i \cdot X_i$$

where w_i is the weight of each criterion and X_i is the normalized spatial layer. The equation computed into the QGIS Raster Calculator was as follows:

$$FRI = 0.311[WUI] + 0.311[FHSZ] + 0.197[VEGETATION\ COVERAGE] + 0.111[HOUSING\ DENSITY] + 0.044[IGNITION\ DENSITY] + 0.026[ROAD\ PROXIMITY]$$

Each raster was multiplied by its corresponding weight and then summed to generate the continuous fire risk surface. The results can be seen in Figure 13. The outcome was validated by overlapping the Fire Risk Index map with historical fire perimeters in the Bay Area, creating a new output where it is possible to see a strong correlation between the moderate to very high categories and the areas burned in previous fires. Figure 14 shows these results.

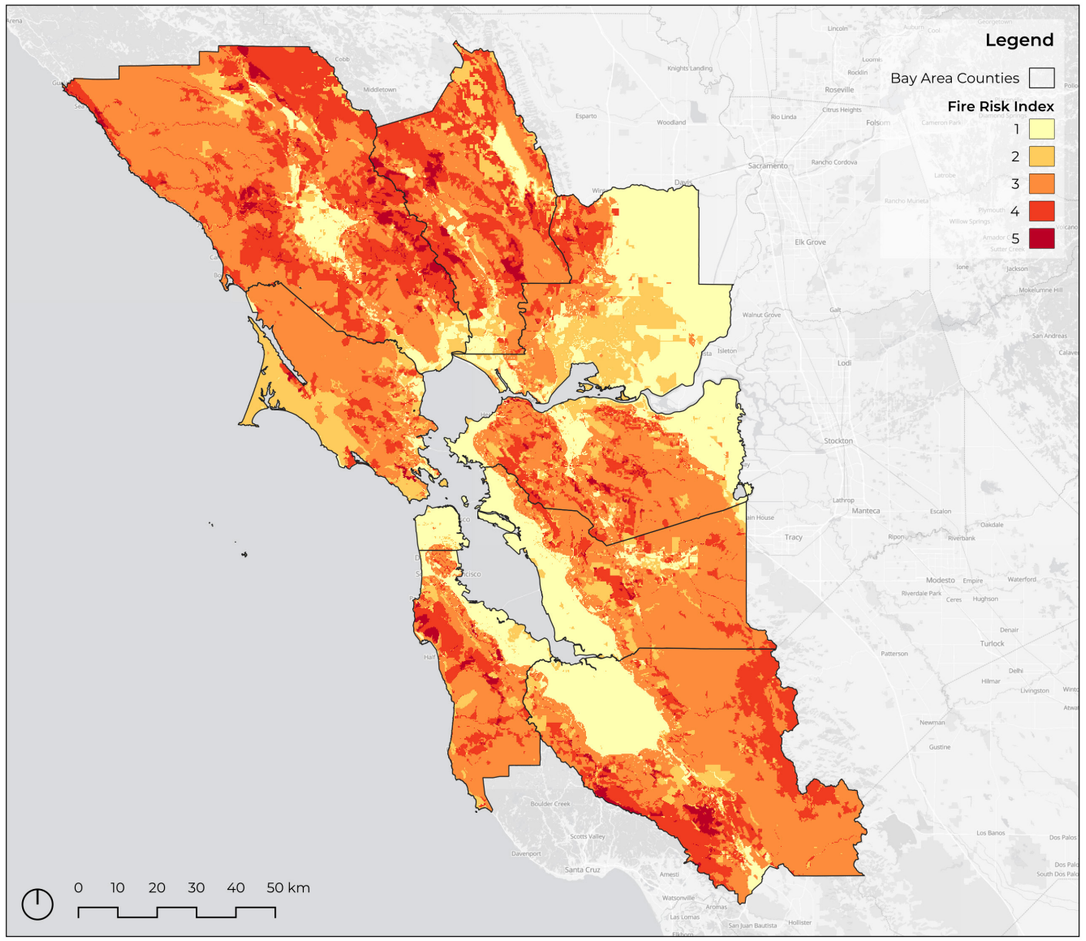

Figure 13 *Fire Risk Index in the Bay Area.*

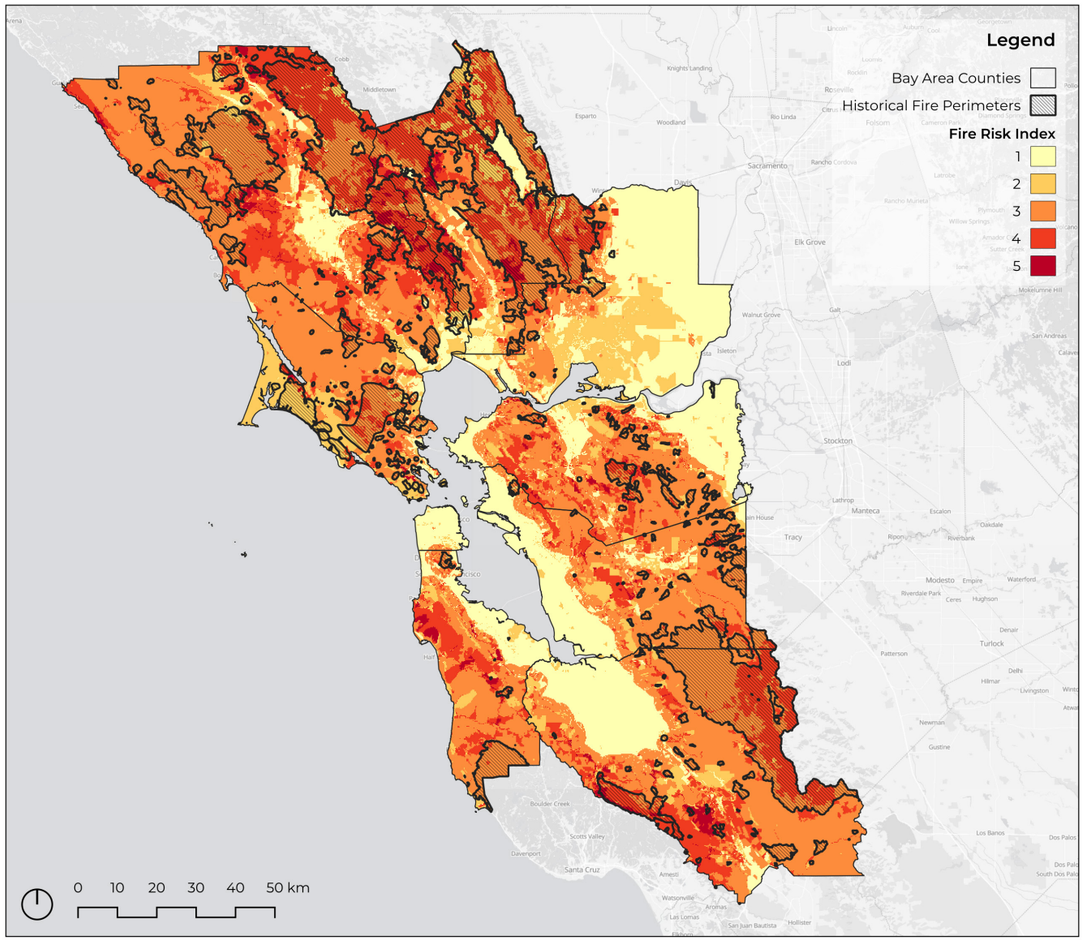

Figure 14 *Fire Risk Index validated by historical fire perimeters.*

7.2 OpenSRA

OpenSRA is an open-source software tool designed to provide a more quantitative and transparent understanding of how natural gas infrastructure behaves during earthquakes in California. Its development responds to a long-standing issue in utility risk assessment, where many existing approaches rely on subjective scoring systems that do not fully represent the uncertainties or the physical fragility of pipelines and storage systems (Largent et al. 2023). By integrating updated scientific models of earthquake occurrence, ground deformation, and infrastructure response within the Performance-Based Earthquake Engineering (PBEE) framework, developed by the Pacific Earthquake Engineering Research Center (PEER), OpenSRA offers a more rigorous and reproducible basis for evaluating seismic risk. The tool was developed through a collaboration among UC Berkeley, Lawrence Berkeley National Laboratory, UC San Diego, the University of Nevada Reno, the NHERI SimCenter, and Slate Geotechnical Consultants, with support from the California Energy Commission (Largent et al. 2024).

A fundamental part of OpenSRA is its representation of the earthquake environment in California. The tool relies on the Uniform California Earthquake Rupture Forecast Version 3 (UCERF3), the official long-term earthquake probability model for the state. UCERF3 synthesizes data from geology, GPS-based crustal deformation, paleoseismic trench records, and historical seismicity to estimate the likelihood of earthquakes across a wide range of magnitudes (Field et al. 2014; USGS Fact Sheet 2015-3009 2015). One notable advancement in UCERF3 is its allowance for multi-fault ruptures, which better reflect the cascading nature of real earthquake events. As a result, UCERF3 anticipates fewer small isolated events and a greater prevalence of large, multi-segment ruptures capable of producing strong, widespread shaking (USGS Fact Sheet 2015-3009 2015). With probabilities exceeding 99% for at least one magnitude 6.7 or greater earthquake within the next 30 years, and a 7% probability of a magnitude 8 event, UCERF3 underscores the need for detailed seismic risk assessments of gas transmission infrastructure, particularly in regions where these systems intersect with elevated fire hazards (USGS Fact Sheet 2008-3027 2008). In this research, UCERF3 serves as the seismic input to OpenSRA, ensuring that the earthquake scenarios considered reflect realistic conditions in the Bay Area. A sample of the UCERF3 input parameters can be seen in Table 10. Rupture traces produced by the software, alongside seismic hazard zones determined by USGS, are represented in Figure 16.

Within OpenSRA, UCERF3 is implemented through probabilistic seismic hazard analysis (PSHA), combining rupture forecasts with NGA-West2 ground-motion prediction equations to estimate shaking intensities at specific locations (Largent et al. 2023). The resulting intensity measures (IMs), including peak ground acceleration, form the first layer of input into the PBEE workflow. The PBEE framework then links these IMs to engineering demand parameters (EDPs), which describe how the ground responds to shaking. For this research, liquefaction-induced settlements and earthquake-triggered landslides were selected as the ground deformation parameters of interest. This choice reflects both their strong influence on buried pipeline behavior and their clear relevance in the Bay Area, where diverse geological conditions, young sedimentary deposits, and steep terrain create susceptibility to both phenomena. Liquefaction and landslides therefore provide a meaningful basis for analyzing how seismic ground failure may compromise gas infrastructure.

These EDPs feed into the next PBEE stage, in which OpenSRA translates ground deformation into damage measures (DMs) for the pipeline segments. The DMs modeled include tensile and compressive strains, which correspond to the primary pipeline failure modes: tensile leakage, tensile rupture, and compressive rupture. These relationships are defined by fragility functions developed from advanced finite element analyses and laboratory testing, enabling OpenSRA to estimate how various levels of ground deformation may generate physical damage in buried steel pipelines (Watson-Lamprey et al. 2022).

The final PBEE step expresses these results as decision variables (DVs), most notably the annual rate of exceedance for each failure mode. An annual rate of 0.01, for example, would imply a roughly 1% chance of the failure occurring in any given year, or approximately a 10% chance over a decade. The PBEE framework described here can be visualized in Figure 17.

This research relies on OpenSRA as the main tool for evaluating seismic risk, and while the software can be used to model any natural gas network, its application here is tailored to the specific characteristics of the Bay Area case study. The region, as previously discussed, offers a compelling context for examining compounding seismic–fire hazards. In this thesis, the software is applied to PG&E's Bay Area gas transmission system, using pipeline data provided by the utility to the software's development team and subsequently made available for this study. The modeled transmission network is shown in Figure 15. Distribution pipelines were not considered, as their data was not made available due to security reasons.

OpenSRA is of particular value because it produces spatially explicit results that can be readily merged with other hazard datasets; its GIS-based outputs make it straightforward to evaluate seismic effects alongside additional spatial information. This capability is especially important in the Bay Area, where the combination of complex geology, steep terrain, and dense development creates conditions in which earthquake-induced pipeline damage may coincide with elevated fire potential. Such interactions between seismic ground failure, pipeline performance, and fire hazards remain understudied, and this thesis therefore contributes to ongoing research by examining how these processes intersect and collectively influence the vulnerability of natural gas transmission infrastructure.

The findings of this research can offer valuable insights for utilities and governing bodies in the Bay Area, helping to inform infrastructure planning, emergency response, and long-term risk mitigation. However, these results should be interpreted carefully, as the region's hazard environment and infrastructure configuration are unique. Because compound hazards are highly place-specific, the outcomes presented here cannot be assumed to apply directly to other regions with different geological, climatic, or operational contexts. Even so, this work illustrates how OpenSRA can be used beyond this case study, providing utilities nationwide with a flexible and rigorous PBEE-based framework for assessing the seismic vulnerability of their own gas networks.

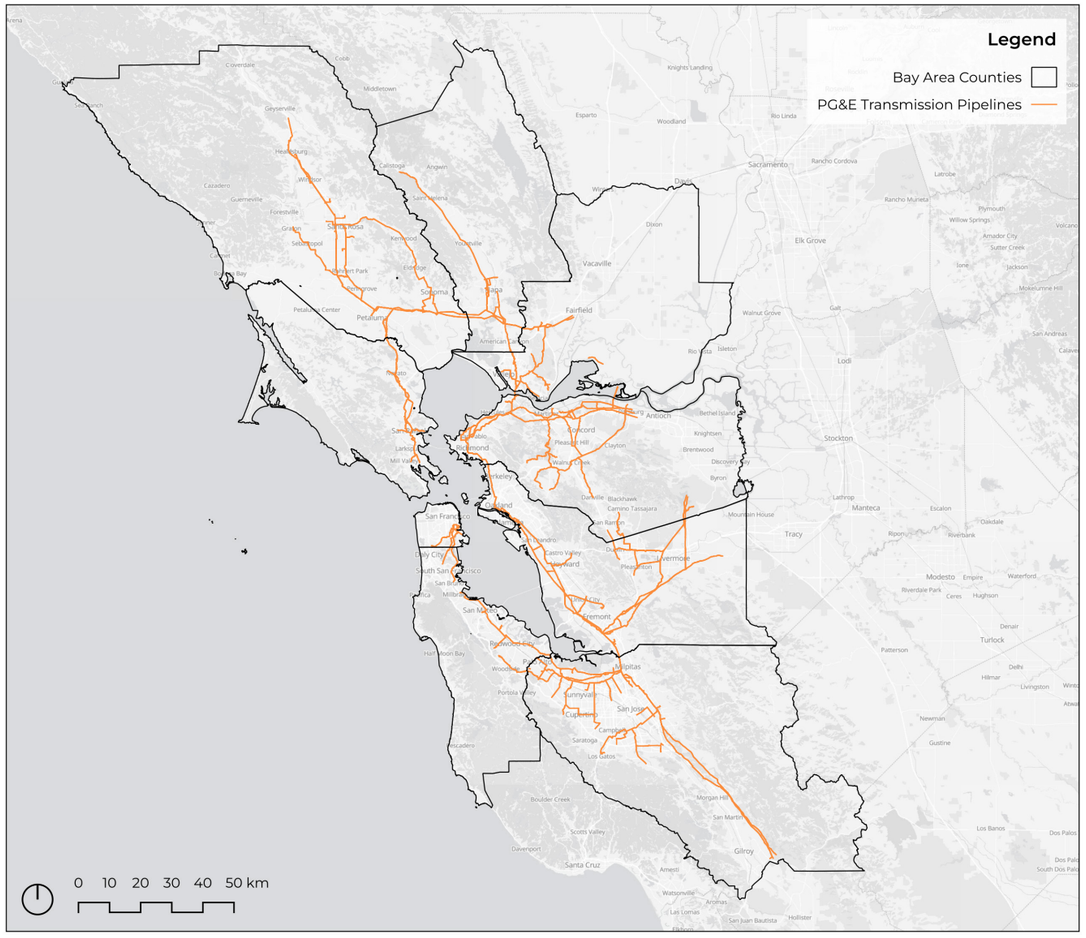

Figure 15 *PG&E gas transmission network in the Bay Area.*

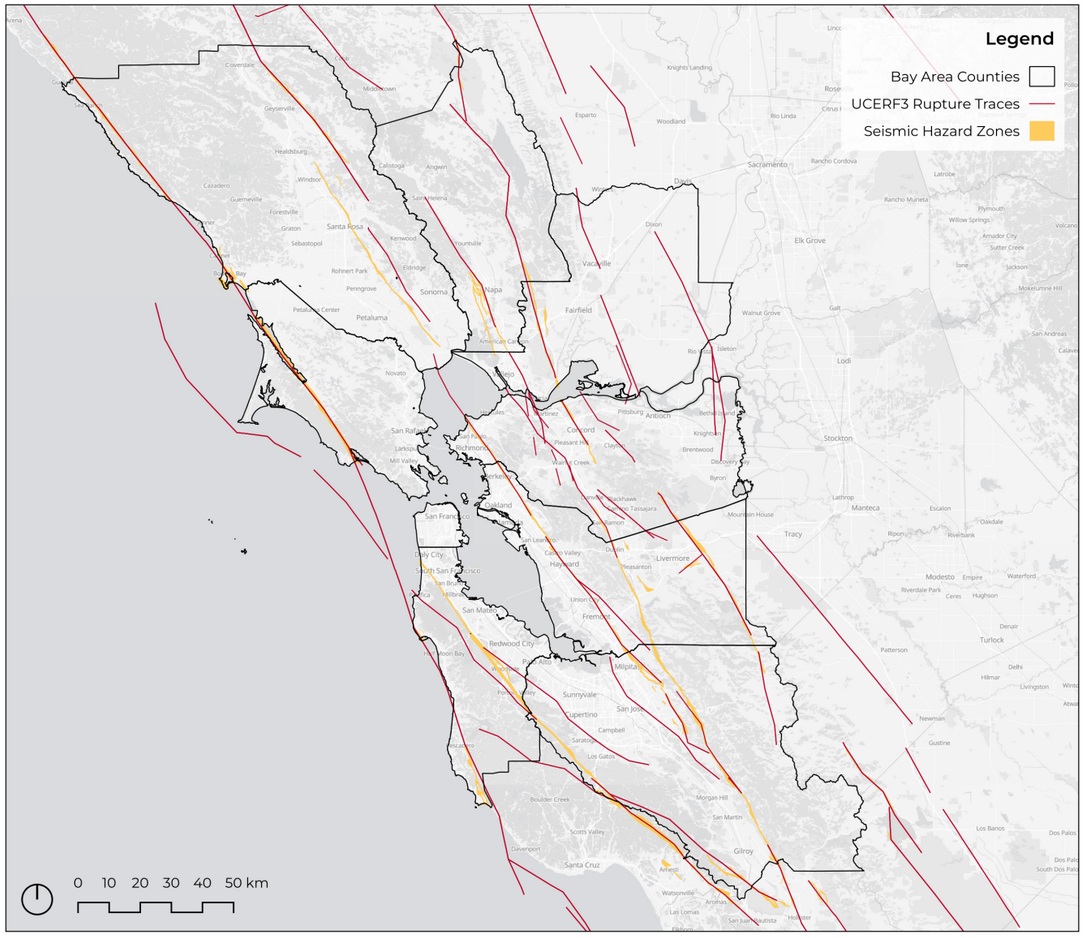

Figure 16 *UCERF3 modelled rupture traces and USGS mapped seismic hazard zones.*

fid	event_id	magnitude	annual_rate	dip	rake	dip_dir	z_tor	z_bor	fault_trace
1	32	6.45	0.000708	90	1.6	58.1	0	14.5	[[-122.499, 38.997, 0.0], [-122.552, 39.047, 0.0], [-122.597, 39.09, 0.0], [-122.603, 39.097, 0.0]]
2	33	6.45	0.000708	90	1.6	58.1	0	14.5	[[-122.603, 39.097, 0.0], [-122.651, 39.149, 0.0], [-122.653, 39.152, 0.0], [-122.714, 39.19, 0.0], [-122.756, 39.216, 0.0], [-122.772, 39.235, 0.0]]
3	34	6.45	0.000708	90	1.6	58.1	0	14.5	[[-122.772, 39.235, 0.0], [-122.817, 39.289, 0.0], [-122.863, 39.342, 0.0], [-122.869, 39.35, 0.0], [-122.914, 39.393, 0.0], [-122.92, 39.398, 0.0]]
4	35	6.45	0.000708	90	1.6	58.1	0	14.5	[[-122.92, 39.398, 0.0], [-122.948, 39.451, 0.0], [-122.956, 39.466, 0.0], [-122.987, 39.507, 0.0], [-123.029, 39.562, 0.0], [-123.046, 39.583, 0.0]]
5	36	6.45	0.000708	90	1.6	58.1	0	14.5	[[-123.046, 39.583, 0.0], [-123.079, 39.613, 0.0], [-123.121, 39.65, 0.0], [-123.137, 39.659, 0.0], [-123.205, 39.696, 0.0], [-123.218, 39.703, 0.0]]
6	37	6.45	0.000708	90	1.6	58.1	0	14.5	[[-123.218, 39.703, 0.0], [-123.263, 39.742, 0.0], [-123.27, 39.748, 0.0], [-123.287, 39.802, 0.0], [-123.288, 39.805, 0.0], [-123.318, 39.862, 0.0]]
7	38	6.45	0.000708	90	1.6	58.1	0	14.5	[[-123.318, 39.862, 0.0], [-123.339, 39.9, 0.0], [-123.356, 39.919, 0.0], [-123.396, 39.963, 0.0], [-123.402, 39.972, 0.0]]
8	39	6.45	0.000708	90	1.6	58.1	0	14.5	[[-123.402, 39.972, 0.0], [-123.438, 40.03, 0.0], [-123.424, 40.077, 0.0], [-123.428, 40.092, 0.0], [-123.445, 40.155, 0.0], [-123.45, 40.171, 0.0]]
9	40	6.95	0.000819	90	1.6	58.1	0	14.5	[[-122.499, 38.997, 0.0], [-122.552, 39.047, 0.0], [-122.597, 39.09, 0.0], [-122.603, 39.097, 0.0], [-122.651, 39.149, 0.0], [-122.653, 39.152, 0.0], [-122.714, 39.19, 0.0], [-122.756, 39.216, 0.0], [-122.772, 39.235, 0.0], [-122.817, 39.289, 0.0], [-122.863, 39.342, 0.0], [-122.869, 39.35, 0.0]]
10	41	6.95	0.000819	90	1.6	58.1	0	14.5	[[-122.869, 39.35, 0.0], [-122.914, 39.393, 0.0], [-122.92, 39.398, 0.0], [-122.948, 39.451, 0.0], [-122.956, 39.466, 0.0], [-122.987, 39.507, 0.0], [-123.029, 39.562, 0.0], [-123.046, 39.583, 0.0], [-123.079, 39.613, 0.0], [-123.121, 39.65, 0.0], [-123.137, 39.659, 0.0], [-123.205, 39.696, 0.0], [-123.218, 39.703, 0.0], [-123.263, 39.742, 0.0], [-123.27, 39.748, 0.0]]
11	42	6.95	0.000819	90	1.6	58.1	0	14.5	[[-123.27, 39.748, 0.0], [-123.287, 39.802, 0.0], [-123.288, 39.805, 0.0], [-123.318, 39.862, 0.0], [-123.339, 39.9, 0.0], [-123.356, 39.919, 0.0], [-123.396, 39.963, 0.0], [-123.402, 39.972, 0.0], [-123.438, 40.03, 0.0], [-123.424, 40.077, 0.0], [-123.428, 40.092, 0.0], [-123.445, 40.155, 0.0], [-123.45, 40.171, 0.0]]
12	43	7.45	0.00069	90	1.6	58.1	0	14.5	[[-122.499, 38.997, 0.0], [-122.552, 39.047, 0.0], [-122.597, 39.09, 0.0], [-122.603, 39.097, 0.0], [-122.651, 39.149, 0.0], [-122.653, 39.152, 0.0], [-122.714, 39.19, 0.0], [-122.756, 39.216, 0.0], [-122.772, 39.235, 0.0], [-122.817, 39.289, 0.0], [-122.863, 39.342, 0.0], [-122.869, 39.35, 0.0], [-122.914, 39.393, 0.0], [-122.92, 39.398, 0.0], [-122.948, 39.451, 0.0], [-122.956, 39.466, 0.0], [-122.987, 39.507, 0.0], [-123.029, 39.562, 0.0], [-123.046, 39.583, 0.0], [-123.079, 39.613, 0.0], [-123.121, 39.65, 0.0], [-123.137, 39.659, 0.0], [-123.205, 39.696, 0.0], [-123.218, 39.703, 0.0], [-123.263, 39.742, 0.0], [-123.27, 39.748, 0.0], [-123.287, 39.802, 0.0], [-123.288, 39.805, 0.0], [-123.318, 39.862, 0.0], [-123.339, 39.9, 0.0], [-123.356, 39.919, 0.0], [-123.396, 39.963, 0.0], [-123.402, 39.972, 0.0], [-123.438, 40.03, 0.0], [-123.424, 40.077, 0.0], [-123.428, 40.092, 0.0], [-123.445, 40.155, 0.0], [-123.45, 40.171, 0.0]]
13	44	7.85	0.00029	90	1.6	58.1	0	14.5	[[-122.499, 38.997, 0.0], [-122.552, 39.047, 0.0], [-122.597, 39.09, 0.0], [-122.603, 39.097, 0.0], [-122.651, 39.149, 0.0], [-122.653, 39.152, 0.0], [-122.714, 39.19, 0.0], [-122.756, 39.216, 0.0], [-122.772, 39.235, 0.0], [-122.817, 39.289, 0.0], [-122.863, 39.342, 0.0], [-122.869, 39.35, 0.0], [-122.914, 39.393, 0.0], [-122.92, 39.398, 0.0], [-122.948, 39.451, 0.0], [-122.956, 39.466, 0.0], [-122.987, 39.507, 0.0], [-123.029, 39.562, 0.0], [-123.046, 39.583, 0.0], [-123.079, 39.613, 0.0], [-123.121, 39.65, 0.0], [-123.137, 39.659, 0.0], [-123.205, 39.696, 0.0], [-123.218, 39.703, 0.0], [-123.263, 39.742, 0.0], [-123.27, 39.748, 0.0], [-123.287, 39.802, 0.0], [-123.288, 39.805, 0.0], [-123.318, 39.862, 0.0], [-123.339, 39.9, 0.0], [-123.356, 39.919, 0.0], [-123.396, 39.963, 0.0], [-123.402, 39.972, 0.0], [-123.438, 40.03, 0.0], [-123.424, 40.077, 0.0], [-123.428, 40.092, 0.0], [-123.445, 40.155, 0.0], [-123.45, 40.171, 0.0]]
14	45	6.75	0.000174	74	35.9	156	0	19.7	[[-122.598, 40.216, 0.0], [-122.522, 40.261, 0.0], [-122.504, 40.269, 0.0], [-122.467, 40.287, 0.0], [-122.404, 40.315, 0.0], [-122.395, 40.32, 0.0], [-122.329, 40.346, 0.0], [-122.3, 40.356, 0.0]]
15	46	6.75	0.000174	74	35.9	156	0	19.7	[[-122.3, 40.356, 0.0], [-122.202, 40.389, 0.0], [-122.193, 40.391, 0.0], [-122.08, 40.416, 0.0], [-121.967, 40.441, 0.0]]
16	47	7.15	0.000118	74	35.9	156	0	19.7	[[-122.598, 40.216, 0.0], [-122.522, 40.261, 0.0], [-122.504, 40.269, 0.0], [-122.467, 40.287, 0.0], [-122.404, 40.315, 0.0], [-122.395, 40.32, 0.0], [-122.329, 40.346, 0.0], [-122.3, 40.356, 0.0], [-122.202, 40.389, 0.0], [-122.193, 40.391, 0.0], [-122.08, 40.416, 0.0], [-121.967, 40.441, 0.0]]
17	54	6.25	0.000733	90	0	60.3	0	10	[[-122.47, 38.225, 0.0], [-122.503, 38.259, 0.0], [-122.537, 38.292, 0.0], [-122.562, 38.33, 0.0]]
18	55	6.25	0.000733	90	0	60.3	0	10	[[-122.562, 38.33, 0.0], [-122.587, 38.368, 0.0], [-122.592, 38.376, 0.0], [-122.617, 38.403, 0.0], [-122.647, 38.435, 0.0], [-122.647, 38.438, 0.0]]
19	56	6.75	0.000455	90	0	60.3	0	10	[[-122.47, 38.225, 0.0], [-122.503, 38.259, 0.0], [-122.537, 38.292, 0.0], [-122.562, 38.33, 0.0], [-122.587, 38.368, 0.0], [-122.592, 38.376, 0.0], [-122.617, 38.403, 0.0], [-122.647, 38.435, 0.0], [-122.647, 38.438, 0.0]]
20	101	6.35	0.000121	70	19.1	27.1	0	12	[[-121.928, 37.121, 0.0], [-121.988, 37.142, 0.0], [-121.992, 37.144, 0.0], [-122.04, 37.173, 0.0]]

Table 10 *Sample UCERF3 input parameters.*

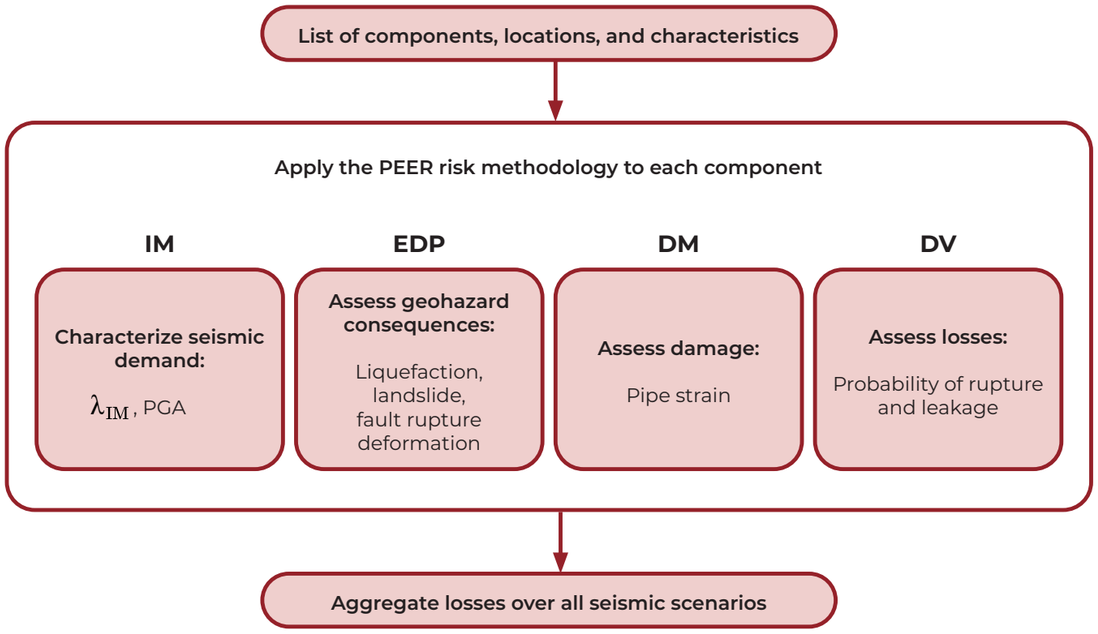

Figure 17 *PEER risk methodology framework applied to underground pipelines. Adapted from (Largent et al.*

7.2.1 Liquefaction Induced Settlements

Liquefaction-induced settlement is a critical geotechnical hazard that can strongly affect the performance of buried infrastructure such as natural gas pipelines. During strong ground shaking, loose and saturated sandy soils may temporarily lose their strength as excess pore water pressures rise, causing the soil to behave like a fluid (Seed and Idriss 1970; Kramer 1996). When the shaking stops and pore pressures dissipate, the soil contracts into a denser state, producing permanent settlement and often uneven downward movement across short distances (Ishihara 1993). Such differential settlement can impose significant strains on pipelines that rely on consistent support along their length.

This hazard is especially relevant in regions like the San Francisco Bay Area, where many urban districts are built on young fill and estuarine deposits that are highly susceptible to liquefaction (Holzer et al. 2002). Historic events, most notably the 1989 Loma Prieta earthquake, illustrated how liquefaction-related settlement and lateral spreading can damage buildings, pavement, and underground utilities, including gas pipelines that contributed to post-earthquake fires (Hamada and O'Rourke 1992). Because pipelines are long, continuous structures, uneven settlement can induce tensile and compressive stresses that exceed design tolerances, leading to joint separation, buckling, rupture, or leakage (O'Rourke and Liu 1999). Gas leakage in densely populated environments can escalate into fire hazards, especially when combined with other lifeline failures such as disrupted water supply (Kiremidjian et al. 2007; O'Rourke 2003).

To analyze potential liquefaction-induced damage to gas pipelines in the Bay area, certain input models were chosen in OpenSRA. They are summarized in Table 11.

	Input
Infrastructure	PG&E Gas Transmission Pipeline Network
Decision Variable	Pipe Compressive Rupture
	Pipe Tensile Rupture
	Pipe Tensile Leakage
Damage Measure	Settlement Induced Pipe Strain
Engineering Demand Parameter	Liquefaction
	Liquefaction Induced Settlement
Intensity Measure	UCERF3
	NGA-West2

Table 11 *Liquefaction OpenSRA framework inputs.*

Findings from the analysis illustrate how the modeled failure mechanisms manifest across the Bay Area pipeline network. Liquefaction-induced damage was represented through the mean annual rate of failure calculated for each pipe segment under both compressive and tensile strain conditions. The model predicted occurrences of tensile rupture and tensile leakage, whereas no instances of compressive rupture were observed. For consistency with the fire hazard results, which already employed a 1 to 5 risk scale, the liquefaction numerical outputs were classified into five damage classes. The mean annual failure rates associated with each failure mode, and their respective classes, are summarized in Table 12.

The OpenSRA damage outputs can be visualized by pipeline segment within the software and exported as vector GIS layers. To develop maps suitable for integration with the Fire Risk Index produced in Section 7.1 (see Figure 13), the exported pipeline damage layers were rasterized in QGIS so that they matched the pixel resolution of the fire map. The vector data for pipeline damage was processed in three separate iterations: one for compressive rupture, one for tensile rupture, and one for tensile leakage. Each resulting raster was then assigned a risk value ranging from 1 to 5. Tensile rupture and tensile leakage layers were classified according to this scale (see Figures 19 and 20), while the compressive rupture raster was assigned a value of 0, reflecting the absence of this failure mode in the liquefaction results and ensuring it would not influence the aggregated damage analysis (see Figure 18).

To generate a comprehensive representation of total liquefaction-related pipeline risk, the compressive-rupture, tensile-rupture, and tensile-leakage rasters were combined by summing their pixel values and subsequently normalizing the output back to a 1-5 scale. The resulting hazard map indicates that liquefaction-related damage potential is highest in flat, low-lying regions, particularly along the margins of the Bay and throughout the inland corridor between San José and Gilroy, where loose, saturated soils are prevalent (see Figure 22).

A validation of these results was conducted by overlaying mapped liquefaction-prone zones onto the outputs. This comparison revealed a strong spatial correspondence between susceptible soils and the locations where pipeline damage was predicted, reinforcing the known association between liquefaction hazards and flatter geomorphic settings (see Figure 23).

A detailed interpretation of these maps, alongside a thorough explanation for the failure modes, is provided in Section 8.2

Liquefaction Mean Annual Rate of Failure			
Normalized	**Compressive Rupture**	**Tensile Rupture**	**Tensile Leakage**
1	0	0.000049 - 0.000093	0.000678 - 0.001104
2	0	0.000093 - 0.000133	0.001104 - 0.001311
3	0	0.000133 - 0.000239	0.001311 - 0.001525
4	0	0.000239 - 0.000567	0.001525 - 0.001953
5	0	0.000567 - 0.000948	0.001953 - 0.002826

Table 12 *Liquefaction mean annual rate. Values were classified on a 1 to 5 scale.*

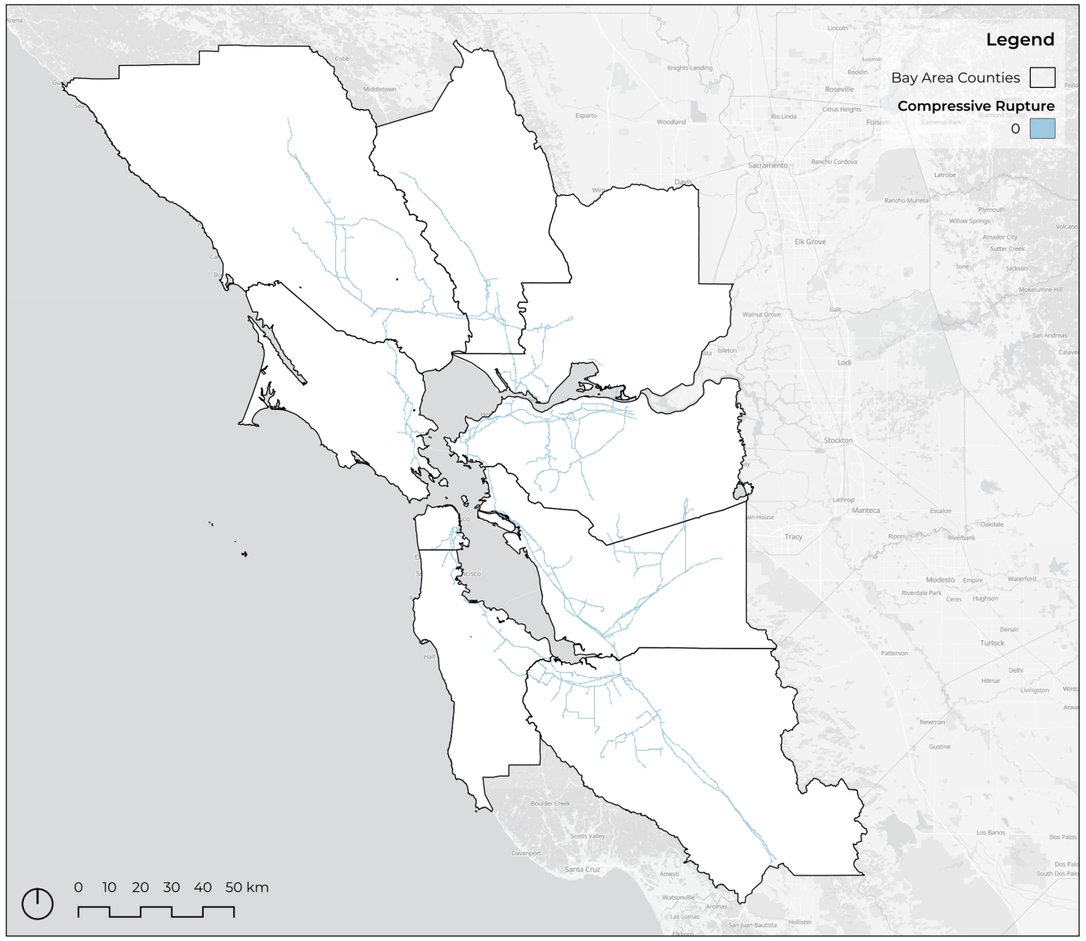

Figure 18 *Liquefaction-induced compressive rupture.*

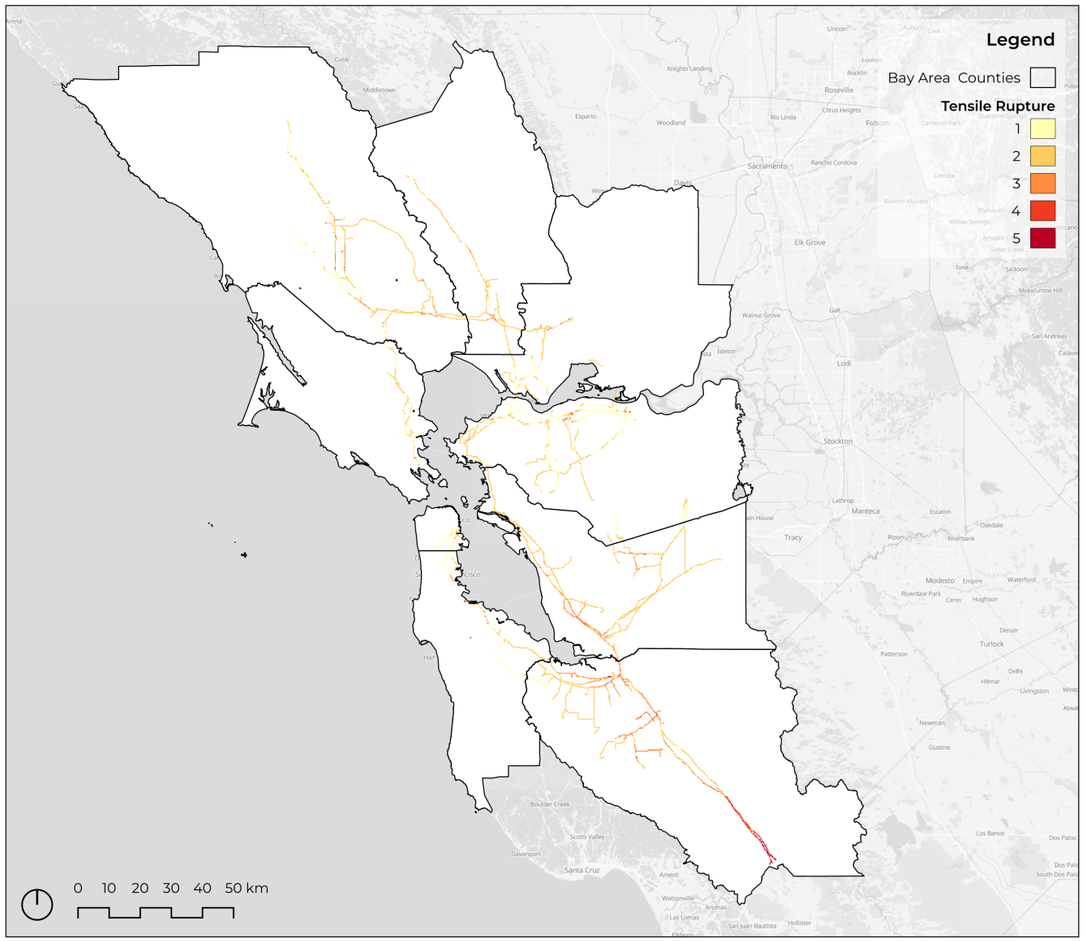

Figure 19 *Liquefaction-induced tensile rupture.*

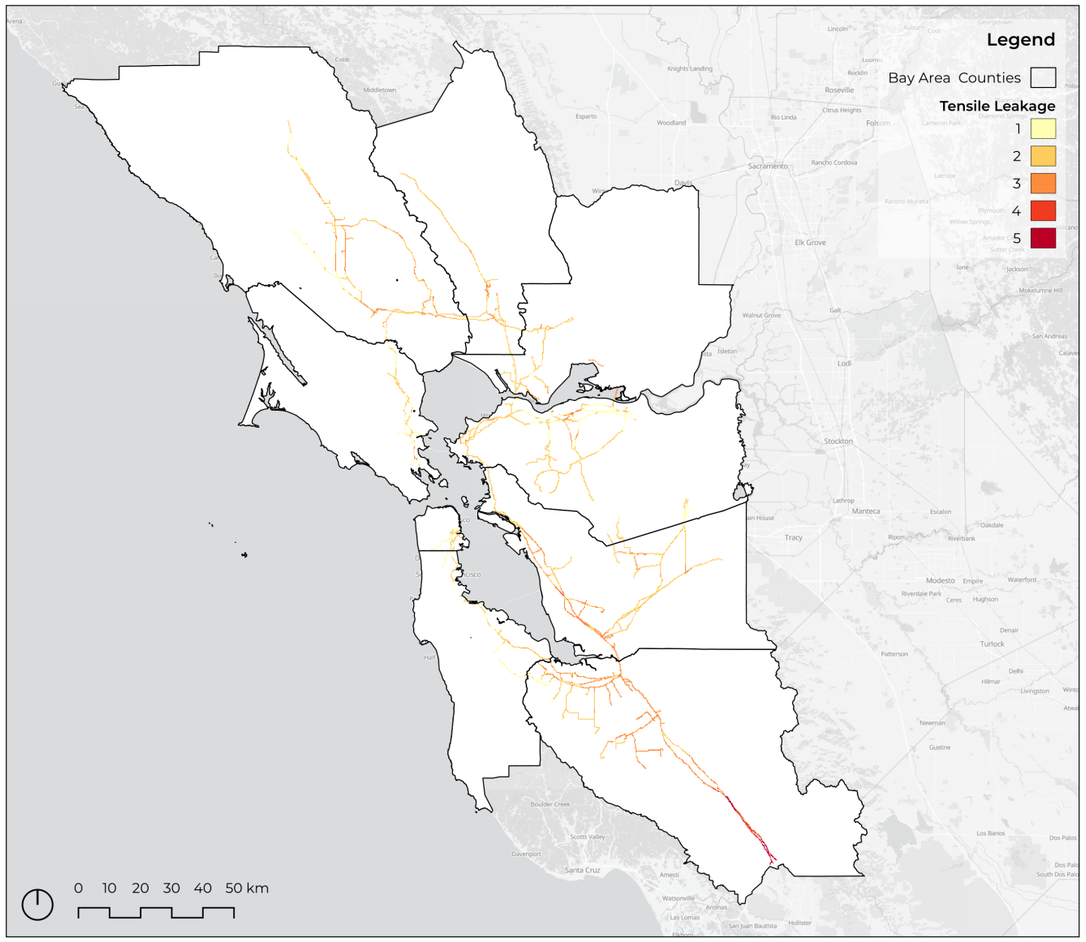

Figure 20 *Liquefaction-induced tensile leakage.*

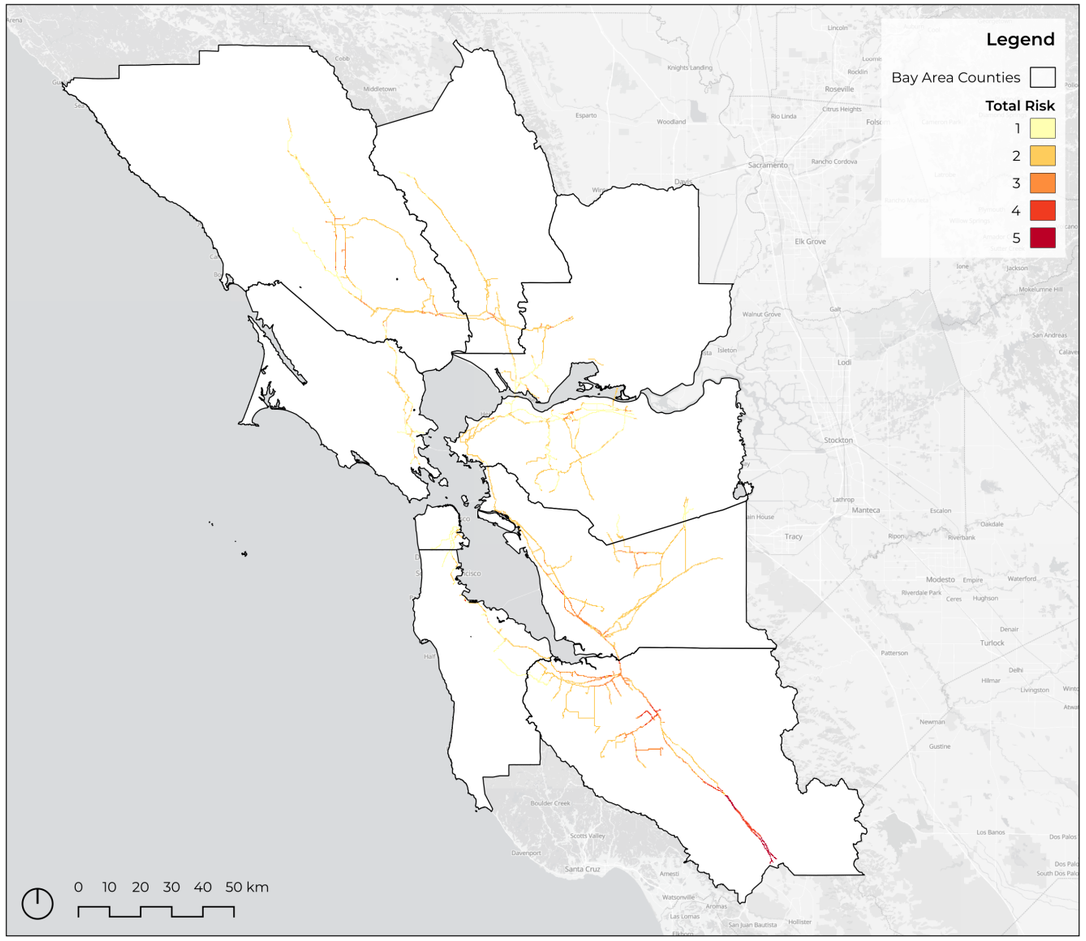

Figure 21 *Total liquefaction risk.*

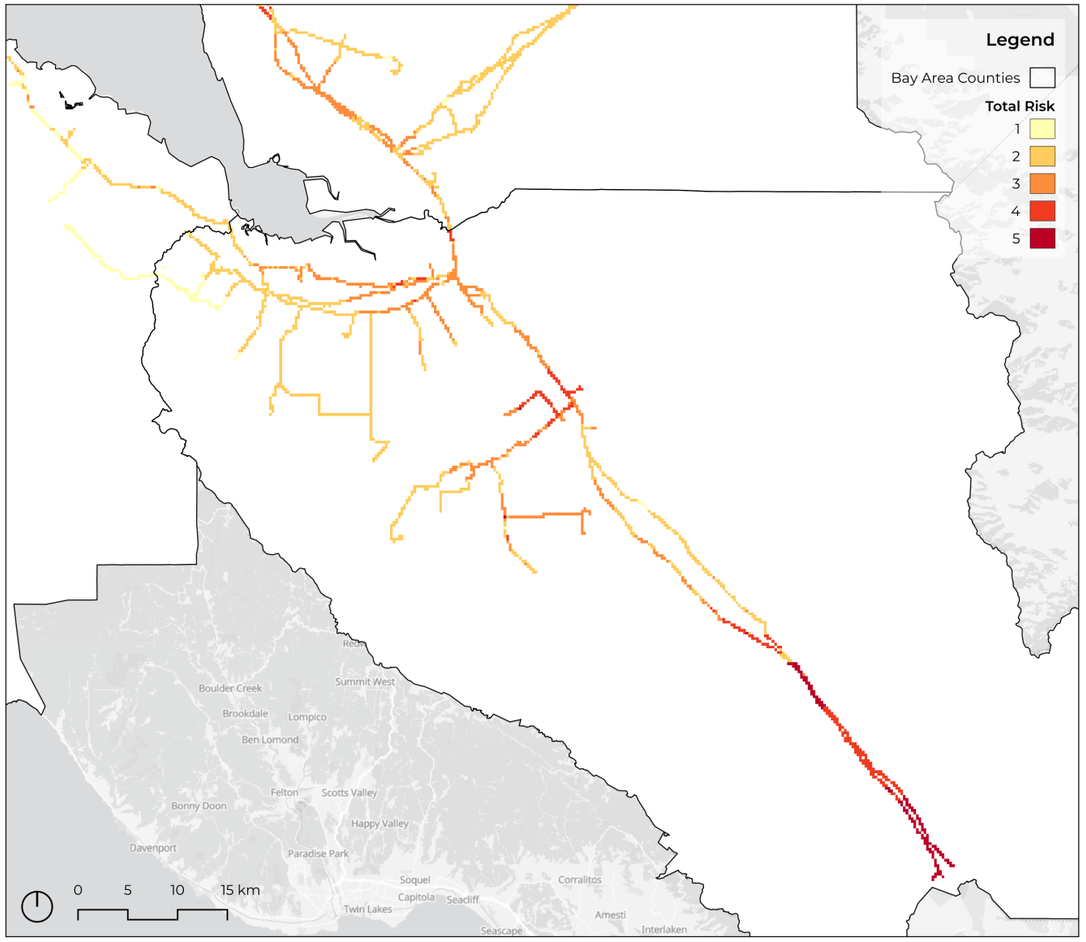

Figure 22 *Total liquefaction risk close-up in Santa Clara county.*

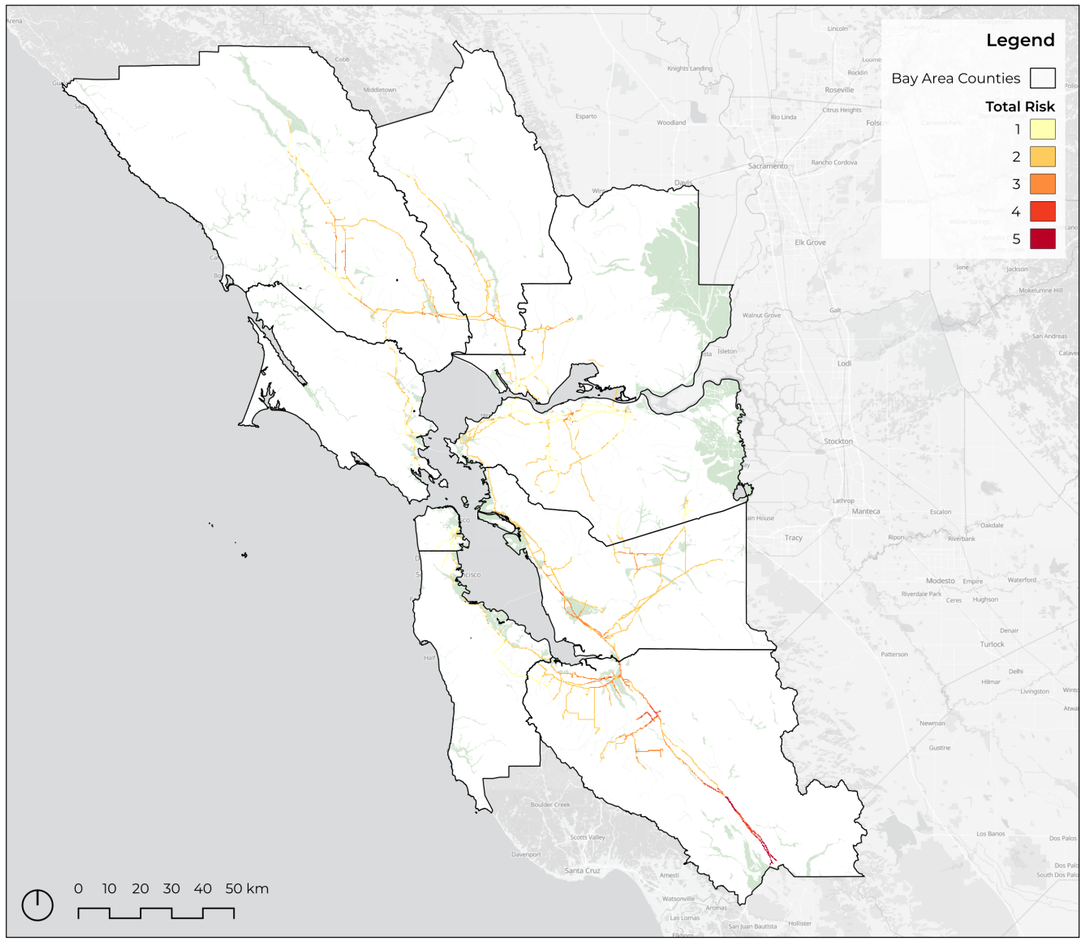

Figure 23 *Total liquefaction risk validated using USGS liquefaction prone zones survey data.*

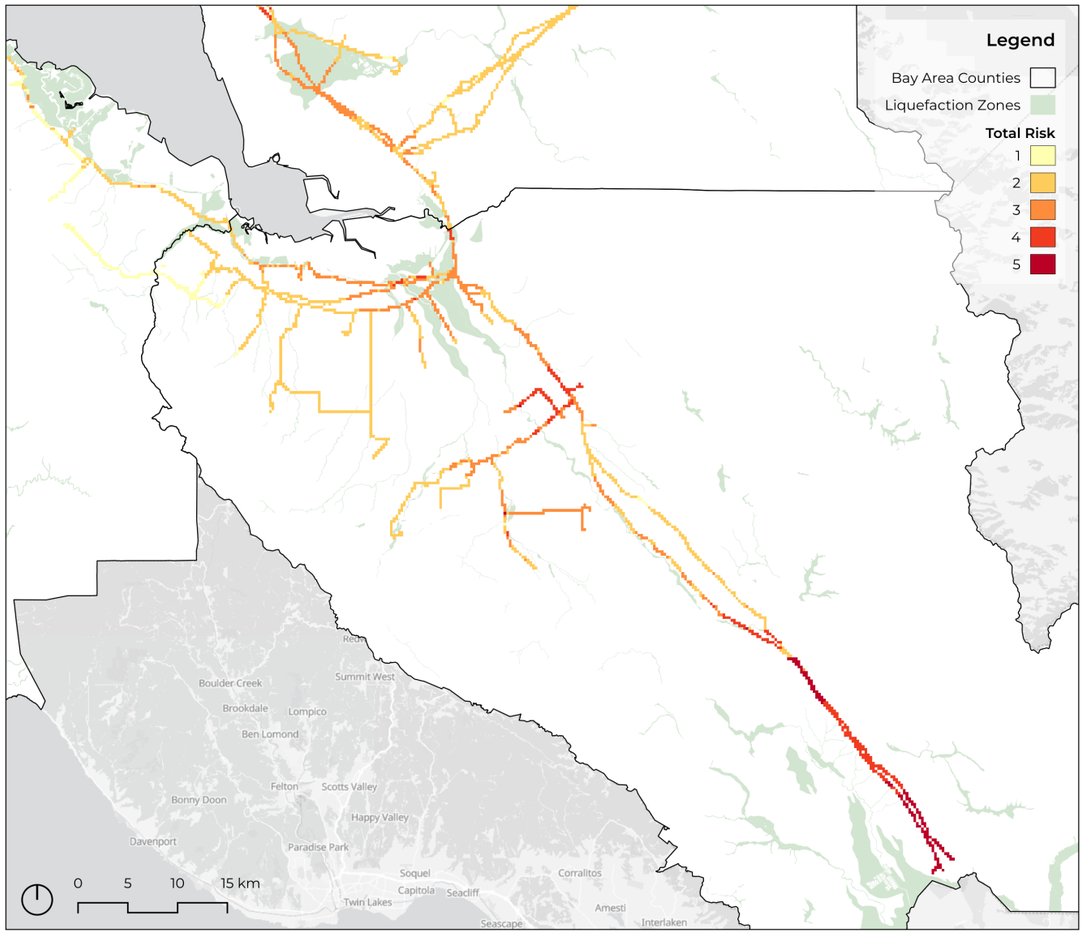

Figure 24 *Total liquefaction risk close-up in Santa Clara county validation. Validated using USGS liquefaction*

7.2.2 Landslides

Earthquake-induced landslides represent another significant secondary hazard that can disrupt natural gas pipeline systems. Strong shaking can destabilize slopes by reducing soil strength, increasing pore water pressures, or generating inertial forces that overcome a slope's resistance (Keefer 1984; Kramer 1996). Resulting slope failures may range from shallow slips and debris flows to deep-seated landslides, often producing ground displacements that far exceed those caused by shaking or liquefaction alone (Jibson 1993). Because many transmission pipelines cross hilly terrain, engineered embankments, and coastal bluffs, landslide susceptibility plays a crucial role in determining their seismic vulnerability.

In the San Francisco Bay Area, steep hills, heterogeneous geology, and high seismicity contribute to widespread landslide potential. Past earthquakes along the San Andreas and Hayward faults have triggered extensive slope failures across both natural and developed terrain. Weak and weathered geological formations, combined with seasonal saturation, heighten this vulnerability. Pipelines crossing such slopes may experience bending, stretching, or compressive forces as ground masses move downslope, potentially causing buckling, rupture, or joint pullout (Hamada and O'Rourke 1992). Landslide-induced ruptures also raise the possibility of gas leakage and ignition, as observed during past earthquakes such as the 1995 Kobe event (Nishida et al. 2024). Furthermore, landslides may block access routes, delay repairs, and damage other lifelines, creating further compounding failures that complicate emergency response (O'Rourke 2003).

To analyze the potential landslide-induced damage to gas pipelines in the Bay Area, the input parameters described in Table 13 were chosen.

	Input
Infrastructure	PG&E Gas Transmission Pipeline Network
Decision Variable	Pipe Compressive Rupture
	Pipe Tensile Rupture
	Pipe Tensile Leakage
Damage Measure	Landslide Induced Pipe Strain
Engineering Demand Parameter	Landslide
Intensity Measure	UCERF3
	NGA-West2

Table 13 *Landslides OpenSRA inputs framework.*

The results of the analysis performed using OpenSRA illustrate the distinct spatial and mechanical behavior of landslide hazards compared to liquefaction. Like the liquefaction analysis, the landslide analysis resulted in mean annual rate of failure values for each pipe segment under compressive and tensile strain, the results of which can be seen in Table 14. In the landslide simulations, compressive rupture was the only damage mode present, while tensile rupture and tensile leakage did not occur. This is due to the way soil behaves under landslide and liquefaction scenarios. This difference in behavior is explained in section 8.2 The values have been assigned 1 to 5 hazard classes like those employed in the liquefaction analysis.

Landslides Mean Annual Rate of Failure			
Normalized	**Compressive Rupture**	**Tensile Rupture**	**Tensile Leakage**
1	0.000000 - 0.000797	0	0
2	0.000797 - 0.002280	0	0
3	0.002280 - 0.003809	0	0
4	0.003809 - 0.006060	0	0
5	0.006060 - 0.012781	0	0

Table 14 ***Landslides mean annual rate.*** *Values were classified on a 1 to 5 scale.*

Since tensile strain damage is non-existent, both rasters were assigned values of 0. This means the total landslide damage map is identical to the compressive-rupture map, since no other damage modes contributed to the combined score.

The results were validated comparing mapped landslide-prone zones with the raster output. This comparison, like liquefaction, revealed a solid spatial correspondence between soils susceptible to landslides and the locations where pipeline damage was predicted, reinforcing the known association between landslide hazards and sloped terrains (see Figures 29 and 30).

A detailed interpretation of these maps, alongside a thorough explanation for the failure modes, is provided in Section 8.2.

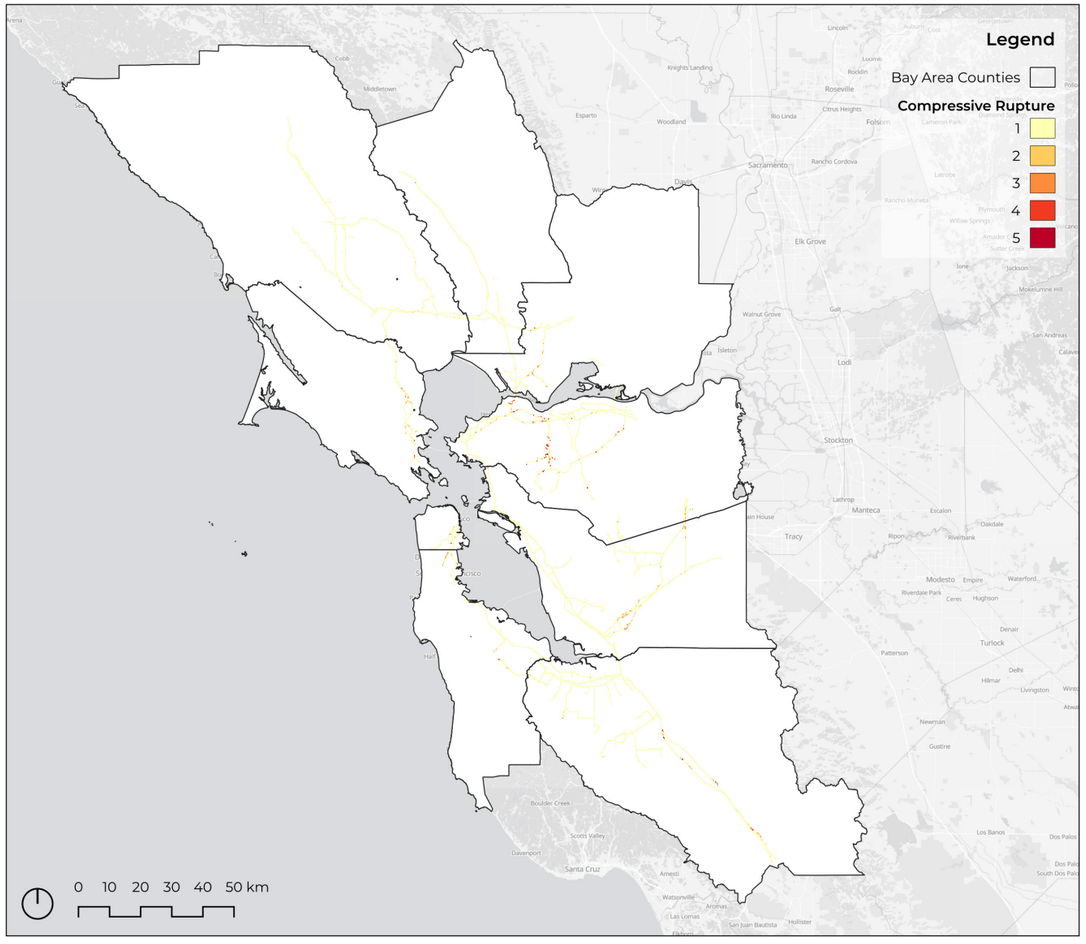

Figure 25 *Landslides-induced compressive rupture.*

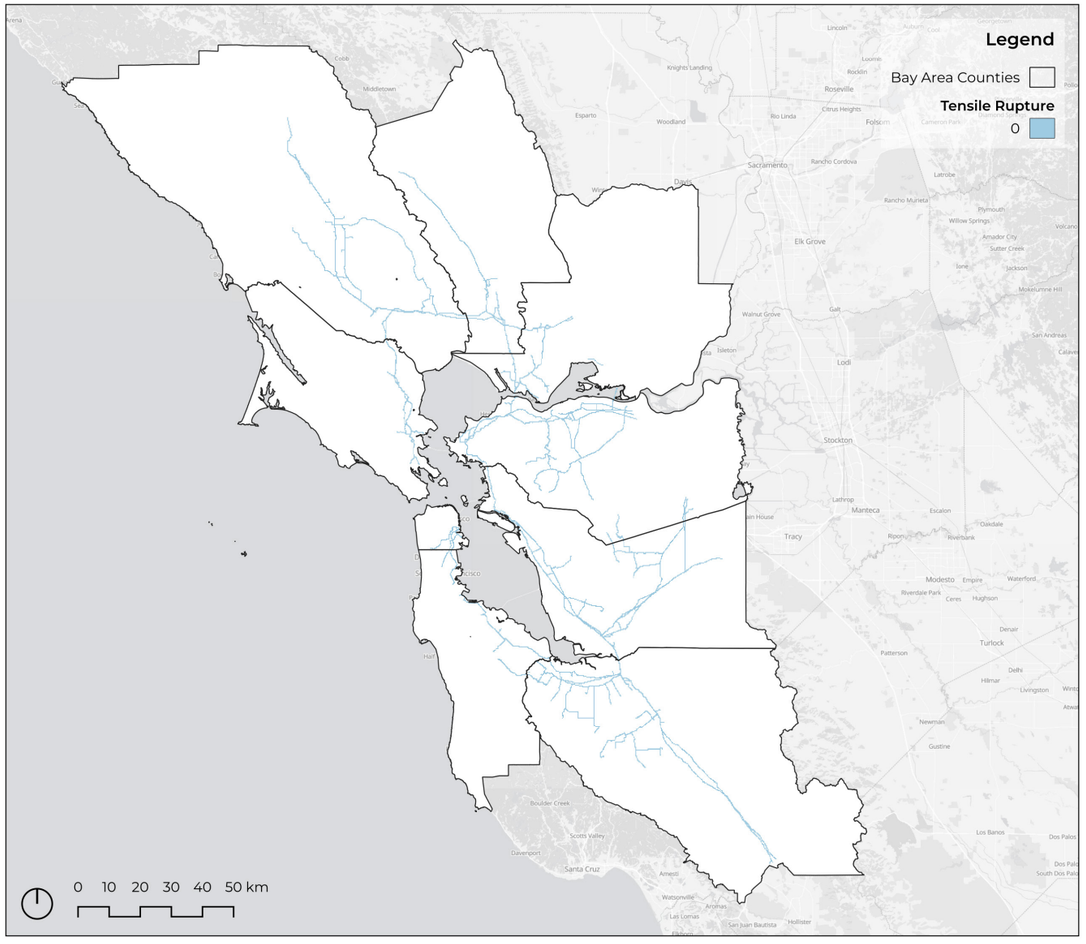

Figure 26 *Landslides-induced tensile rupture.*

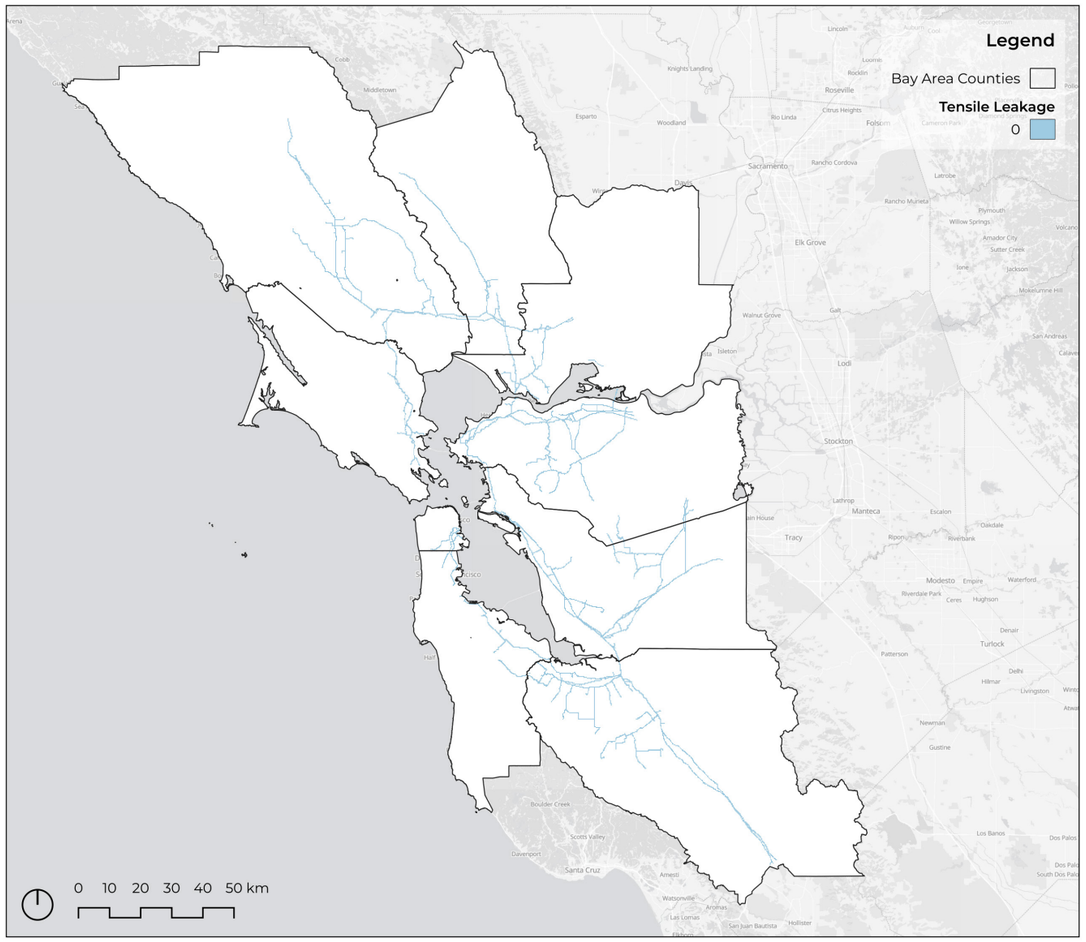

Figure 27 *Landslides-induced tensile leakage.*

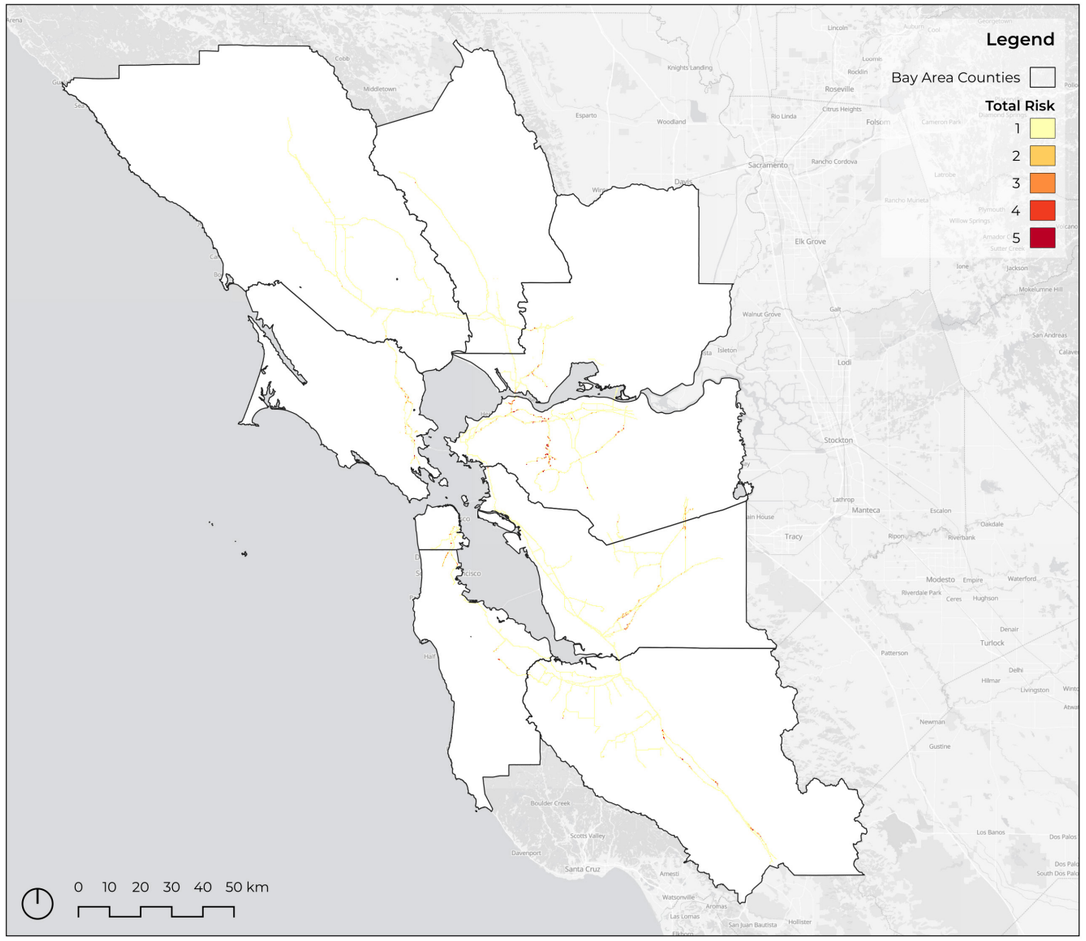

Figure 28 *Total landslide risk.*

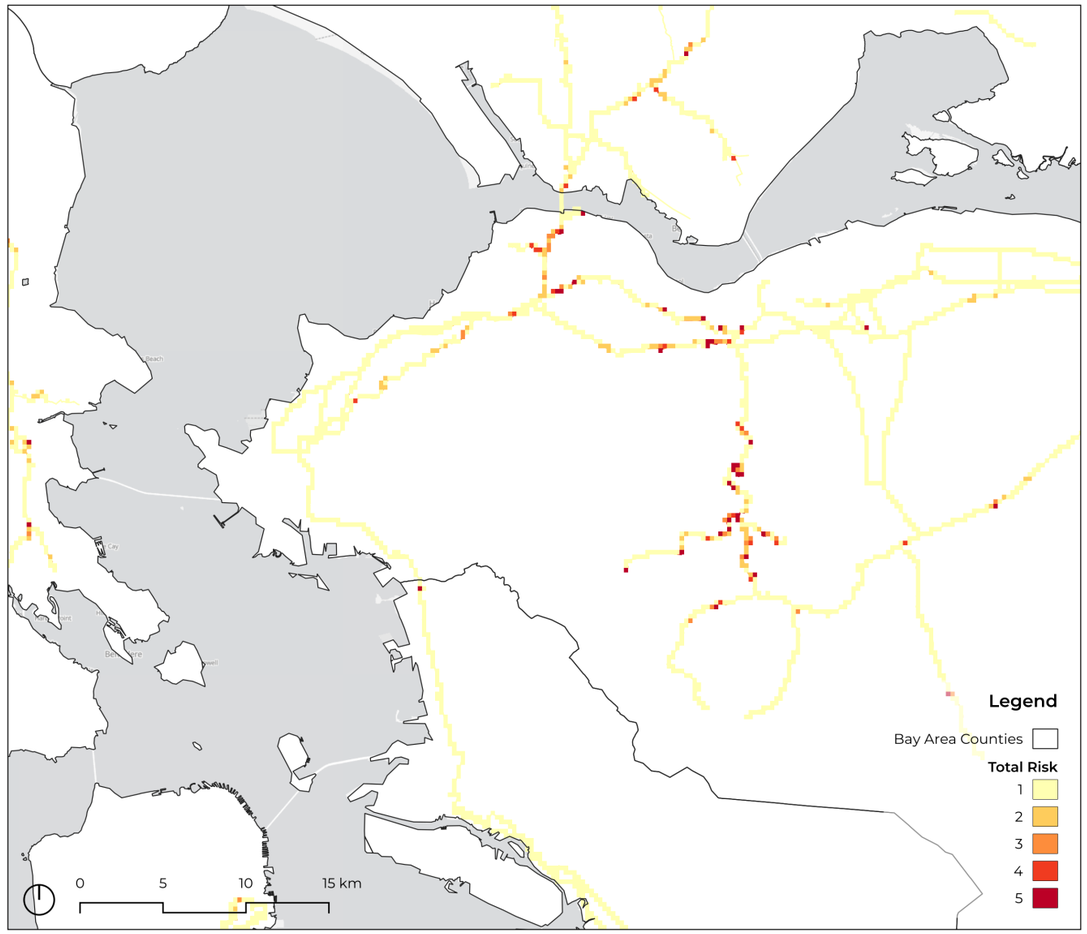

Figure 29 *Total landslide risk close-up in Contra Costa county. Validated using USGS landslides prone zones survey data.*

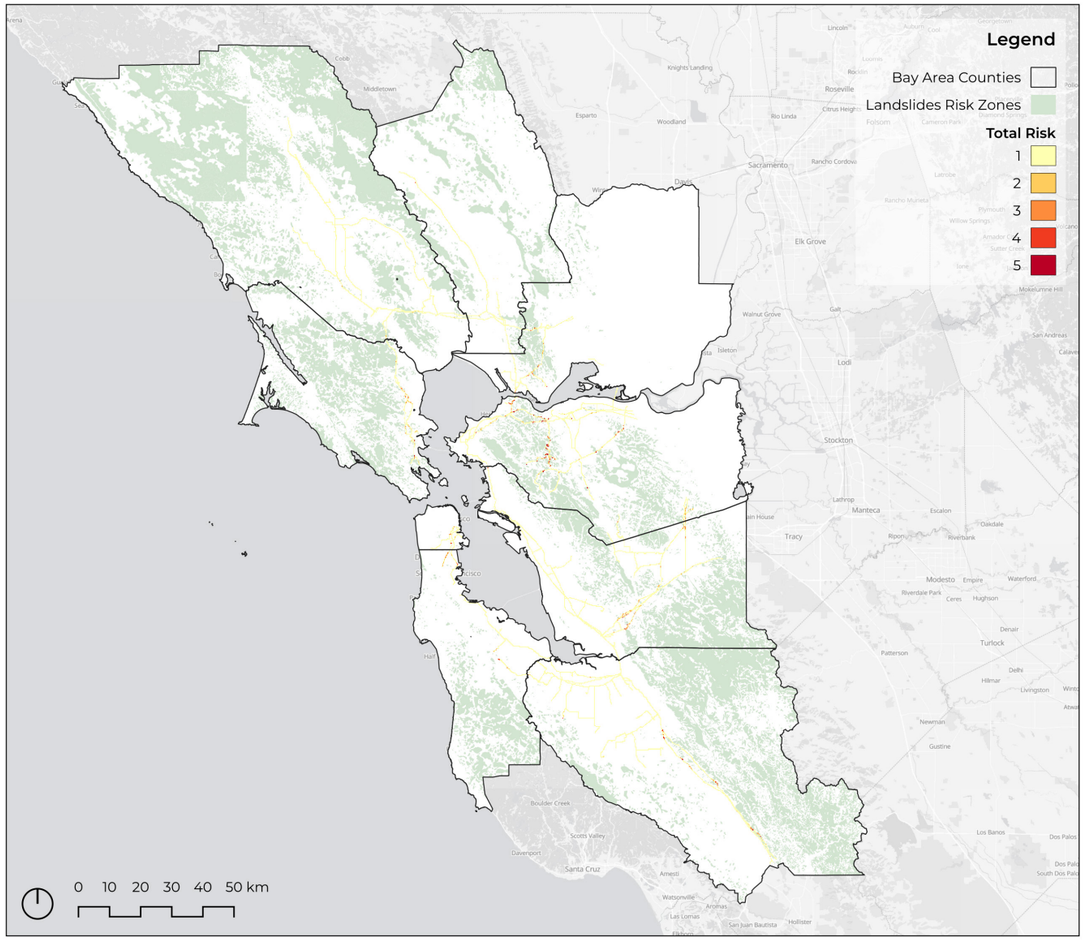

Figure 30 *Total landslide risk validated using USGS landslide prone zones survey data.*

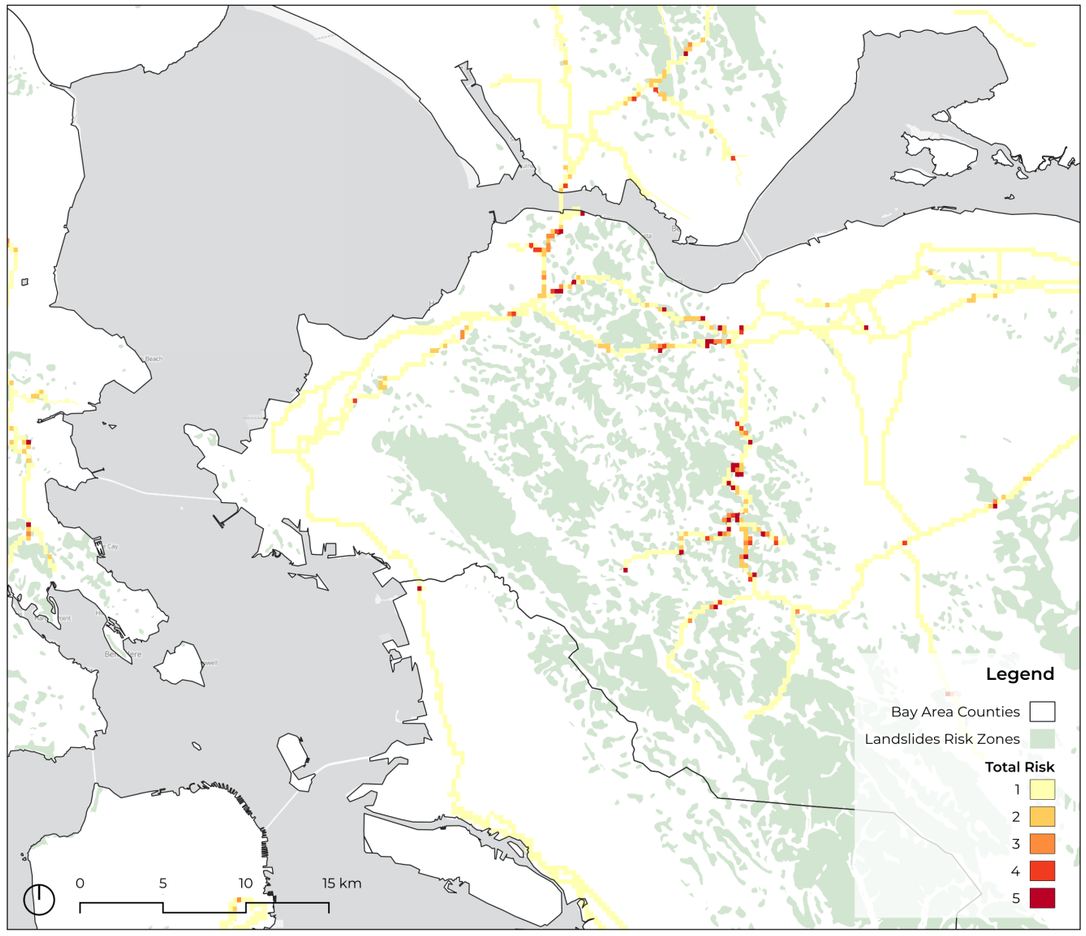

Figure 31 ***Total landslide risk close-up in Contra Costa county validation.*** *Validated using USGS landslide prone zones survey data.*

7.3 Compound Hazard Analysis

The results presented in this section build directly on the datasets and procedures developed in sections 6.1 and 6.2. After constructing a fire risk index map and two seismic-induced damage vulnerability maps for the Bay Area transmission pipeline network, these outputs were further examined to understand their potential compound effects. Because earthquake-related pipeline fragility and fire potential do not occur in isolation, a combined analysis was required to determine how these hazards interact spatially and to identify the pipeline segments most exposed to multiple risk factors simultaneously.

To achieve this, three different analytical methods chosen by the author were applied, each offering a distinct lens through which to interpret the relationship between the two hazard surfaces. The objective was not only to compare the spatial patterns produced by each method but also to evaluate which approach most effectively supports the broader goal of identifying pipeline segments subject to high, moderate, or low levels of combined hazard. This multi-method structure is essential given the critical role of gas transmission pipelines: they represent an infrastructure system fundamental to the functioning of daily life, yet one that also poses significant danger when exposed to compounding natural hazards. By clarifying the conditions under which these pipelines are at elevated risk of failure, the analysis contributes to the development of a maintenance and replacement framework that can assist utility operators in prioritizing interventions. Such insights help promote both operational awareness within gas companies and broader public safety efforts aimed at protecting human life and the environment.

The three analytical methods employed were the additive hazard index, the matrix hazard index, and the binary hazard index, names coined by the author and based on reasoning, according to the different results the research aimed to achieve. The additive index is the most straightforward and visually intuitive, but its simplicity can lead to potential misrepresentation because it collapses different hazard combinations into identical values. The matrix index provides the most comprehensive perspective for the purposes of this thesis: it retains the distinct contributions of both fire risk and pipeline vulnerability and thus allows for a more nuanced interpretation of their interaction. The binary index, in contrast, offers a targeted view of the most severe overlapping conditions and is particularly useful for identifying top-priority areas in emergency response or rapid decision-making contexts.

Together, these three methods form the basis of the results presented in this section, allowing for a detailed examination of how compound hazards affect the Bay Area's transmission pipeline system and offering crucial insights into where the network may require increased maintenance, reinforcement, or modernization.

Method 1: Additive Hazard Index

To generate a continuous estimate of earthquake-induced pipeline hazard that integrates both structural fragility and fire potential, an additive hazard index was calculated by combining the two normalized raster layers (each classified on a 1-5 scale). This approach assumes that both dimensions, earthquake-induced pipeline damage potential and fire hazard, contribute jointly and approximately equally to the overall hazard environment. Let P denote the pipeline damage class and F the fire potential class for a given pixel; the combined hazard score H is therefore defined as:

$$H_a = P + F$$

This formulation produces values ranging from 2 (minimum combined hazard: 1 + 1) to 10 (maximum: 5 + 5) and preserves the ordinal meaning of the input classes while creating a smooth, continuous surface of combined hazard intensity across the study area.

To make the comparison with other components of the analysis easier, the additive index H_a was normalized back to a 1-5 scale using a linear transformation:

$$H_{a,n} = 1 + \frac{(H_a - 2)}{(10 - 2)} \times 4$$

The resulting normalized index was then grouped into five hazard intensity classes reflecting very low to very high combined hazard. These classes maintain approximate equality while retaining ordinal separation, allowing for intuitive visualization and interpretation. The results can be seen in Table 15.

Hazard Class	Threshold (H)
5	H ≥ 4.2
4	3.4 ≤ H < 4.19
3	2.6 ≤ H < 3.39
2	1.8 ≤ H < 2.59
1	H < 1.8

Table 15 *Additive risk reclassification ranges.*

The principal strength of the additive method lies in its simplicity and transparency: the formulation is intuitive, easily reproducible, and straightforward to communicate to both technical and nontechnical audiences. The additive score directly increases when either pipeline fragility or fire potential rises, ensuring that higher individual risk levels appropriately contribute to higher joint hazard estimates. Additionally, because the method produces a continuous surface, it captures gradual spatial transitions that may be overlooked by more categorical approaches, making it an effective tool for broad regional screening.

However, the additive method also exhibits notable limitations. By assigning equal weight to pipeline fragility and fire potential, it implicitly assumes that both factors contribute symmetrically to overall hazard, an assumption that may not fully align with real-world dynamics or operational priorities. Furthermore, the method does not distinguish between different combinations of values that yield the same total, even though the underlying hazard implications of these scenarios may differ substantially. As a result, extreme values in one factor can mask moderate contributions in the other, potentially obscuring important nuances in joint hazard patterns. Despite these constraints, the additive index remains useful as an initial, high-level representation of overall earthquake-fire hazard across the Bay Area.

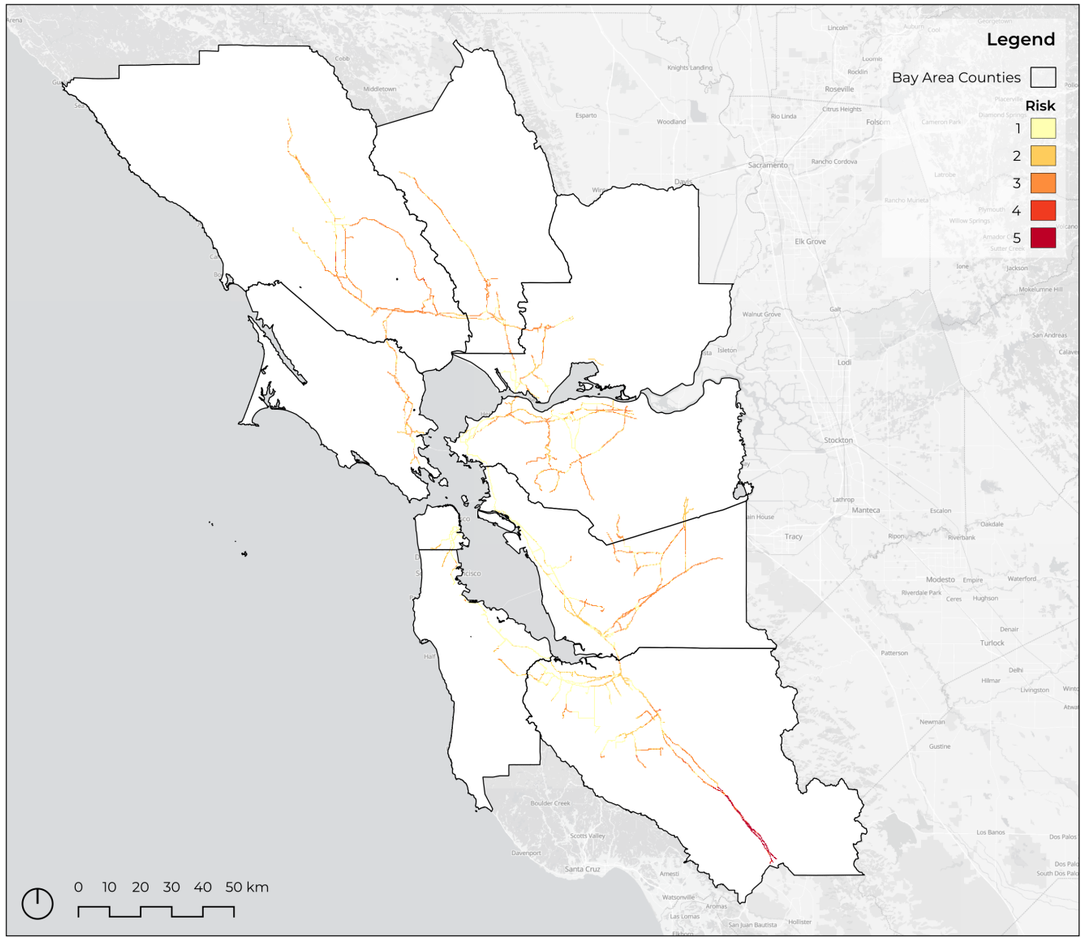

Figure 32 *Additive liquefaction risk.*

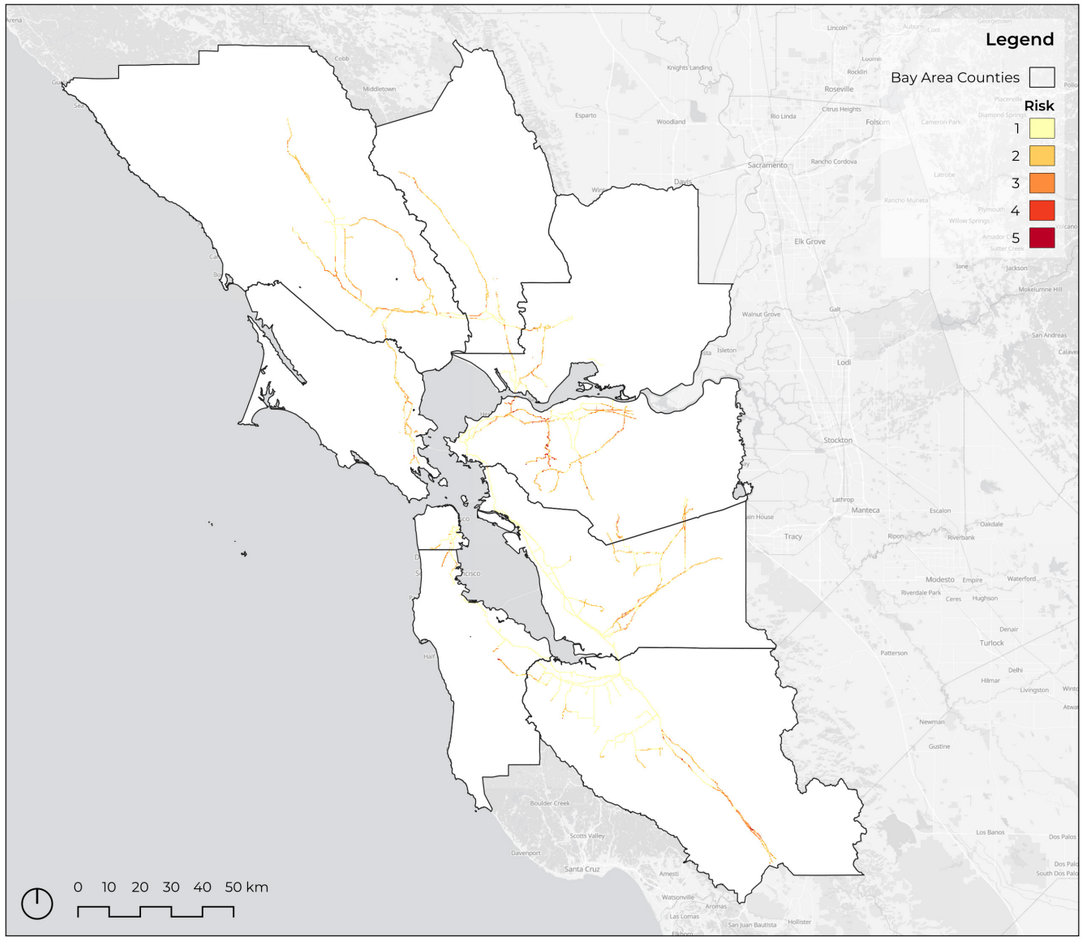

Figure 33 *Additive landslides risk.*

Method 2: Matrix Hazard Index

Method 2 employs a joint hazard matrix to characterize the interaction between earthquake-induced pipeline fragility and fire potential at a given pixel level. This approach preserves the full set of possible combinations between the two input rasters (both classified on a 1-5 scale) while allowing a direct interpretation of how these two hazards overlap spatially. Each pixel is assigned a two-digit code ranging from 11 to 55, where the first digit corresponds to the pipeline fragility class Pand the second digit corresponds to the fire potential class *F*. As an example, a pixel coded as 55 indicates the simultaneous presence of the highest pipeline fragility and highest fire potential, whereas a value of 11 reflects minimal hazard in both dimensions.

To facilitate quantitative comparison and visualization, the matrix values were further transformed into a joint hazard score. The two digits were first separated into their individual components, and a combined score was calculated as the arithmetic mean:

$$H = \frac{P + F}{2}$$

This formulation retains the independence and interpretability of the original hazard components while generating a continuous measure of combined hazard on a 1-5 scale. The resulting values were then grouped into five classes representing very low, low, moderate, high, and very high joint hazard conditions. In this classification scheme, pixels with H ≥ 4.5 were assigned to the Very High class, while those with H < 2.0 were assigned to the Very Low class, with intermediate classes defined using equidistant thresholds (see Table 16). Each of the 25 matrix codes (11-55) was subsequently reclassified into one of these five hazard categories according to its computed value of *H* (see Table 17). This direct mapping ensures that no information is lost in the transition from the matrix representation to the final hazard layer.

Hazard Class	Threshold (H)
5	H ≥ 4.5
4	4.0 ≤ H < 4.5
3	3.0 ≤ H < 4.0
2	2.0 ≤ H < 3.0
1	H < 2.o

Table 16 *Matrix risk reclassification ranges.*

The matrix method provides several important advantages. Its principal strength lies in its ability to preserve the full structure of the two-dimensional hazard space, allowing combinations of pipeline fragility and fire potential to be examined explicitly rather than collapsed prematurely into a single continuous score. This makes the method particularly effective for interpreting the joint behavior of hazards; combinations such

Hazard Class	Matrix Values (P, F)
5	45, 54, 55
4	35, 44, 53
3	15, 24, 25, 33, 42, 43, 51, 52
2	13, 14, 22, 23, 31, 32, 41
1	11, 12, 21

Table 17 *Matrix values classified by risk.*

as high pipeline fragility with moderate fire potential, or moderate pipeline fragility with high fire potential, remain distinguishable and can be analyzed in detail. The method also offers strong interpretability, as the two-digit codes transparently reflect the underlying hazard components and their contributions to the final classification. This interpretability is valuable for communicating results to stakeholders and for understanding the drivers of high-hazard outcomes.

Despite its clarity and flexibility, the matrix method also introduces certain limitations. The discrete nature of the matrix codes can produce a map with many classes, some of which may occur infrequently, resulting in visual complexity and potential difficulty in discerning broader spatial patterns. The method also requires an additional step of reclassification to convert the matrix codes into a more manageable number of hazard categories, and the choice of classification thresholds introduces some degree of subjectivity. While the arithmetic mean provides a balanced way to integrate both hazard components, it implicitly applies equal weighting, which may not always reflect operational priorities or physical processes. Furthermore, although the matrix captures all combinations, it does not inherently quantify the relative severity of different pairings without the additional step of reclassification.

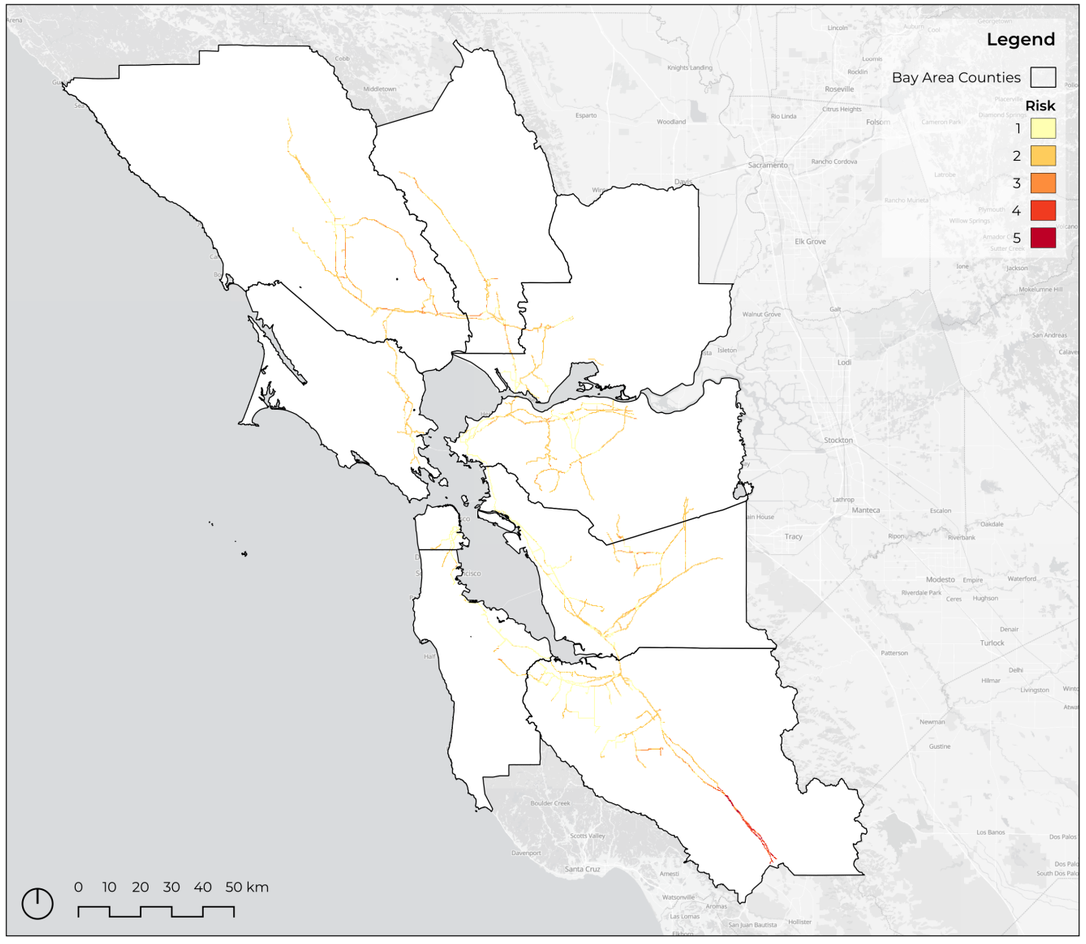

Figure 34 *Matrix liquefaction risk.*

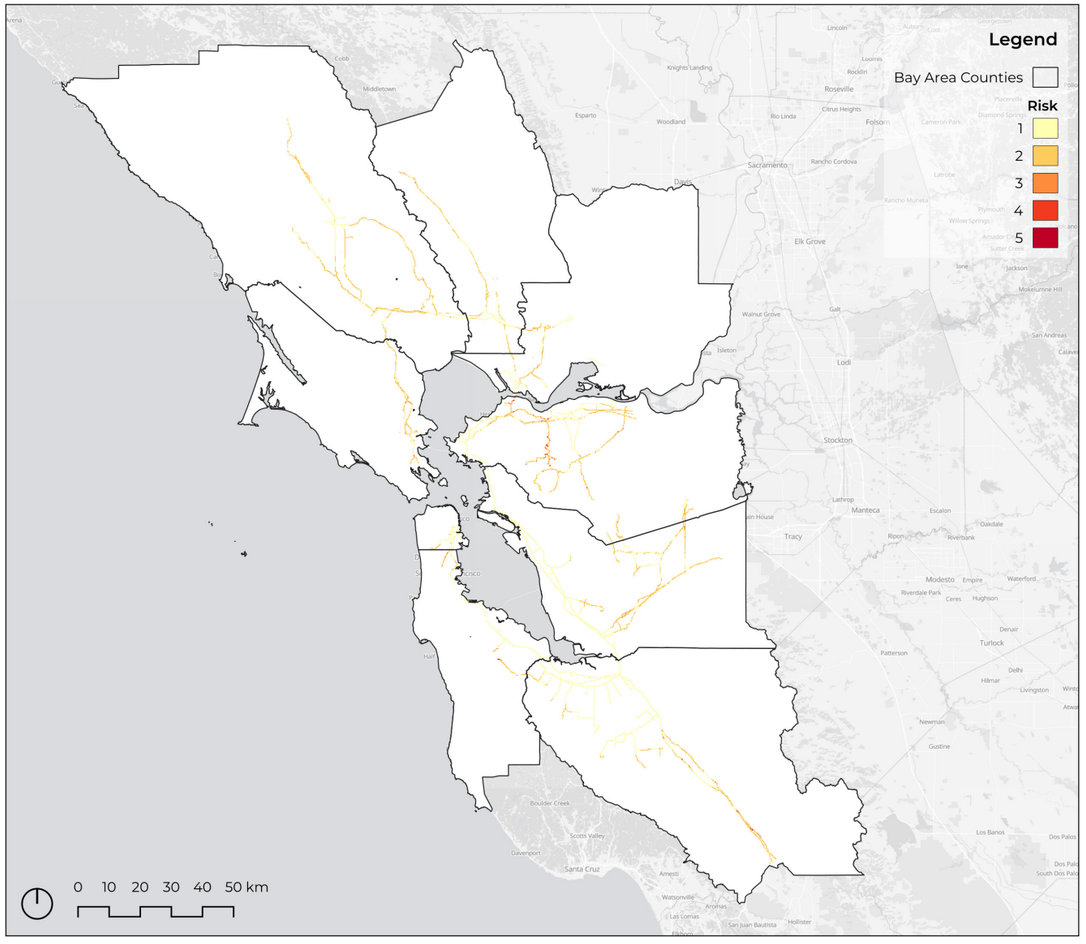

Figure 35 *Matrix landslides risk.*

Method 3: Binary Hazard Index

Whereas Methods 1 and 2 focus on continuous gradations in hazard conditions, Method 3 aims to identify only those areas where earthquake-induced pipeline fragility and fire potential simultaneously reach high levels. This binary hotspot detection approach isolates the most severe co-occurrences of risk factors and is therefore particularly relevant for emergency management, hazard mitigation policy, and targeted maintenance interventions. The method classifies a pixel as a high-risk hotspot if both the pipeline fragility class P and the fire potential class F meet or exceed 4. Formally, the hotspot score H_h is defined as:

$$H_h = \begin{cases} 1, & \text{if } P \geq 4 \text{ and } F \geq 4 \\ 0, & \text{otherwise} \end{cases}$$

The resulting raster is strictly binary, distinguishing only between critical overlap zones (value 1) and all other areas (value 0). To assess the sensitivity of the hotspot classification to the chosen threshold, a supplementary evaluation was conducted using a relaxed threshold of $P \geq 3$ and $F \geq 3$, enabling an examination of how the spatial distribution of hotspots responds to broader inclusion criteria.

The hotspot approach offers a clear advantage in its interpretability and operational clarity. By presenting only the most severe joint hazard conditions, the method effectively highlights locations where immediate action, inspection, or reinforcement may be warranted. This clarity makes the hotspot map particularly useful for decision-makers who require rapid identification of priority areas without the complexity of gradient-based models. The method is also stringent in its identification of severe co-occurrence, ensuring that only genuinely high-risk conditions are highlighted and that moderate-risk areas do not dilute the analysis.

Nevertheless, the strengths of the hotspot method are accompanied by important limitations. Because the classification depends entirely on a predefined threshold, results can vary substantially depending on whether the cutoff is set at ≥ 4, ≥ 3, or some other value, introducing an element of subjectivity into the analysis. The binary nature of the output also leads to a significant loss of information, as all non-hotspot areas are treated uniformly even when they differ substantially in their underlying risk composition. Transitional zones that may still pose meaningful hazard, such as areas with high pipeline fragility but only moderate fire potential, are excluded entirely from the hotspot category, which may underrepresent their significance in a broader risk management context. Consequently, the hotspot approach is best interpreted as a complementary decision-support layer rather than a full replacement for continuous hazard models.

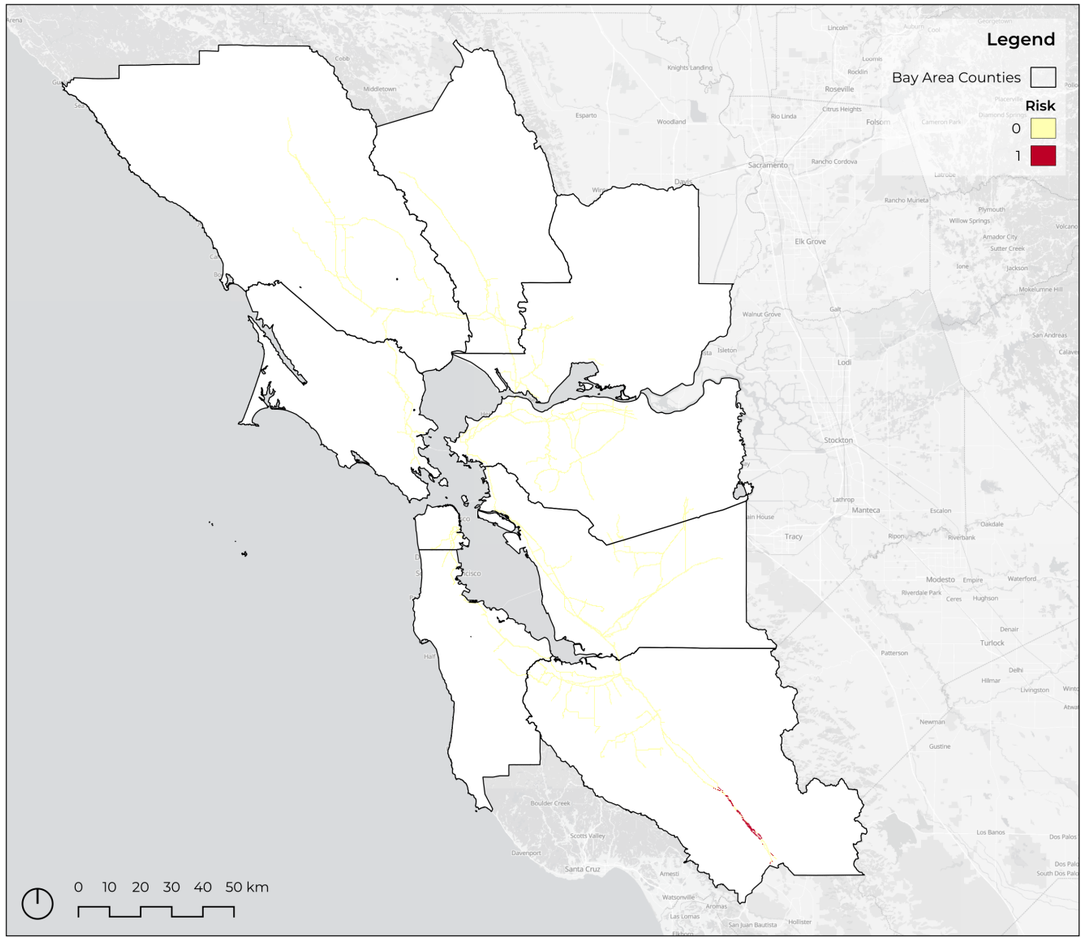

Figure 36 *Binary liquefaction risk.*

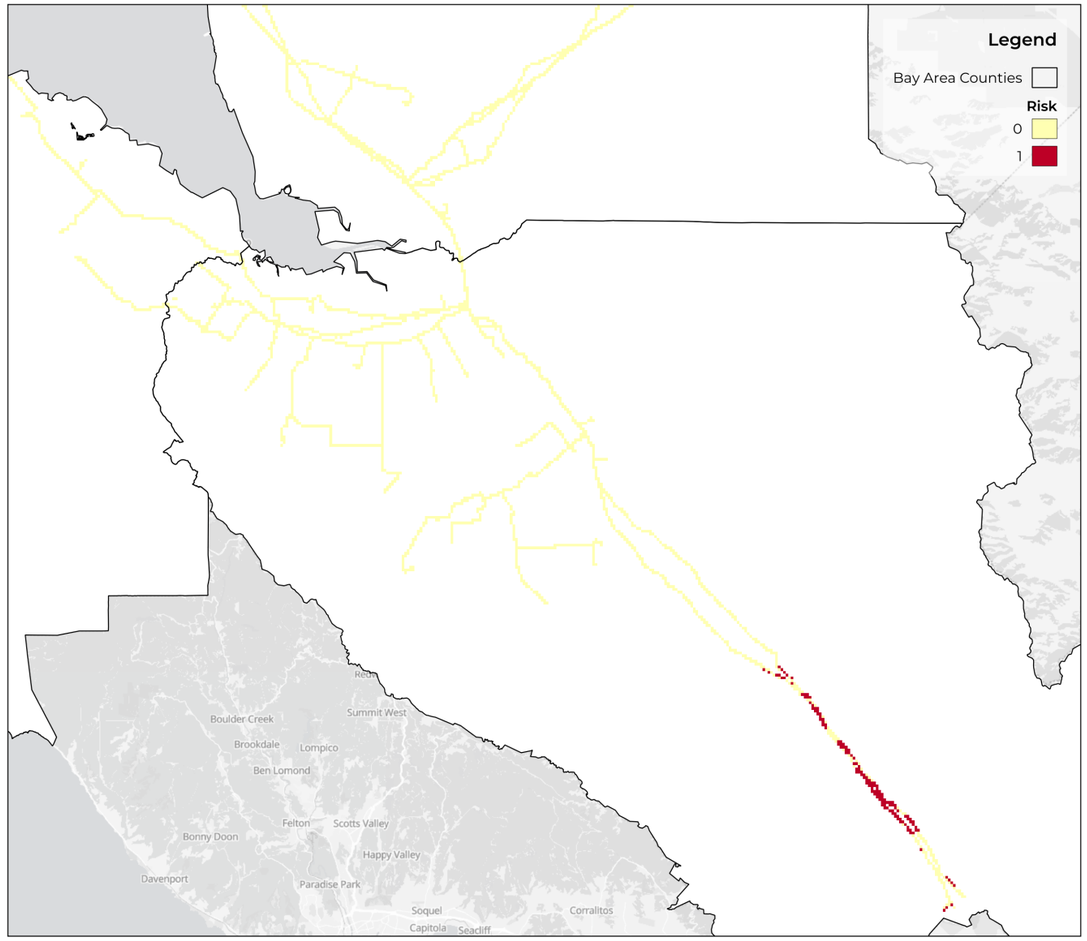

Figure 37 *Binary liquefaction risk close-up.*

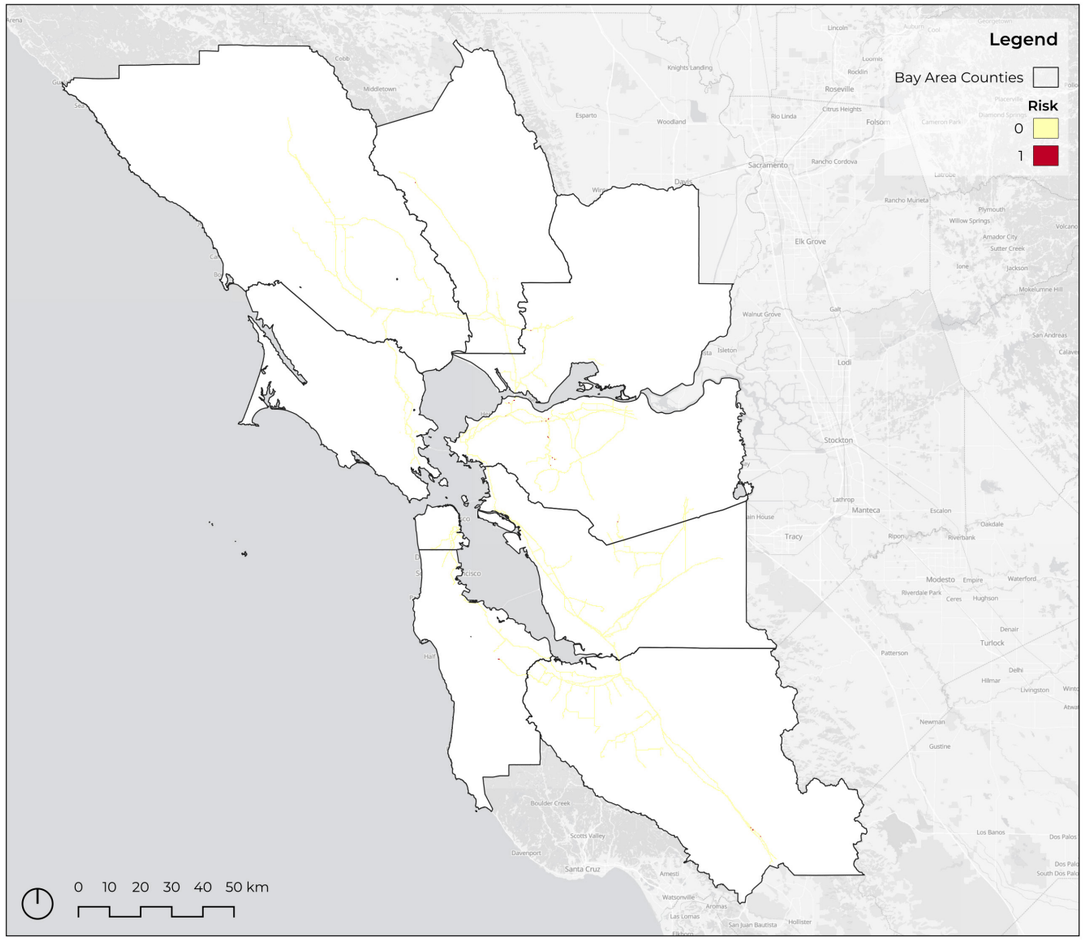

Figure 38 *Binary landslides risk.*

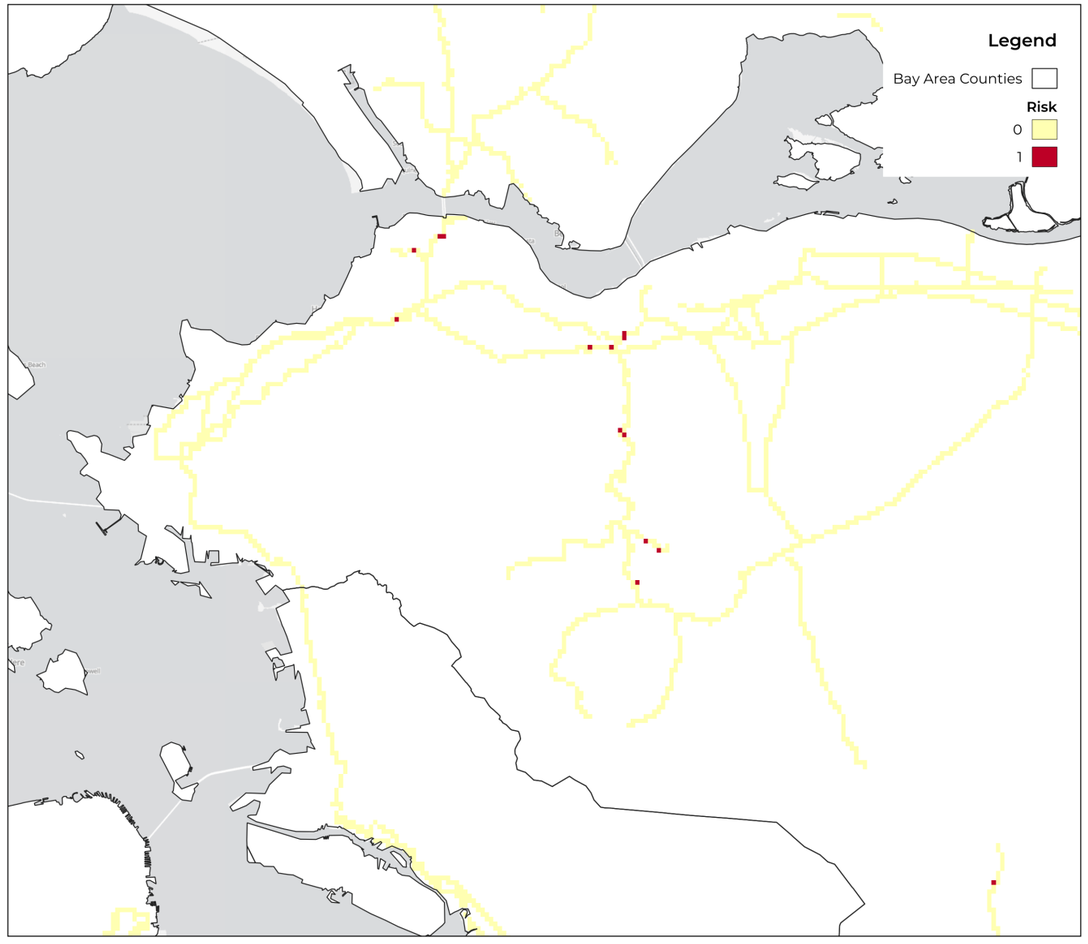

Figure 39 *Binary landslides risk close up.*

8. RESULTS AND DISCUSSION

8.1 Wildfire Hazard

The fire risk map for the San Francisco Bay Area (see Figure 13) illustrates a distinct spatial structure in wildfire susceptibility, shaped primarily by topography, vegetation distribution, and the degree of urbanization. The lowest risk zones, shown in yellow, are concentrated in the region's most urbanized, flat, and heavily modified landscapes, while the highest risk zones, shown in dark orange and red, dominate the vegetated uplands and mountainous areas.

San Francisco County stands out clearly as the area with the smallest overall fire risk. As one of the most densely populated counties in the United States, it contains minimal natural vegetation and virtually no Wildland-Urban Interface (WUI) zones. Its built landscape, coastal setting, and lack of extensive fuel beds produce a nearly continuous swath of low-risk classification, making it the least susceptible county in the region to fire activity.

Along the bayshore, a consistent pattern emerges across San Mateo, Santa Clara, and Alameda Counties. Each shows a broad corridor of low fire risk adjacent to the shoreline, reflecting the flat terrain, absence of steep slopes, and fragmented or urbanized land covers in these areas. Moving inland, fire risk increases progressively as these counties transition into hillier terrain. Here, the landscape shifts toward denser vegetation, stronger fuel continuity, and more extensive WUI zones, creating the conditions associated with medium to very high risk. Santa Clara County is the main exception to the general bayshore pattern: its interior low-risk corridor extends much farther inland than in San Mateo or Alameda, reaching deep into the Santa Clara Valley and encompassing San José and its surrounding communities. This reflects a wide expanse of urban development and relatively open valley floor that limits fuel availability.

In contrast, Marin, Sonoma, and Napa Counties exhibit some of the highest fire risk values in the region. Their rugged topography, extensive forest and shrubland cover, and large continuous tracts of natural vegetation drive the concentration of high and very high risk zones. The mountainous terrain of western Marin, the forested areas of Napa's eastern ridges, and the chaparral and oak dominated foothills of Sonoma form an extensive surface of the upper three categories of fire risk. Small pockets of low risk do appear along their edges near the Bayshore, particularly around San Pablo Bay and the lower-lying areas near Santa Rosa, Sonoma, and Napa City, where flatter topography and reduced vegetation moderate fire potential.

Solano County is one of the counties with the smallest overall fire risk, second only to San Francisco. Much of its landscape, particularly toward the Sacramento Valley, consists of flatter terrain, agricultural areas, and lower-density vegetation, resulting in extensive low-risk zones. Like Marin, Napa, and Sonoma, Solano also has additional low-risk stretches along the San Pablo Bay shoreline, reinforcing the pattern of reduced susceptibility in low-lying coastal plains.

Contra Costa County displays a more mixed pattern, with very high fire risk concentrated in its central upland areas, called the East Bay Hills, where steep hills and continuous vegetation create favorable conditions for wildfire spread. In contrast, the low-risk zones cluster along the San Francisco Bay margin to the west and extend eastward toward the flatter lands in the direction of Stockton These gradients reflect

the county's sharp topographic transitions between its coastal plain, interior valleys, and the elevated ridges of the Diablo Range.

Overall, the map highlights a consistent regional dynamic: low fire risk aligns with urbanization, valley floors, and flat coastal plains, while high risk dominates the vegetated, mountainous belts that frame the Bay Area. This spatial pattern closely mirrors historical fire occurrences (see Figure 14) and underscores the role of topography, vegetation, and land use in shaping the region's wildfire susceptibility.

8.2 Seismic Hazard

The seismic hazard analysis performed on OpenSRA reveals clear patterns of both liquefaction and landslide susceptibility in the San Francisco Bay Area, exposing pipelines across the entire region. These patterns reflect the region's fault system, local soil conditions, and, most important, the distribution of critical infrastructure across the counties. The OpenSRA results clearly highlight areas where modeled seismic activity is most likely to disrupt the gas network.

The liquefaction-prone soils of the area pose a substantial threat to gas pipelines, as buried infrastructure can experience displacement, joint separation, and rupture when saturated soils lose strength under intense shaking.

This study found that gas pipelines exposed to earthquake-induced liquefaction tend to experience tensile damage, with both rupture and leakage happening at different points, while compressive failures do not occur at all. This can be explained by how liquefied soil behaves and how pipelines interact with it.

As the soil liquefies, it loses much of its strength and can no longer firmly support the pipeline. As a result, the pipe may become partly unsupported while the surrounding ground moves in different directions. Ground movements such as settlement or lateral spreading usually pull the soil apart rather than push it together, meaning the ground suffers horizontal extension. Parts of the pipeline that remain anchored in firmer soil resist this movement, causing the pipe to stretch and bend. These forces increase tensile strain and can lead to cracking or rupture. In contrast, compressive failure, which requires the pipe to be pushed together, rarely occurs during liquefaction because the ground almost never shortens in these conditions. Instead, the weakened soil moves in a way that causes extension, not compression. Even when bending causes some compression on one side of the pipe, the tension on the other side is usually larger and controls the failure.

This explains why tensile damage was observed in the modeled pipeline while compressive damage was not. These findings closely match patterns observed in major international earthquakes, such as the 1964 Niigata earthquake, where widespread liquefaction and lateral spreading caused severe deformation and tensile failures in buried utilities (Hamada and O'Rourke 1992). This emphasizes the need to consider tensile strain capacity and ground movement patterns when evaluating pipeline performance in liquefaction-prone areas.

The results seen in the previous section (see Figures 21 and 22) paint the picture of the immense impact liquefaction-induced settlement damage has in the San Francisco Bay Area. Significant portions of the Bay shoreline and valley floors exhibit high liquefaction potential due to their composition of artificial fill, alluvial soils, and shallow groundwater. Notable hotspots include the shore margins of the Alameda, Contra Costa, Santa Clara and San Mateo counties, with high liquefaction susceptibility going from Richmond all the way past Freemont, and around the bay towards Palo Alto. It is also present in the low stretches of land between Sonoma and Santa Rosa, and all around Napa. It is also highly present in the low-lying portions of the Santa Clara Valley going from San Jose all the way to Gilroy, with this stretch being the one with the highest susceptibility score.

In addition to liquefaction, the Bay Area is also at risk of experiencing major landslides. Landslide-prone slopes can greatly endanger gas pipelines, as the infrastructure can experience loading, bending, and rupture when unstable ground masses rapidly shift downslope during seismic activity.

This research found that earthquake-induced landslides caused compressive damage to the gas pipelines, while no tensile rupture or leakage occurred. This outcome is, similar to liquefaction, mainly due to how the ground moves during a landslide and how said movement impacts buried pipelines.

During a landslide, the soil mass typically moves downslope and toward stable ground, causing the ground to shorten rather than stretch. This means the ground is suffering horizontal compression. Because parts of the pipeline remain anchored in stable soil, the moving soil effectively pushes the pipe, creating compression. Situations that would pull the pipeline apart and create tension, like during liquefaction, are much less common in landslides and were not present in the scenarios analyzed.

Furthermore, the way a pipe interacts with the surrounding soil also favors compression as the main loading type. When a pipe is pushed, the soil provides strong resistance, which builds up significant compressive forces on it. However, when the pipe is pulled, the soil offers much less resistance or may even separate from the pipe, allowing tension to be relieved before it can cause serious damage.

Additionally, steel pipelines can usually tolerate more tensile strain without failing, but they are much more vulnerable to buckling and wrinkling under compression. Even moderate compressive strains can lead to local instability, especially when the pipe is confined by soil.

Overall, this combination of factors explains why compressive rupture occurred during landslides simulation while tensile damage did not. It is possible to draw a comparison between these findings and those of a landslide-related pipeline failure reported in the literature. In March 2019, a major landslide in Taleqan, Iran, triggered by extreme rainfall, caused a 16-inch natural gas pipeline to rupture when the downslope soil movement pushed the pipe, creating high compressive forces and bending at a girth weld (Vasseghi et al. 2021). Although this event was rainfall-induced, the comparison should not be undermined as the damage mechanism is directly relevant to earthquake-induced landslides as well, seeing as both hazards generate similar patterns of ground movement that place buried pipelines under intense compression and localized deformation. These results stress that pipeline design and evaluation in regions vulnerable to landsliding must prioritize the management of compressive deformation and the mitigation of buckling hazards.

Drawing from the previous section, Figure 28 makes it clear that landslides-induced damage, although present, is not as problematic a deformation mechanism in the Bay Area as liquefaction. This can be clearly seen when comparing Figures 21 and 28. However, the area still shows some significant damage hotspots. The region of highest concern is in the East Bay Hills, especially in the part right to the north of the city of Lafayette. It is also somewhat present along the shore on the Carquinez Strait, between the cities of Martinez and Crockett. Less significant damage is also present to the east of Marin county, in an area of the Diablo Range to the east of the city of Freemont, and very sparsely along the stretch between San Jose and Gilroy.

8.3 Compound Hazard

The three hazard modelling approaches applied in section 7.3 of this study, (1) the additive hazard index, (2) the matrix hazard index, and (3) the binary hazard index, offer different perspectives on the interaction between earthquake-induced pipeline fragility and fire potential. Although all rely on the same underlying 1-5 normalized input rasters, each method conceptualizes and represents the multi-hazard environment in distinct ways, thereby influencing both the interpretation and the practical applicability of the results.

Method 1, the additive hazard index, provides a smooth and continuous spatial representation of compound hazard by summing the pipeline fragility and fire potential values. This produces a gradient-like surface in which hazard intensity increases whenever either input increases. The strength of this method lies in its simplicity and ease of interpretation: it clearly illustrates regional patterns and broad transitions in multi-hazard exposure. However, the additive approach also has significant limitations. By collapsing two hazard dimensions into a single total, it may obscure meaningful differences between combinations that produce the same sum. For instance, a pixel with extremely fragile pipelines but low fire potential may be assigned the same score as an area with moderate fragility and moderate fire potential, despite the distinct hazard dynamics implied by each scenario. Moreover, the method assumes equal weighting of the two hazard components, an assumption that may not always reflect operational or physical realities.

Method 3, the binary hotspot detection approach, offers a different perspective by isolating only the most severe co-occurrences of high pipeline fragility and high fire potential. It identifies a pixel as a hotspot only when both input values exceed a defined threshold, thereby producing a clear and decisive delineation of the most critical areas. This method is effective for highlighting zones that may warrant urgent attention from managers or emergency response planners. Yet its stark binary structure leads to substantial information loss: all areas that fall below the chosen threshold, even if only marginally, are treated uniformly despite potentially significant underlying differences in hazard levels. Furthermore, hotspot identification is inherently sensitive to the choice of threshold, and modest adjustments can cause substantial changes in the spatial extent of the resulting high-risk zones. As such, Method 3 is valuable as a supplementary diagnostic layer but less suitable as a primary modelling framework.

Positioned between these two approaches, Method 2, the joint risk matrix, offers a more balanced and information-rich representation of the multi-hazard landscape. By encoding each pixel using a two-digit value that preserves both the pipeline fragility and fire potential classes, the method retains the full structure of the combined hazard space. This makes it possible to distinguish between different combinations that would otherwise be collapsed into the same value under an additive approach, for example, high pipeline fragility with moderate fire risk versus moderate fragility with high fire risk. The subsequent reclassification into joint hazard categories provides a generalized yet transparent summary of these combinations while maintaining fidelity to the underlying drivers of risk. Unlike Method 3, Method 2 avoids abrupt cutoffs and preserves nuance across intermediate hazard levels. Unlike Method 1, it does not obscure the internal composition of hazard contributions.

A more practical, map-based explanation of the methods helps show why the matrix approach is especially useful for this study. When looking at the resulting maps, the additive method consistently shows higher risk levels for both liquefaction and landslides (see Figures 21, 23, 28 and 30), often making long sections of pipeline appear more vulnerable than they actually are. This can create the impression that many more pipelines need urgent attention, which may shift focus away from the areas where the risk is truly serious. In many cases, segments marked as high risk in the additive map are reduced to moderate risk when evaluated with the matrix method, giving a more realistic picture of where the most important problems are.

These differences matter for planning and decision-making. The matrix method provides a clearer view of how hazard intensity and pipeline vulnerability interact, helping authorities identify the areas that genuinely require immediate action. This allows resources, such as maintenance work, monitoring efforts, or emergency planning, to be directed to the segments where failure would have the most significant impact. For this study, the matrix map is therefore the most reliable tool for understanding the real distribution of pipeline risk.

After those highest-priority segments have been dealt with, the additive map becomes useful as a secondary reference. Because it tends to give higher values overall, it highlights additional pipelines that may not require urgent intervention but could still benefit from long-term monitoring or future upgrades. In this sense, the additive method helps identify medium-priority areas once the most critical ones have already been addressed.

The binary method, however, goes in the opposite direction. It underestimates risk by showing only the pipeline segments that fall into the very high risk category. This means it ignores all other segments that still represent a potential threat. As a result, the binary map is too simplified for effective planning, since it overlooks many areas that should not be ignored.

The comparison of the three methods suggests that each plays a distinct role in characterizing multi-hazard interactions. Method 1 is useful for visualizing regional hazard gradients; Method 3 is effective for identifying the most critical overlap zones; but Method 2, through its explicit preservation of the individual hazard components and their combinations, offers the clearest and most analytically robust depiction of the interaction between pipeline fragility and fire potential, making it the most suitable for governing bodies in charge of monitoring, fixing and upgrading the network, as well as to emergency responders and planners.

8.4 Implications for Infrastructure, Government and Communities

The multi-hazard assessment presented in this thesis demonstrates how wildfire potential interacts with earthquake-induced liquefaction and landslide-related pipeline fragility across the San Francisco Bay Area. These findings have important implications for infrastructure managers, public agencies, and the communities that rely on this critical network.

Implications for Infrastructure Management

The analysis shows that liquefaction is the most widespread and damaging seismic hazard for gas pipelines in the region. Because liquefaction-induced ground deformation predominantly generates tensile forces, pipeline operators should prioritize engineering strategies that enhance tensile strain capacity, improve joint flexibility, and mitigate vulnerability to lateral spreading. High-priority corridors include the low-lying bayshore margins in Alameda, Contra Costa, San Mateo, and Santa Clara Counties, as well as the Santa Clara Valley and the Napa-Sonoma lowlands.

Although landslide-induced pipeline damage is less spatially extensive, its consequences are structurally severe. Landslides impose compressive and bending forces that can lead to buckling and rupture, failure modes to which steel pipelines are particularly vulnerable. Hotspots identified in the East Bay Hills, the Carquinez Strait, and parts of the Diablo Range require targeted mitigation such as slope stabilization, soil-strengthening measures, and enhanced monitoring. Importantly, because landslides occur on steep slopes, any pipeline failure in these areas carries an elevated risk of igniting fires that can propagate rapidly through the slopes. This means that even relatively small landslide-related pipeline failures can escalate into larger, fast-moving fire incidents, amplifying their potential impact on infrastructure and surrounding communities.

The matrix compound hazard method supports infrastructure planning by distinguishing between hazard combinations that would otherwise be obscured. For pipeline operators, this provides a clearer basis for prioritizing inspections, upgrades, and emergency planning in locations where pipeline fragility and fire potential converge most critically.

Implications for Government Agencies and Emergency Planning

For state, regional, and county agencies, the compound hazard findings underline the need for integrated seismic and wildfire preparedness strategies. Again, the matrix method offers the most realistic representation of where hazards interact, making it a valuable decision-support tool for allocating resources, enforcing safety standards, and coordinating emergency response efforts.

Liquefaction-prone areas that coincide with moderate or high wildfire susceptibility are especially important for government planning, as post-earthquake gas leakage could trigger fires in regions where suppression is more difficult. In contrast, landslide-prone regions require a different focus: because these areas are steep and heavily vegetated, they not only expose pipelines to compressive rupture but also present terrain conditions highly conducive to fire spread. Steep slopes accelerate flame movement, increase radiant heat transfer, and allow fires to grow more rapidly than in flat terrain. This amplifies the importance of pre-event mitigation, early detection systems, and rapid suppression capacity in hillside counties such as Marin, Contra Costa, Alameda, and Sonoma.
These patterns justify greater interagency coordination between fire authorities, geotechnical units, and pipeline regulators, ensuring that emergency plans incorporate both the probability of pipeline failure and the fire behavior characteristics of the surrounding terrain.

Implications for Communities and Public Safety

For communities, the results clarify where seismic damage to pipelines is most likely and how such damage could interact with local wildfire conditions. Residents in liquefaction-prone urban corridors face elevated risks of gas leakage and potential ignition following major earthquakes. Public outreach and preparedness programs, such as emergency shutoff awareness, evacuation planning, and household resilience measures, can directly reduce these risks.

Communities located in or near landslide-prone hillsides face a dual vulnerability: the possibility of pipeline rupture due to ground compression, and the significantly higher fire propagation potential typical of sloped terrain. Fires that start in these areas can grow more rapidly, spread farther, and reach communities faster. They can also block important transportation corridors and isolate populations. This underscores the need for strengthened public education around fire behavior in steep landscapes, improved defensible space practices, fuel management, and participation in neighborhood evacuation and alert systems.

Finally, the compound hazard maps produced in this study can support transparent risk communication, helping communities understand not only which hazards they face, but how those hazards interact. This enables residents, local leaders, and emergency organizations to plan more effectively and build resilience.

8.5 Limitations of the Study

Despite the structured approach used in this thesis, several limitations must be acknowledged. These stem mainly from data availability, methodological simplifications, and the challenges of modeling complex, overlapping hazards in the San Francisco Bay Area.

First, the study relies on spatial datasets that differ in age and how often they are updated. Seismic hazard layers reflect long-term probabilities, while wildfire datasets, especially fuel and vegetation information, capture conditions from past years rather than current states. Because vegetation and fire behavior are changing rapidly due to climate change, the hazard maps used here may not fully represent present-day or future conditions.

Second, limitations in pipeline data affect the precision of the fragility analysis. The transmission pipeline network used in this study comes directly from PG&E, which ensures that the information regarding these large-diameter pipelines is highly accurate. However, this analysis does not include the distribution pipeline network, which is typically more extensive and reaches deeper into residential neighborhoods. Distribution pipeline data is not available due to security reasons and the absence

of this data reduces the completeness of the analysis, since damage to distribution pipelines could significantly influence local risk patterns and affect areas not reached by the transmission system.

Third, the hazard integration method is static and does not account for real-time or cascading interactions. For example, an earthquake-induced gas leak during extreme wind conditions would pose a very different fire risk than a leak on a calm, humid day. The model also does not include factors such as fire suppression capacity, road closures, or water system failures, which can strongly influence disaster outcomes. These dynamic processes fall outside the scope of this spatial overlay approach but are important in real events.

Fourth, the weighting choices used to combine hazard layers introduce some subjectivity to the study. Although weights were informed by existing literature, alternative choices could reflect different priorities or assumptions, and no sensitivity analysis was performed to test how different weights might change the results.

Finally, the study focuses on physical hazards and pipeline vulnerability but does not integrate social vulnerability factors that shape how communities experience and recover from disasters. Characteristics such as income, age, disability, race, immigrant status, linguistic isolation, and access to transportation or health services strongly influence a community's exposure and resilience. Including such metrics would allow for a more complete understanding of who is most at risk, but this requires additional datasets and a broader modeling framework than what was used in this thesis.

8.6 Future Research

The results of this study highlight several promising avenues for advancing multi-hazard analysis and regional resilience planning in the San Francisco Bay Area.

A priority direction is the development of dynamic, event-based hazard models that simulate the progression of earthquake-fire interactions in real time. This could include modeling pipeline rupture likelihood under varying wind conditions, fuel moisture levels, and seasonal fire-weather extremes (such as Diablo winds). Integrating dynamic emergency response variables like travel-time delays, water system failures, and communication disruptions would provide a more realistic representation of cascading disaster scenarios.

Another important direction is the incorporation of climate change projections into both wildfire and seismic-related hazard models. As vegetation composition, drought intensity, and fire-weather conditions shift, the spatial distribution of wildfire susceptibility will change accordingly. Future models should integrate downscaled climate scenarios to assess how hazard patterns may evolve over coming decades and to guide long-term adaptation planning.

Expanding multi-hazard assessments to incorporate social vulnerability metrics also represents an important next research step. Pairing physical hazard exposure with indicators such as transportation access, housing quality, and public health burdens would allow researchers to identify communities where limited adaptive capacity intersects with high hazard levels. This would support more equitable prioritization of mitigation resources and emergency planning.

Finally, future research should explore cross-jurisdictional coordination frameworks that reflect the regional nature of Bay Area hazards. Earthquakes, wildfires, and pipeline systems transcend municipal boundaries, yet planning and response capacities vary widely between jurisdictions. Multi-county data-sharing agreements, integrated scenario planning, and joint emergency-response exercises could significantly enhance resilience. Research into collaborative governance models would help bridge these gaps and support a more unified regional approach to compound hazard management.

9. CONCLUSION

The research conducted in this thesis illustrates how California's evolving hazard environment requires analytical approaches capable of addressing the interconnected nature of natural disasters and the vulnerabilities of critical infrastructure. Earthquakes, landslides, liquefaction, and the pressures of climate and development intersect in ways that challenge long-standing assumptions about how infrastructure performs under stress. Among the systems most exposed to this shifting reality are natural gas networks, lifelines that operate quietly beneath the surface but whose failure during earthquakes can trigger consequences far beyond the initial ground shaking. Understanding how these failures emerge, and how different hazards converge to shape them, has become more than a technical question; it is a matter of public safety, energy security, and long-term resilience.

This work responds to that need by bringing together tools and perspectives that have rarely been integrated. Through the combination of OpenSRA's performance-based modeling with spatial multi-criteria analysis, the research forms a methodological bridge between detailed engineering assessment and regional hazard evaluation. Instead of treating liquefaction, landslides, and other ground-failure mechanisms as isolated phenomena, the framework allows them to be examined together, highlighting how they co-occur, reinforce each other, and ultimately influence pipeline behavior along different segments of the network. This represents a notable step forward in a field where compound hazards are often acknowledged but seldom quantified with such clarity.

The results make these interactions tangible. Liquefaction emerges as a defining driver of risk in the Bay Area, with clear patterns of tensile rupture and leakage in low-lying, water-saturated zones. The absence of compressive rupture in the modeled scenario helps refine the understanding of how local geologic conditions translate into distinct performance outcomes. The combined risk map, produced by normalizing and synthesizing the hazard layers, underscores these patterns visually and analytically: the highest concentrations of vulnerability trace the shorelines, floodplains, and sedimentary basins stretching from the central Bay to the Santa Clara Valley. Such insights offer a level of precision that is valuable not only to researchers but also to utilities seeking to target investments, prioritize inspections, or plan emergency response strategies.

Beyond the specific findings, the broader contribution of the research lies in the emergence of a methodological framework that is adaptable, transparent, and scalable. Its structure, open-source, data-driven, and grounded in performance-based engineering, makes it relevant not only for the Bay Area but for utility operators throughout California and the United States. As hazards become more interconnected and infrastructure systems more stressed, methods capable of capturing these interactions are no longer optional; they are essential. This thesis demonstrates how such an approach can be constructed and applied in practice, turning complex scientific models into decision-support tools with real operational value.

At the same time, the work opens pathways for future enhancement. Higher-resolution geotechnical data, richer pipeline attribute information, and the incorporation of additional compounding factors, such as rainfall-triggered slope instability or post-earthquake fire ignition, would deepen the analytical power of the framework. As data availability expands and hazard modeling advances, the methodology presented here can evolve into an even more comprehensive system for anticipating,

visualizing, and mitigating risk.

Instead of viewing the findings as an end point, this research positions itself as the beginning of a larger shift in how critical infrastructure risk is understood. The methodology developed here demonstrates that complex hazard interactions can be translated into tools that directly support decision-making, but it also reveals how much untapped potential remains. As utilities move toward modernization, climate pressures intensify, and expectations for reliability grow, the ability to anticipate system behavior under multi-hazard conditions will increasingly define the difference between reactive management and true resilience. The framework introduced in this work offers a blueprint for that evolution, not as a fixed solution, but as a foundation that future researchers, practitioners, and agencies can expand, refine, and adapt. Its value lies not only in the insights it generates today but in the doors it opens for integrating new data, new models, and new ways of thinking about infrastructure in a hazard-prone world. In this sense, the thesis contributes more than an assessment: it marks a turning point toward a more holistic, science-driven, and anticipatory approach to safeguarding lifeline systems.

10. BIBLIOGRAPHY

Aagaard, Brad T., J. Luke Blair, John Boatwright, et al. 2016. “Earthquake Outlook for the San Francisco Bay Region 2014–2043.” In Fact Sheet, Nos. 2016–3020. U.S. Geological Survey. https://doi.org/10.3133/fs20163020.

Abatzoglou, John T., and A. Park Williams. 2016. “Impact of Anthropogenic Climate Change on Wildfire across Western US Forests.” Proceedings of the National Academy of Sciences 113 (42): 11770–75. https://doi.org/10.1073/pnas.1607171113.

Ackerly, David D., William K. Cornwell, Stuart B. Weiss, Lorraine E. Flint, and Alan L. Flint. 2015. “A Geographic Mosaic of Climate Change Impacts on Terrestrial Vegetation: Which Areas Are Most at Risk?” PLOS ONE 10 (6): e0130629. https://doi.org/10.1371/journal.pone.0130629.

Adaktylou, Nektaria, Dimitris Stratoulias, and Rick Landenberger. 2020. “Wildfire Risk Assessment Based on Geospatial Open Data: Application on Chios, Greece.” ISPRS International Journal of Geo-Information 9 (9): 516. https://doi.org/10.3390/ijgi9090516.

Alasiri, Muhannad R., Rachel Chicchi, and Amit H. Varma. 2021. “Post-Earthquake Fire Behavior and Performance-Based Fire Design of Steel Moment Frame Buildings.” Journal of Constructional Steel Research 177 (February): 106442. https://doi.org/10.1016/j.jcsr.2020.106442.

Alexander, David, and Gianluca Pescaroli. 2019. “What Are Cascading Disasters?” UCL Open Environment 1. https://doi.org/10.14324/111.444/ucloe.000003.

Alexandre, Patricia M., Susan I. Stewart, Nicholas S. Keuler, et al. 2016. “Factors Related to Building Loss Due to Wildfires in the Conterminous United States.” Ecological Applications 26 (7): 2323–38. https://doi.org/10.1002/eap.1376.

Amiri, Afshin, Silvio Gumiere, and Hossein Bonakdari. 2025. “Firestorm in California: The New Reality for Wildland-Urban Interface Regions.” Urban Climate 62 (August): 102528. https://doi.org/10.1016/j.uclim.2025.102528.

Amos, Colin B., Pascal Audet, William C. Hammond, Roland Bürgmann, Ingrid A. Johanson, and Geoffrey Blewitt. 2014. “Uplift and Seismicity Driven by Groundwater Depletion in Central California.” Nature 509 (7501): 483–86. https://doi.org/10.1038/nature13275.

Bain, Christopher A. 2023. “Seismic Performance of Natural Gas Transmission Pipelines Affected by Ground Failure.” UC Berkeley.

Bain, Christopher A., Thomas D. O’Rourke, and Jonathan D. Bray. 2024. “Pipeline Response to Seismic Displacement at Balboa Boulevard during the 1994 Northridge Earthquake.” Journal of Geotechnical and Geoenvironmental Engineering 150 (2): 04023139. https://doi.org/10.1061/JGGEFK.GTENG-11886.

Balch, Jennifer K., Bethany A. Bradley, John T. Abatzoglou, R. Chelsea Nagy, Emily J. Fusco, and Adam L. Mahood. 2017. “Human-Started Wildfires Expand the Fire Niche across the United States.” Proceedings of the National Academy of Sciences 114 (11): 2946–51. https://doi.org/10.1073/pnas.1617394114.

Baquedano Juliá, Pilar, Tiago Miguel Ferreira, and Hugo Rodrigues. 2021. “Post-Earthquake Fire Risk Assessment of Historic Urban Areas: A Scenario-Based Analysis Applied to the Historic City Centre of Leiria, Portugal.” International Journal of Disaster Risk Reduction 60 (June): 102287. https://doi.org/10.1016/j.ijdrr.2021.102287.

Bay Area Census. 2020. “Population.” https://census.bayareametro.gov/population.

Bondi, Brittany, and Alyssa Kaewwilai. 2020. “Flooding, Landslides, Wildfires, Air Pollution, and Income: Risk in California.” Gettysburg Social Sciences Review 4 (1). https://cupola.gettysburg.edu/gssr/vol4/iss1/3.

Botzen, W. J. Wouter, Olivier Deschenes, and Mark Sanders. 2019. “The Economic Impacts of Natural Disasters: A Review of Models and Empirical Studies.” Review of Environmental Economics and Policy 13 (2): 167–88. https://doi.org/10.1093/reep/rez004.

Brett, Lou, Christopher J. White, Daniela I. V. Domeisen, Bart Van Den Hurk, Philip Ward, and Jakob Zscheischler. 2025. “Review Article: The Growth in Compound Weather and Climate Event Research in the Decade since SREX.” Natural Hazards and Earth System Sciences 25 (8): 2591–611. https://doi.org/10.5194/nhess-25-2591-2025.

Burrough, P.A., and R.A. McDonnell. 1998. Principles Of Geographical Information Systems. Oxford University Press.

CAL FIRE. n.d. “California Department of Forestry and Fire Protection.” CAL FIRE. Accessed November 29, 2025. https://www.fire.ca.gov/.

Cal OES. 2023. “State of California Hazard Mitigation Plan.”

Calviño-Cancela, María, María L. Chas-Amil, Eduardo D. García-Martínez, and Julia Touza. 2016. “Wildfire Risk Associated with Different Vegetation Types within and Outside Wildland-Urban Interfaces.” Forest Ecology and Management 372 (July): 1–9. https://doi.org/10.1016/j.foreco.2016.04.002.

Chow, Fotini Katopodes, Katelyn A. Yu, Alexander Young, et al. 2022. “High-Resolution Smoke Forecasting for the 2018 Camp Fire in California.” Bulletin of the American Meteorological Society 103 (6): E1531–52. https://doi.org/10.1175/BAMS-D-20-0329.1.

Chuvieco, E., I. Aguado, S. Jurdao, et al. 2014. “Integrating Geospatial Information into Fire Risk Assessment.” International Journal of Wildland Fire 23 (5): 606–19. https://doi.org/10.1071/WF12052.

Cohen, Jack D. 2000. “Preventing Disaster: Home Ignitability in the Wildland-Urban Interface.” Journal of Forestry 98 (3): 15–21. https://doi.org/10.1093/jof/98.3.15.

Comfort, Louise K. 2021. “Networks within Networks: Scaling Response Operations in the Lightning Complex Fires in Northern California, August 2020.” E3S Web of Conferences 331: 04016. https://doi.org/10.1051/e3sconf/202133104016.

Costafreda-Aumedes, Sergi, Carles Comas, and Cristina Vega-Garcia. 2016. “Spatio-Temporal Configurations of Human-Caused Fires in Spain through Point Patterns.” Forests 7 (9): 185. https://doi.org/10.3390/f7090185.

CRED. 2025. “Disaster Year In Review 2024.” May 13. https://reliefweb.int/report/world/cred-crunch-newsletter-issue-no-78-may-2025-disaster-year-review-2024.

Cruz, Ana Maria, and Maria Camila Suarez-Paba. 2019. “Advances in Natech Research: An Overview.” Progress in Disaster Science 1 (May): 100013. https://doi.org/10.1016/j.pdisas.2019.100013.

Dahl, Kristina A., John T. Abatzoglou, Carly A. Phillips, et al. 2023. “Quantifying the Contribution of Major Carbon Producers to Increases in Vapor Pressure Deficit and Burned Area in Western US and Southwestern Canadian Forests.” Environmental Research Letters 18 (6): 064011. https://doi.org/10.1088/1748-9326/acbce8.

Dashti, Shahin, Barlas Ozden Caglayan, and Negar Dashti. 2025. “Post-Earthquake Fire Resistance in Structures: A Review of Current Research and Future Directions.” Applied Sciences 15 (6): 3311. https://doi.org/10.3390/app15063311.

Debats Garrison, Jessica, and Travis E. Huxman. 2020. “A Tale of Two Suburbias: Turning up the Heat in Southern California’s Flammable Wildland-Urban Interface.” Cities 104 (September): 102725. https://doi.org/10.1016/j.cities.2020.102725.

Delforge, Damien, Valentin Wathelet, Regina Below, et al. 2025. “EM-DAT: The Emergency Events Database.” International Journal of Disaster Risk Reduction 124 (June): 105509. https://doi.org/10.1016/j.ijdrr.2025.105509.

Do, Vivian, Heather McBrien, Nina M. Flores, et al. 2023. “Spatiotemporal Distribution of Power Outages with Climate Events and Social Vulnerability in the USA.” Nature Communications 14 (1): 2470. https://doi.org/10.1038/s41467-023-38084-6.

Edgeley, Catrin M., Alexander M. Evans, Sarah E. Devenport, Gabriel Kohler, Zoë M. Zamudio, and William D. DeGrandpre. 2025. “Preventing Human-Caused Wildfire Ignitions on Public Lands: A Review of Best Practices.” Forest Science 71 (4): 493–521. https://doi.org/10.1007/s44391-025-00025-9.

Eguchi, Ronald T., James D. Goltz, Craig E. Taylor, et al. 1998. “Direct Economic Losses in the Northridge Earthquake: A Three-Year Post-Event Perspective.” Earthquake Spectra 14 (2): 245–64. https://doi.org/10.1193/1.1585998.

Ermagun, Alireza, Diego Thompson, Farshid Vahedifard, and Roxane Cohen Silver. 2025. “Emergency Managers’ Challenges with Wildfires and Related Cascading Hazards in California.” Journal of Environmental Management 374 (February): 124008. https://doi.org/10.1016/j.jenvman.2024.124008.

Farid, Arvin, Md Khorshed Alam, Venkata Siva Naga Sai Goli, et al. 2024. “A Review of the Occurrence and Causes for Wildfires and Their Impacts on the Geoenvironment.” Fire 7 (8): 295. https://doi.org/10.3390/fire7080295.

Feng, Xu, Loretta J. Mickley, Jed O. Kaplan, Makoto Kelp, Yang Li, and Tianjia Liu. 2024. “Large Role of Anthropogenic Climate Change in Driving Smoke Exposure across the Western United States from 1992 to 2020.” Version 1. Preprint, arXiv. https://doi.org/10.48550/ARXIV.2412.03733.

Field, E. H., R. J. Arrowsmith, G. P. Biasi, et al. 2014. “Uniform California Earthquake Rupture Forecast, Version 3 (UCERF3) - The Time-Independent Model.” Bulletin of the Seismological Society of America 104 (3): 1122–80. https://doi.org/10.1785/0120130164.

Fielding Reid, Harry. 1910. The California Earthquake of April 18, 1906. Carnegie Institution of Washington.

Fiorucci, Paolo, Umberto Pernice, Giorgio Meschi, Andrea Trucchia, and Enrico Ponte. 2024. “Technical Guidelines for Forest Fire Risk Assessment.” CIMA.

Fournier, Eric Daniel, Stephanie Pincetl, and Samantha Smithies. 2025. “Gas Decommissioning in California.”

Fraser, Andrew M., Mikhail V. Chester, and B. Shane Underwood. 2022. “Wildfire Risk, Post-Fire Debris Flows, and Transportation Infrastructure Vulnerability.” Sustainable and Resilient Infrastructure 7 (3): 188–200. https://doi.org/10.1080/23789689.2020.1737785.

Gall, Melanie, Kevin A. Borden, and Susan L. Cutter. 2009. “When Do Losses Count?: Six Fallacies of Natural Hazards Loss Data.” Bulletin of the American Meteorological Society 90 (6): 799–810. https://doi.org/10.1175/2008BAMS2721.1.

Gigović, Ljubomir, Gordana Jakovljević, Dragoljub Sekulović, and Miodrag Regodić. 2018. “GIS Multi-Criteria Analysis for Identifying and Mapping Forest Fire Hazard: Nevesinje, Bosnia and Herzegovina.” Tehnicki Vjesnik - Technical Gazette 25 (3). https://doi.org/10.17559/TV-20151230211722.

Golding, Brian, ed. 2022. Towards the “Perfect” Weather Warning: Bridging Disciplinary Gaps through Partnership and Communication. Springer International Publishing. https://doi.org/10.1007/978-3-030-98989-7.

Gong, Dapeng, Long Sun, and Tongxin Hu. 2024. “Characterizing the Occurrence of Wildland-Urban Interface Fires and Their Important Factors in China.” Ecological Indicators 165 (August): 112179. https://doi.org/10.1016/j.ecolind.2024.112179.

González, David J.X., Rachel Morello-Frosch, Zehua Liu, et al. 2024. “Wildfires Increasingly Threaten Oil and Gas Wells in the Western United States with Disproportionate Impacts on Marginalized Populations.” One Earth 7 (6): 1044–55. https://doi.org/10.1016/j.oneear.2024.05.013.

Goodchild, Michael F. 2006. “GIS and Disasters: Planning for Catastrophe.” Computers, Environment and Urban Systems 30 (3): 227–29. https://doi.org/10.1016/j.compenvurbsys.2005.10.004.

Greenberg, Miriam, Hillary Angelo, Elena Losada, and Christopher C. Wilmers. 2024. “Relational Geographies of Urban Unsustainability: The Entanglement of California’s Housing Crisis with WUI Growth and Climate Change.” Proceedings of the National Academy of Sciences 121 (32): e2310080121. https://doi.org/10.1073/pnas.2310080121.

Greene, Randal, Rodolphe Devillers, Joan E. Luther, and Brian G. Eddy. 2011. “GIS-Based Multiple-Criteria Decision Analysis.” Geography Compass 5 (6): 412–32. https://doi.org/10.1111/j.1749-8198.2011.00431.x.

Guo, Yongxuan, Jianghao Wang, Yong Ge, and Chenghu Zhou. 2024. “Global Expansion of Wildland-Urban Interface Intensifies Human Exposure to Wildfire Risk in the 21st Century.” Science Advances 10 (45): eado9587. https://doi.org/10.1126/sciadv.ado9587.

Hamada, M., and T. D. O’Rourke. 1992. Case Studies of Liquefaction and LifelinePerformance During Past Earthquakes. NCEER-92-0001.

Hardebeck, Jeanne L., and Tomomi Okada. 2018. “Temporal Stress Changes Caused by Earthquakes: A Review.” Journal of Geophysical Research: Solid Earth 123 (2): 1350–65. https://doi.org/10.1002/2017JB014617.

Holzer, Thomas L., Selcuk Toprak, and Michael J. Bennett. 2002. “Liquefaction Potential Index and Seismic Hazard Mapping in the San Francisco Bay Area, California.” 2: 1699–706.

Hua, Jiahao, Taicong Chen, and Jingyao Zhang. 2025. “Vulnerability Evaluation of Post-Earthquake Fire Ignition of Building Structures.” Journal of Building Engineering 109 (September): 113058. https://doi.org/10.1016/j.jobe.2025.113058.

Huffman, David W., John Paul Roccaforte, Judith D. Springer, and Joseph E. Crouse. 2020. “Restoration Applications of Resource Objective Wildfires in Western US Forests: A Status of Knowledge Review.” Fire Ecology 16 (1): 18. https://doi.org/10.1186/s42408-020-00077-x.

Ibarrarán Viniegra, María Eugenia, Matthias Ruth, Sanjana Ahmad, and Marisa London. 2009. “Climate Change and Natural Disasters: Macroeconomic Performance and Distributional Impacts.” Environment, Development and Sustainability 11 (3): 549–69. https://doi.org/10.1007/s10668-007-9129-9.

Ishihara, K. 1993. “Liquefaction and Flow Failure during Earthquakes.” Géotechnique 43 (3): 351–451. https://doi.org/10.1680/geot.1993.43.3.351.

IUFRO and PROFOR. 2020. “Managing Wildfires in a Changing Climate.” International Bank for Reconstruction and Development/The World Bank. https://www.profor.info/content/managing-wildfires-changing-climate.

Jibson, R. 1993. “PREDICTING EARTHQUAKE-INDUCED LANDSLIDE DISPLACEMENTS USING NEWMARK’S SLIDING BLOCK ANALYSIS.” Transportation Research Record, 9–17.

Jones, Lucile M., Richard Bernknopf, Dale Cox, et al. 2008. The ShakeOut Scenario. Open-File Report 2008-1150. Open-File Report. U.S. Geological Survey.

Kaku, Kazuya. 2019. “Satellite Remote Sensing for Disaster Management Support: A Holistic and Staged Approach Based on Case Studies in Sentinel Asia.” International Journal of Disaster Risk Reduction 33 (February): 417–32. https://doi.org/10.1016/j.ijdrr.2018.09.015.

Kanamori, Hiroo, and Emily E Brodsky. 2004. “The Physics of Earthquakes.” Reports on Progress in Physics 67 (8): 1429–96. https://doi.org/10.1088/0034-4885/67/8/R03.

Keane, Robert E., James K. Agee, Peter Fulé, et al. 2008. “Ecological Effects of Large Fires on US Landscapes: Benefit or Catastrophe?A.” International Journal of Wildland Fire 17 (6): 696–712. https://doi.org/10.1071/WF07148.

Keefer, David K. 1984. “Landslides Caused by Earthquakes.” Geological Society of America Bulletin 95: 406–21.

Keeley, Jon E., and Alexandra D. Syphard. 2018. “Historical Patterns of Wildfire Ignition Sources in California Ecosystems.” International Journal of Wildland Fire 27 (12): 781–99. https://doi.org/10.1071/WF18026.

Keeley, Jon E., and Alexandra D. Syphard. 2019. “Twenty-First Century California, USA, Wildfires: Fuel-Dominated vs. Wind-Dominated Fires.” Fire Ecology 15 (1): 24, s42408-019-0041–0. https://doi.org/10.1186/s42408-019-0041-0.

Keeley, Jon, and Alexandra Syphard. 2016. “Climate Change and Future Fire Regimes: Examples from California.” Geosciences 6 (3): 37. https://doi.org/10.3390/geosciences6030037.

Kharb, Aditi, Sandesh Bhandari, Maria Moitinho De Almeida, Rafael Castro Delgado, Pedro Arcos González, and Sandy Tubeuf. 2022. “Valuing Human Impact of Natural Disasters: A Review of Methods.” International Journal of Environmental Research and Public Health 19 (18): 11486. https://doi.org/10.3390/ijerph191811486.

Kim, Man-Jae, and Hee-Kwon Lee. 2023. “Long-Term Patterns of Earthquakes Influenced by Climate Change: Insights from Earthquake Recurrence and Stress Field Changes across the Korean Peninsula during Interglacial Periods.” Quaternary Science Reviews 321 (December): 108369. https://doi.org/10.1016/j.quascirev.2023.108369.

Kiremidjian, Anne, James Moore, Yue Yue Fan, Ozgur Yazlali, Nesrin Basoz, and Meredith Williams. 2007. “Seismic Risk Assessment of Transportation Network Systems.” Journal of Earthquake Engineering 11 (3): 371–82. https://doi.org/10.1080/13632460701285277.

Kramer, Steven L. 1996. Geotechnical Earthquake Engineering. Prentice-Hall International Series in Civil Engineering and Engineering Mechanics. Prentice Hall.

Krausmann, Elisabeth, Serkan Girgin, and Amos Necci. 2019. “Natural Hazard Impacts on Industry and Critical Infrastructure: Natech Risk Drivers and Risk Management Performance Indicators.” International Journal of Disaster Risk Reduction 40 (November): 101163. https://doi.org/10.1016/j.ijdrr.2019.101163.

Kürüm Varolgüneş, Fatma, and Sadık Varolgüneş. 2025. “Post-Earthquake Fires (PEFs) in the Built Environment: A Systematic and Thematic Review of Structural Risk, Urban Impact, and Resilience Strategies.” Fire 8 (6): 233. https://doi.org/10.3390/fire8060233.

Largent, M, B Zheng, J Watson-Lamprey, et al. 2024. “OPENSRA: A SOFTWARE FOR

SEISMIC RISK ANALYSIS OF NATURAL GAS INFRASTRUCTURE.” Paper presented at World Conference on Earthquake Engineering.

Largent, Micaela, Jonathan Bray, Jennie Watson-Lamprey, and Norman Abrahamson. 2023. “Developing Software to Assess the Seismic Risk of Natural Gas Infrastructure: OpenSRA.” Frontiers in Built Environment 9 (June): 1176919. https://doi.org/10.3389/fbuil.2023.1176919.

Lee, Selina, Rachel Davidson, Norihito Ohnishi, and Charles Scawthorn. 2008. “Fire Following Earthquake - Reviewing the State-of-the-Art of Modeling.” Earthquake Spectra 24 (4): 933–67. https://doi.org/10.1193/1.2977493.

Legislative Analyst’s Office. 2019. “Main Types of Disasters and Associated Trends.” https://lao.ca.gov/Publications/Report/3918?utm_source=chatgpt.com.

Li, Shu, and Tirtha Banerjee. 2021. “Spatial and Temporal Pattern of Wildfires in California from 2000 to 2019.” Scientific Reports 11 (1): 8779. https://doi.org/10.1038/s41598-021-88131-9.

Li, Yijiang, Kibaek Kim, Sven Leyffer, Matt Menickelly, Lawrence Paul Lewis, and Joshua Bergerson. 2024. “Modeling and Solving Cascading Failures across Interdependent Infrastructure Systems.” Version 1. Preprint, arXiv. https://doi.org/10.48550/ARXIV.2407.16796.

Lo, Helen, Seth Blumsack, Paul Hines, and Sean Meyn. 2019. “Electricity Rates for the Zero Marginal Cost Grid.” The Electricity Journal 32 (3): 39–43. https://doi.org/10.1016/j.tej.2019.02.010.

Lotfi, Nafiseh, Behrouz Behnam, and Farzad Peyman. 2021. “A BIM-Based Framework for Evacuation Assessment of High-Rise Buildings under Post-Earthquake Fires.” Journal of Building Engineering 43 (November): 102559. https://doi.org/10.1016/j.jobe.2021.102559.

Loudermilk, E. Louise, Joseph J. O’Brien, Scott L. Goodrick, Rodman R. Linn, Nicholas S. Skowronski, and J. Kevin Hiers. 2022. “Vegetation’s Influence on Fire Behavior Goes beyond Just Being Fuel.” Fire Ecology 18 (1): 9, s42408-022-00132–39. https://doi.org/10.1186/s42408-022-00132-9.

Ly, Laura. 2019. “Merrimack Valley Gas Explosions Were Caused by Weak Management, Poor Oversight, NTSB Says | CNN.” September 24. https://edition.cnn.com/2019/09/24/us/ma-gas-explosions-cause/index.html.

MacCarthy, James, Jessica Richter, Sasha Tyukavina, Mikaela Weisse, and Nancy Harris. 2024. The Latest Data Confirms: Forest Fires Are Getting Worse. August 13. https://www.wri.org/insights/global-trends-forest-fires.

Malczewski, Jacek. 1999. GIS and Multicriteria Decision Analysis. Wiley.

Marlon, Jennifer R., Patrick J. Bartlein, Daniel G. Gavin, et al. 2012. “Long-Term Perspective on Wildfires in the Western USA.” Proceedings of the National Academy of Sciences 109 (9). https://doi.org/10.1073/pnas.1112839109.

Martin, Glen. 2008. “Taking the Heat.” Bay Nature. https://baynature.org/article/taking-the-heat/.

Masoudvaziri, Nima, Fernando Szasdi Bardales, Oguz Kaan Keskin, Amir Sarreshtehdari, Kang Sun, and Negar Elhami-Khorasani. 2021. “Streamlined Wildland-Urban Interface Fire Tracing (SWUIFT): Modeling Wildfire Spread in Communities.” Environmental Modelling & Software 143 (September): 105097. https://doi.org/10.1016/j.envsoft.2021.105097.

Mazhin, Sadegh Ahmadi, Mehrdad Farrokhi, Mehdi Noroozi, et al. 2021. “Worldwide Disaster Loss and Damage Databases: A Systematic Review.” Journal of Education and Health Promotion 10 (1). https://doi.org/10.4103/jehp.jehp_1525_20.

McLauchlan, Kendra K., Philip E. Higuera, Jessica Miesel, et al. 2020. “Fire as a Fundamental Ecological Process: Research Advances and Frontiers.” Journal of Ecology 108 (5): 2047–69. https://doi.org/10.1111/1365-2745.13403.

Mell, William E., Samuel L. Manzello, Alexander Maranghides, David Butry, and Ronald G. Rehm. 2010. “The Wildland–Urban Interface Fire Problem – Current Approaches and Research Needs.” International Journal of Wildland Fire 19 (2): 238–51. https://doi.org/10.1071/WF07131.

Moftakhari, Hamed, and Amir AghaKouchak. 2019. “Increasing Exposure of Energy Infrastructure to Compound Hazards: Cascading Wildfires and Extreme Rainfall.” Environmental Research Letters 14 (10): 104018. https://doi.org/10.1088/1748-9326/ab41a6.

Mousavi, Shahab, Ashutosh Bagchi, and Venkatesh K.R. Kodur. 2008. “Review of Post-Earthquake Fire Hazard to Building Structures.” Canadian Journal of Civil Engineering 35 (7): 689–98. https://doi.org/10.1139/L08-029.

Murray, Alan T., Jiwon Baik, Vanessa Echeverri Figueroa, et al. 2023. “Developing Effective Wildfire Risk Mitigation Plans for the Wildland Urban Interface.” International Journal of Applied Earth Observation and Geoinformation 124 (November): 103531. https://doi.org/10.1016/j.jag.2023.103531.

Narayanaraj, Ganapathy, and Michael C. Wimberly. 2012. “Influences of Forest Roads on the Spatial Patterns of Human- and Lightning-Caused Wildfire Ignitions.” Applied Geography 32 (2): 878–88. https://doi.org/10.1016/j.apgeog.2011.09.004.

NASA. 2024. The Effects of Climate Change. Climate Change. https://science.nasa.gov/climate-change/effects/.

Nemeth, Noelle, Malcolm S. Johnson, Gabi Mocatta, and Erin Hawley. 2024. “Communicational Responses for Compound Natural Hazards: A Systematic Review.” International Journal of Disaster Risk Reduction 115 (December): 105041. https://doi.org/10.1016/j.ijdrr.2024.105041.

Nishida, Rira, Ayane Sasaki, Tetsuo Tobita, Yasuko Kuwata, and Koji Ichii. 2024. “The Effect of Lifeline Damage to Other Lifeline Networks: A Past Experience in Kobe and Future Perspective of Interrelationship Effect on Electricity and Gas.” Japanese Geotechnical Society Special Publication 10 (60): 2398–401. https://doi.org/10.3208/jgssp.v10.P2-09.

Nishino, Tomoaki. 2023. “Post-Earthquake Fire Ignition Model Uncertainty in Regional Probabilistic Shaking–Fire Cascading Multi-Hazard Risk Assessment: A Study of Earthquakes in Japan.” International Journal of Disaster Risk Reduction 98 (November): 104124. https://doi.org/10.1016/j.ijdrr.2023.104124.

Oliveira, Tiago M., Ana M. G. Barros, Alan A. Ager, and Paulo M. Fernandes. 2016. “Assessing the Effect of a Fuel Break Network to Reduce Burnt Area and Wildfire Risk Transmission.” International Journal of Wildland Fire 25 (6): 619. https://doi.org/10.1071/WF15146.

O’Rourke, Michael J., and Xuejie Liu. 1999. Response of Buried Pipelines Subject to Earthquake Effects. Multidisciplinary Center for Earthquake Engineering Research.

O’Rourke, T. D., and M. C. Palmer. 1994. Northridge, California Earthquake of January 17, 1994: Performance of Gas Transmission Pipelines. NCEER-94-0011. Cornell University.

O'Rourke, T.D. 2003. Critical Infrastructure, Interdependencies, and Resilience. The Bridge.

Petak, William J., and Shirin Elahi. 2001. "The Northridge Earthquake, USA, and Its Economic and Social Impacts." Proceedings of the EuroConference (Laxenburg, Austria).

Piccinelli, Roberta, Elisabeth Krausmann, and Europäische Kommission, eds. 2013. Analysis of Natech Risk for Pipelines: A Review. EUR 26371. Publications Office of the European Union. https://doi.org/10.2788/42532.

Pitilakis, Kyriazis, Maria Alexoudi, Sotiris Argyroudis, Olivier Monge, and Christophe Martin. 2006. "Earthquake Risk Assessment of Lifelines." Bulletin of Earthquake Engineering 4 (4): 365–90. https://doi.org/10.1007/s10518-006-9022-1.

Plafker, George. 1969. "Tectonics of the March 27, 1964, Alaska Earthquake." Geological Survey Professional Paper 543-I. https://pubs.usgs.gov/pp/0543i/.

Qiu, Minghao, Deyang Chen, Makoto Kelp, Jing Li, Guanyu Huang, and Mahdieh Danesh Yazdi. 2025. "The Rising Threats of Wildland-Urban Interface Fires in the Era of Climate Change: The Los Angeles 2025 Fires." The Innovation 6 (5): 100835. https://doi.org/10.1016/j.xinn.2025.100835.

Quarantelli, E. L. 2000. EMERGENCIES, DISASTER AND CATASTROPHES ARE DIFFERENT PHENOMENA. University of Delaware.

Radeloff, V. C., R. B. Hammer, S. I. Stewart, J. S. Fried, S. S. Holcomb, and J. F. McKeefry. 2005. "THE WILDLAND–URBAN INTERFACE IN THE UNITED STATES." Ecological Applications 15 (3): 799–805. https://doi.org/10.1890/04-1413.

Radeloff, Volker C., David P. Helmers, H. Anu Kramer, et al. 2018. "Rapid Growth of the US Wildland-Urban Interface Raises Wildfire Risk." Proceedings of the National Academy of Sciences 115 (13): 3314–19. https://doi.org/10.1073/pnas.1718850115.

Ren, A. Z., and X. Y. Xie. 2004. "The Simulation of Post-Earthquake Fire-Prone Area Based on GIS." Journal of Fire Sciences 22 (5): 421–39. https://doi.org/10.1177/0734904104042440.

Rentschler, Jun, Melda Salhab, and Bramka Arga Jafino. 2022. "Flood Exposure and Poverty in 188 Countries." Nature Communications 13 (1): 3527. https://doi.org/10.1038/s41467-022-30727-4.

Ricotta, Carlo, Sofia Bajocco, Daniela Guglietta, and Marco Conedera. 2018. "Assessing the Influence of Roads on Fire Ignition: Does Land Cover Matter?" Fire 1 (2): 24. https://doi.org/10.3390/fire1020024.

Saaty, R.W. 1987. "The Analytic Hierarchy Process - What It Is and How It Is Used." Mathematical Modelling 9 (3–5): 161–76. https://doi.org/10.1016/0270-0255(87)90473-8.

Saaty, Thomas L. 1990. "How to Make a Decision: The Analytic Hierarchy Process." European Journal of Operational Research 48 (1): 9–26. https://doi.org/10.1016/0377-2217(90)90057-I.

Sapsis, David, Tadashi Moody, and James Thorne. 2022. Indicators of Climate Change in California | Wildfires. No. 4. California Environmental Protection Agency, OEHHA.

Saran, Anshu, Gurdeep Singh Raina, Diem Ha Bui, and Parvinder Pal Singh. 2024. "Aging Midstream Supply Chain in the Oil and Gas Industry: Issues and AI-Based Solutions." Journal of Energy and Development 49 (2). https://doi.org/10.56476/jed.v49i2.25.

Sauber, Jeanne M., and Natalia A. Ruppert. 2013. "Rapid Ice Mass Loss: Does It Have an Influence on Earthquake Occurrence in Southern Alaska?" In Geophysical Monograph Series, edited by Jeffrey T. Freymueller, Peter J. Haeussler, Robert L. Wesson, and Göran Ekström. American Geophysical Union. https://doi.org/10.1029/179GM21.

Sauber, Jeanne, Chris Rollins, Jeffrey T. Freymueller, and Natalia A. Ruppert. 2021. "Glacially Induced Faulting in Alaska." In Glacially-Triggered Faulting, 1st ed., edited by Holger Steffen, Odleiv Olesen, and Raimo Sutinen. Cambridge University Press. https://doi.org/10.1017/9781108779906.026.

Saunders, Kate R., Owen Forbes, Jess K. Hopf, et al. 2025. "Data-Driven Recommendations for Enhancing Real-Time Natural Hazard Warnings." One Earth 8 (5): 101274. https://doi.org/10.1016/j.oneear.2025.101274.

Scawthorn, C. 1986. "Fire Following Earthquake." Fire Safety Science 1: 971–79. https://doi.org/10.3801/IAFSS.FSS.1-971.

Scawthorn, C., T. D. O'Rourke, and F. T. Blackburn. 2006. "The 1906 San Francisco Earthquake and Fire - Enduring Lessons for Fire Protection and Water Supply." Earthquake Spectra 22 (2_suppl): 135–58. https://doi.org/10.1193/1.2186678.

Scawthorn, Charles, Keith Porter, Mahmoud Khater, et al. 1992. "Utility Performance Aspects, Liquefaction Study, Marina and Sullivan Marsh Areas, San Francisco, California."

Schaeffer, Roberto, E. Lisa F. Schipper, Daniel Ospina, et al. 2025. "Ten New Insights in Climate Science 2024." One Earth 8 (6): 101285. https://doi.org/10.1016/j.oneear.2025.101285.

Schencking, J. Charles. 2013. The Great Kantō Earthquake and the Chimera of National Reconstruction in Japan. Columbia University Press. https://doi.org/10.7312/sche16218.

Schmidt, Kevin M., Stephen D. Ellen, and David M. Peterson. 2014. "Deformation from the 1989 Loma Prieta Earthquake near the Southwest Margin of the Santa Clara Valley, California." Geosphere 10 (6): 1177–202. https://doi.org/10.1130/GES01095.1.

Seed, H Bolton, and I M Idriss. 1970. A SIMPLIFIED PROCEDURE FOR EVALUATING SOIL LIQUEFACTION POTENTIAL. EERC 70-9. University of California, Berkeley.

Seismic Safety Commission. 1995. Northridge Earthquake: Turning Loss to Gain. CSSC 95-01. California Seismic Safety Commission. https://ssc.ca.gov/forms_pubs/ssc95-01/.

Sfetsos, Athanasios, Frederique Giroud, Alice Clemencau, et al. 2021. "Assessing the Effects of Forest Fires on Interconnected Critical Infrastructures under Climate Change. Evidence from South France." Infrastructures 6 (2): 16. https://doi.org/10.3390/infrastructures6020016.

Shives, Erin, Tzu-Hsin Karen Chen, and Karen C. Seto. 2025. "Multiple Hazards and Exposure in California: A Space-Time Analysis of Temperature, Drought, and Wildfire." International Journal of Disaster Risk Reduction 120 (April): 105391. https://doi.org/10.1016/j.ijdrr.2025.105391.

Short, K. C. 2014. "A Spatial Database of Wildfires in the United States, 1992-2011." Earth System Science Data 6 (1): 1–27. https://doi.org/10.5194/essd-6-1-2014.

Syphard, Alexandra D., Volker C. Radeloff, Jon E. Keeley, et al. 2007. "HUMAN INFLUENCE ON CALIFORNIA FIRE REGIMES." Ecological Applications 17 (5): 1388–402. https://doi.org/10.1890/06-1128.1.

Syphard, Alexandra D., Heather Rustigian-Romsos, Michael Mann, Erin Conlisk, Max A. Moritz, and David Ackerly. 2019. "The Relative Influence of Climate and Housing

Development on Current and Projected Future Fire Patterns and Structure Loss across Three California Landscapes." Global Environmental Change 56 (May): 41–55. https://doi.org/10.1016/j.gloenvcha.2019.03.007.

Taccaliti, Flavio, Raffaella Marzano, Tina L. Bell, and Emanuele Lingua. 2023. "Wildland–Urban Interface: Definition and Physical Fire Risk Mitigation Measures, a Systematic Review." Fire 6 (9): 343. https://doi.org/10.3390/fire6090343.

Tam, Laura, and Laurie A. Johnson. 2020. Safety First: Improving Hazard Resilience in the Bay Area. SPUR Regional Strategy.

Thapa, Samrajya Bikram, Jeffrey S. Jenkins, and Anthony Leroy Westerling. 2023. "Perceptions of Wildfire Management Practices in a California Wildland-Urban Interface." Environmental Advances 12 (July): 100382. https://doi.org/10.1016/j.envadv.2023.100382.

Thomas, Alyssa S. 2024. "Inequities in Wildfire Risk Distribution to People and Their Communities." One Earth 7 (6): 956–58. https://doi.org/10.1016/j.oneear.2024.05.018.

Thonicke, K., A. Spessa, I. C. Prentice, S. P. Harrison, L. Dong, and C. Carmona-Moreno. 2010. "The Influence of Vegetation, Fire Spread and Fire Behaviour on Biomass Burning and Trace Gas Emissions: Results from a Process-Based Model." Biogeosciences 7 (6): 1991–2011. https://doi.org/10.5194/bg-7-1991-2010.

Tian, Yuan, Minting Lu, Zhen Xu, and Jingyi Ren. 2025. "A Fire Following Earthquake Spread Model Considering Building Height and Its Application to Real-World Events." International Journal of Disaster Risk Reduction 118 (February): 105261. https://doi.org/10.1016/j.ijdrr.2025.105261.

Turco, Marco, John T. Abatzoglou, Sixto Herrera, et al. 2023. "Anthropogenic Climate Change Impacts Exacerbate Summer Forest Fires in California." Proceedings of the National Academy of Sciences 120 (25): e2213815120. https://doi.org/10.1073/pnas.2213815120.

Twigg, John. 2003. "The Human Factor in Early Warnings: Risk Perception and Appropriate Communications." In Early Warning Systems for Natural Disaster Reduction, edited by Jochen Zschau and Andreas Küppers. Springer Berlin Heidelberg. https://doi.org/10.1007/978-3-642-55903-7_4.

UCAR. 2025. "Predictions of Future Global Climate." https://scied.ucar.edu/learning-zone/climate-change-impacts/predictions-future-global-climate.

Ueno, Junichi, N Hassani, S Fujita, et al. 2004. "Research and Development on Fragility of Components for the Gas Distribution System in Greater Tehran, Iran." World Conference on Earthquake Engineering.

UNISDR. 2015. "Sendai Framework for Disaster Risk Reduction 2015-2030." June 29. https://www.undrr.org/publication/sendai-framework-disaster-risk-reduction-2015-2030.

US EPA, OAR. 2024. "Future of Climate Change." Overviews and Factsheets. March 27. https://www.epa.gov/climatechange-science/future-climate-change.

USGS Fact Sheet 2008-3027. 2008. Fact Sheet. Fact Sheet.

USGS Fact Sheet 2015-3009. 2015. Fact Sheet. Fact Sheet.

Vasseghi, Akbar, Ebrahim Haghshenas, Aram Soroushian, and Masoumeh Rakhshandeh. 2021. "Failure Analysis of a Natural Gas Pipeline Subjected to Landslide." Engineering Failure Analysis 119 (January): 105009. https://doi.org/10.1016/j.engfailanal.2020.105009.

Vernick, Daniel. 2025. "Is Climate Change Increasing the Risk of Disasters?" World Wildlife Fund. https://www.worldwildlife.org/resources/explainers/is-climate-change-increasing-the-risk-of-disasters/.

Vitorino, Hugo, Vahid Khiali, and Hugo Rodrigues. 2024. "Post-Earthquake Fire Risk and Loss Assessment in Urban Areas." Innovative Infrastructure Solutions 9 (1): 26. https://doi.org/10.1007/s41062-023-01333-0.

Watson-Lamprey, Jannie, Micaela Largent, and Barry Zheng. 2022. Performance-Based Earthquake Engineering Assessment Tool for Natural Gas Storage and Pipeline Systems.

Weiss, Stu, Alan Flint, Lorraine Flint, Healy Hamilton, Miguel Fernandez, and Lisa Micheli. 2013. Climate Scenarios for San Francisco Bay Area. A Dwight Center for Conservation Science.

Westerling, A. L., B. P. Bryant, H. K. Preisler, et al. 2011. "Climate Change and Growth Scenarios for California Wildfire." Climatic Change 109 (S1): 445–63. https://doi.org/10.1007/s10584-011-0329-9.

Westerling, Anthony LeRoy. 2016. "Increasing Western US Forest Wildfire Activity: Sensitivity to Changes in the Timing of Spring." Philosophical Transactions of the Royal Society B: Biological Sciences 371 (1696): 20150178. https://doi.org/10.1098/rstb.2015.0178.

Wilkin, Katherine M., David Benterou, and Amanda M. Stasiewicz. 2025. "High Fire Hazard Wildland Urban Interface (WUI) Residences in California Lack Voluntary and Mandated Wildfire Risk Mitigation Compliance in Home Ignition Zones." International Journal of Disaster Risk Reduction 124 (June): 105435. https://doi.org/10.1016/j.ijdrr.2025.105435.

Williams, A. Park, John T. Abatzoglou, Alexander Gershunov, et al. 2019. "Observed Impacts of Anthropogenic Climate Change on Wildfire in California." Earth's Future 7 (8): 892–910. https://doi.org/10.1029/2019EF001210.

Yegian, M. K., G. V. Ghahraman, G. Gazetas, P. Dakoulas, and N. Makris. 1995. "The Northridge Earthquake of 1994: Ground Motions and Geotechnical Aspects." 1. http://scholarsmine.mst.edu/icrageesd/03icrageesd/session14/1.

Zscheischler, Jakob, Seth Westra, Bart J. J. M. Van Den Hurk, et al. 2018. "Future Climate Risk from Compound Events." Nature Climate Change 8 (6): 469–77. https://doi.org/10.1038/s41558-018-0156-3.

DAD
Dipartimento
di Architettura
e Design

Politecnico di Torino
December 2025